AWARD NUMBER:
W81XWH-13-1-0140

TITLE:
Targeting Common but Complex Proteoglycans on Breast Cancer Cells and Stem Cells Using Evolutionary Refined Malaria Proteins

PRINCIPAL INVESTIGATOR:
Mads Daugaard

CONTRACTING ORGANIZATION: **University of British Columbia**
Vancouver V6T1Z3

REPORT DATE:
August 2016

TYPE OF REPORT:
Annual Report

PREPARED FOR: U.S. Army Medical Research and Materiel Command
Fort Detrick, Maryland 21702-5012

REPORT DOCUMENTATION PAGE

Form Approved OMB No. 0704-0188

1. REPORT DATE	2. REPORT TYPE	3. DATES COVERED
August 2016	Annual	15 Jul 2015 – 14 Jul 2016

4. TITLE AND SUBTITLE
Targeting Common but Complex Proteoglycans on Breast Cancer Cells and Stem Cells Using Evolutionary Refined Malaria Proteins

5a. CONTRACT NUMBER
W81XWH-13-1-0140

5b. GRANT NUMBER
W81XWH-13-1-0140

5c. PROGRAM ELEMENT NUMBER

6. AUTHOR(S)
Mads Daugaard

E-Mail: mdaugaard@prostatecentre.com

5d. PROJECT NUMBER

5e. TASK NUMBER

5f. WORK UNIT NUMBER

7. PERFORMING ORGANIZATION NAME(S) AND ADDRESS(ES)
The University of British Columbia
The University Industry
Liaison Office
6190 Agronomy Rd, #102
Vancouver, BC V6T 1Z3

8. PERFORMING ORGANIZATION REPORT NUMBER

9. SPONSORING / MONITORING AGENCY NAME(S) AND ADDRESS(ES)
U.S. Army Medical Research and Materiel Command
Fort Detrick, Maryland 21702-5012

10. SPONSOR/MONITOR'S ACRONYM(S)

11. SPONSOR/MONITOR'S REPORT NUMBER(S)

12. DISTRIBUTION / AVAILABILITY STATEMENT
Approved for Public Release; Distribution Unlimited

13. SUPPLEMENTARY NOTES

14. ABSTRACT
In the past year of the project we have successfully produced recombinant VAR2CSA that binds with high affinity and high specificity to breast cancer cells and breast cancer tissue biopsies. We have demonstrated that the protein binds to distinct secondary modified proteoglycans exclusively present on breast cancer cells and that targeting these with recombinant VAR2CSA interferes with key functions of the cancer cell like growth, migration and invasion.

15. SUBJECT TERMS
Cancer, breast cancer, treatment, malaria protein

16. SECURITY CLASSIFICATION OF:			17. LIMITATION OF ABSTRACT	18. NUMBER OF PAGES	19a. NAME OF RESPONSIBLE PERSON
a. REPORT	b. ABSTRACT	c. THIS PAGE			USAMRMC
Unclassified	Unclassified	Unclassified	Unclassified	75	19b. TELEPHONE NUMBER *(include area code)*

Table of Contents

1. INTRODUCTION:

In pregnant women, parasite-infected red blood cells express a protein that binds to a distinct sugar structure present only on certain cells of the placenta. This highly evolved binding system enables the parasite to evade clearance and infect placental cells, thereby causing pregnancy-associated malaria outbreaks in epidemic regions of the world. Prior to this application we discovered that human breast cancer cells express this same carbohydrate structure, which is present on human placental cells. The sugar structure likely enables breast cancer cells to migrate and invade surrounding normal tissue, and plays a role in metastatic spread of the cancer. This raised the intriguing possibility that we could use this naturally refined parasite-host interaction mechanism as a tool to specifically bind human breast cancer cells and inhibit their metastatic potential. The aim of the project was to combine our individual expertise in cancer biology (Dr. Daugaard) and parasitology (Dr. Salanti) to investigate the potential of exploiting the interaction between the malarial protein, called VAR2CSA, and the breast cancer-associated sugar structure as a novel approach to inhibit growth and metastatic growth of different subtypes of breast cancers.

NOTE: The below reporting relates to work performed at University of Copenhagen (Dr. Salanti) and University of British Columbia (Dr. Daugaard) under the partnering PI mechanism.

2. KEYWORDS:

Breast cancer, Malaria, treatment, metastasis, Recombinant protein, drug conjugate

3. ACCOMPLISHMENTS:

We have successfully produced recombinant VAR2CSA (rVAR2) that binds with high affinity and high specificity to breast cancer cells and breast cancer tissue biopsies [1]**(Figures 1A, 2A, 3A-B, S3A, and Table S1);** [2]**(Figure 2A, Table 1)**. We have demonstrated that the protein binds to distinct secondary modified proteoglycans exclusively present on breast cancer cells and that targeting these with rVAR2 interferes with key functions of the cancer cell like growth, migration and invasion [1]**(Figures 4H, 4J-K, S4D);** [3]**(Figs. 1C, 4D).** *In vivo* data supports the use of using toxin-conjugated rVAR2 to effectively target and treat breast cancer [1]**(Figures 7A-D, 7H-M)**. There are no deviations to the agreed research plan and all major tasks are on schedule (see below section for breakdown of results).

What were the major goals of the project?

Aim 1: To identify the highest-affinity cancer cell line-binding recombinant VAR2CSA variant, and facilitate high-throughput synthesis of VAR2CSA for pre-clinical and clinical use

Aim 2: To identify the endogenous ligand of VAR2CSA on breast cancer cells

Aim 3: To dissect the affected intracellular pathways following VAR2CSA-ligand interactions and to investigate the link between CSPG signaling, migration, and invasion in human breast cancer

Aim 4: To evaluate the use of recombinant VAR2CSA as a diagnostic tool in immunohistochemistry and tissue microarray (TMA) applications of breast cancer
Aim 5: To couple cytotoxic compounds to recombinant VAR2CSA and test these conjugates *in vitro* for their ability to induce tumor cell-selective cell death
Aim 6: To establish proof-of-concept for a targeting strategy using both uncoupled and toxin-coupled VAR2CSA *in vitro* and in mouse models

What was accomplished under these goals?
Aim 1: A stable expression system for the production of rVAR2 has been tested and validated in Shuffle *E. coli* cells. As evident by the 3 publications[1-3], we have been able to produce sufficient amounts of recombinant protein for this project. We are currently trying to move the expression system into insect cells and are in the process of mutating glycosylation sites in the rVAR2 protein (as glycosylation of the protein inhibits its activity). The produced proteins have been tested for binding affinity and specificity to a panel of cancer cell lines, and we have shown that both the eukaryotic and prokaryotic produced proteins binds all tested breast cancer cells with high affinity (1nM) and high specificity [1]**(Figs. 1G-H, 2B-F, 2H-J, S2A-E, S4A-C, Table S1)**. Scale-up batches were made available for subsequent *in vivo* and *in vitro* experiments. Accordingly, the work related to aim 1 is fully accomplished, although scheduled synthesis of rVAR2 proteins will continue for the remaining of this project (anticipated 10%).
Location: University of Copenhagen
Accomplished: 90%

Aim 2: To identify the endogenous ligand of VAR2CSA on breast cancer cells.
To conduct the work outlined in major work task II, we tested a number of different purification technologies including the TAP-TAG approach. It turned out that the best approach was not the TAP-TAG, but a column-based approach where recombinant VAR2CSA was immobilized within a purification column. Using this approach, we have until now successfully identified a number of proteoglycans that interact with the recombinant malaria protein VAR2CSA when sulfated on carbon 4 of the CS backbone [1]**(Figs. 4E-K, Table S5)**. We have identified two major breast cancer-associated proteoglycans, CSPG4 and CD44, as modified with CS and expression of these has been validated using western [1]**(Figs. 4F, K)** blot confocal microscopy [1]**(Figs. 4E, J)**. Accordingly, the work within *major work task II* is accomplished but work on expanding the source material to include more cell lines and primary tissue is ongoing.
Location: University of British Columbia and University of Copenhagen
Accomplished: 50%

Aim 3: To dissect the affected intracellular pathways following VAR2CSA-ligand interactions and to investigate the link between CSPG signaling, migration, and invasion in human breast cancer
We have with success investigated the internalization patterns of recombinant VAR2CSA and found that the protein internalize into intracellular structures within 15-20 minutes after addition

to the tumor cell culture and that it ends up in the lysosomal compartment [1]**(Figs. 5A-D)**. We have identified the main signaling pathway affected by recombinant VAR2CSA (Integrin signaling) and validated this biochemically and functionally [3]**(Figs. 1A-E, 2A-F, 3A-G, 4A-G, Table 1)**. Ongoing work focuses on elucidating the mechanism of internalization and by which CS affects cell motility.
Location: University of British Columbia and University of Copenhagen
Accomplished: 50%

Aim 4: To evaluate the use of recombinant VAR2CSA as a diagnostic tool in immunohistochemistry and tissue microarray (TMA) applications of breast cancer
Aim 4 has progressed according to plan. We have successfully established an IHC procedure for high-throughput tissue analysis on the VentureDiscovery platform [1]**(Figs. 1A-E)**. An important finding here is that fixed tissue cannot be subjected antigen retrieval procedures (otherwise used for most IHC antibodies), as this process destroys the glycosaminoglycan target on the tissue. Based on this we have identified the optimal concentration of the recombinant VAR2CSA to be 500 pM in this assay. The optimized protocol is based on a primary incubation of a V5-tagged VAR2CSA, followed by a secondary incubation with a mouse monoclonal anti-V5 antibody, finalized by a detection step using anti mouse-HRP. The high throughput screening of breast cancer tissues, has been initiated. The first round of data demonstrates that that we bind approximately 80-90% of the breast tumor specimens on the test array [1]**(Figs. 2B, S3A)**. We have furthermore developed a biosensor method for analyzing binding kinetics of VAR2CSA directly to primary breast tumor specimens [2]**(Figs. 1A-C, 2A-C, Table 1)**. Ongoing work focuses on refining methodology and expanding the IHC and biosensor-based analysis in larger cohorts of patients.
Location: University of British Columbia
Accomplished: 50%

Aim 5: To couple cytotoxic compounds to recombinant VAR2CSA and test these conjugates *in vitro* for their ability to induce tumor cell-selective cell death
To facilitate coupling of saporin to VAR2CSA we have made a VAR2CSA protein with a biotin acceptor site and procured saporin coupled to streptavidin. However, we have failed to directly couple saporin to VAR2CSA without significantly reducing affinity of VAR2CSA to CS. Therefore, during the project period we developed a more clinical relevant toxin conjugation strategy in collaboration with Kairos Therapeutics (now Zymeworks). A cell cytotoxin, KT886, was successfully conjugated to recombinant VAR2CSA and the drug conjugate effective kills breast cancer cells in vitro [1]**(Figs. 7A-C)**. We are currently making improvements of this strategy, testing new VDC generations in breast cancer cells on an ongoing basis.
Location: University of British Columbia and University of Copenhagen
Accomplished: 50%

Aim 6: To establish proof-of-concept for a targeting strategy using both uncoupled and toxin-coupled VAR2CSA *in vitro* and in mouse models

The work outlined in aim 6 has progressed according to plan with minor deviations to the SOW. All subtasks were performed with the exception of the radiolabelling, which we did not manage to perform due to technical issues. We are currently working on getting a viable radiolabeling method established. Using our VAR2-Drug Conjugate (Aim 5), we have demonstrated strong proof of concept for this strategy to target breast cancer [1]**(Figs. 7A-C).** We have also investigated the functional consequences of unconjugated VAR2CSA binding to breast cancer cells, and in vitro we have a strong effect on the adhesion phenotype [3]**(Figs. 3D)**. In other programs directed at other types of cancer we have evaluated the in vivo effect on tumor growth using recombinant unconjugated VAR2CSA and the conclusion is that we have an effect on migration of cells but not on growth [3]**(Fig. 6A-F)**. For a clinical validation of the concept we would prefer to have an effect on tumor growth hence we decided to focus our efforts on the *in vivo* validation of a VAR2-Drug Conjugate. Hence we established an efficacy model using the highly aggressive syngeneic (immunocompetent) mouse model of metastatic murine breast cancer cells. 4T1 breast cancer cells were efficiently bound by rVAR2 in a concentration and CSA-dependent manner [1]**(Fig. 7H)**. Moreover, the VAR2CSA drug conjugate demonstrated strong cytotoxicity in 4T1 cells in vitro, which could be completely rescued by competition with soluble CSA [1]**(Fig. 7I)**. Injection of luciferase positive-4T1 cells in the left ventricle of the heart of C57BL/6 mice resulted in aggressive bone metastasis with an overall penetrance of 50%–60% [1]**(Fig. 7J)**. The bone metastases invaded into adjacent muscle and showed strong CSA expression as analyzed by rVAR2-based immunohistochemistry (IHC) [1]**(Fig. 7K)**. Notably, of the mice with 4T1 bone metastases, five out of six mice in the VAR2CSA drug conjugate-treated group were still alive at the end of the study (day 54) with no detectable metastases, while all control-treated mice died with metastatic disease ($p = 0.0196$) [1]**(Fig. 7L)**. Indeed, the VAR2CSA drug conjugate-treatment significantly increased survival of mice with 4T1 bone metastasis as compared to control-treated mice [1]**(Fig. 7M)**. Toxicity studies as well as additional xenograft models using triple-negative breast cancer cells are planed for in year 2 and 3.

Location: University of British Columbia

Accomplished: 50%

What opportunities for training and professional development have the project provided?

The VPC is a UBC and National Centre of Excellence, with collaborative links across on-campus and hospital-based research facilities, and is internationally recognized as a comprehensive and integrated cancer research and treatment facility. The VPC uniquely integrates many critical components of translational research under one organization, facilitating seamless management of the complex processes involved in discovery, preclinical development, commercialization, and clinical research in close partnership with national clinical trials and research networks as well as the industry. A major strength of the VPC is the proximity of its clinical and basic research programs, oriented to direct discovery research and translate these discoveries towards the clinical arena. As part of our collaborative research project, we share

several trainees that spend time both in Copenhagen and at the VPC/UBC. When trainees are at Dr. Daugaard's laboratory at the VPC they enjoy unrestricted access to 60,000 square foot integrated laboratory at the Jack Bell and Robert Ho Research Buildings as well as to core infrastructure and technology platforms to support our research project. The Daugaard lab is located in the 3rd floor in the Robert Ho Research Building and on the 5th floor of the Jack Bell Research Centre. It is comprised of a research laboratory and a molecular pathology core facility. As such, the work environment for our trainees has elements of both basic and translational cancer research and provides an optimal framework for professional development.

How were the results disseminated to communities of interest?
The first article describing this novel strategy was published in October 2015 in *Cancer Cell* followed up by a manuscript in *Sens Biosensing Research* published in July 2016 (Attached to this report). Following the publication our institutions made press releases about the publication. These press releases were well adopted by the international news medias, and Daugaard and Salanti have to date given more than 100 interviews about the research both in national as well as international medias ranging from local newspapers to national broadcasted TV. In addition to this we have presented the results at numerous international scientific conferences.

What do you plan to do during the next reporting period to accomplish the goals?
Aim 1. Continue scheduled synthesis of rVAR2 proteins for this project.
Aim 2. Expanding the source material to include more cell lines and primary tissue.
Aim 3. Elucidate the mechanism of internalization and by which CSA affects cell motility.
Aim 4. Refine methodology and expand the IHC and biosensor-based analysis in larger cohorts of breast cancer patients.
Aim 5. Improving and testing new VDC generations in breast cancer cells.
Aim 6: Toxicity studies as well as additional xenograft models using triple-negative breast cancer cells are planed for in year 2 and 3. Continue effort on radiolabeling of VAR2CSA.

4. IMPACT
What was the impact on the development of the principal discipline(s) of the project?
For the first time we demonstrate how an evolutionary evolved pathogen derived protein can be used to target malignant tissue. Furthermore we describe for the first time the presence of a uniquely cancer associated modification, which will form the basis for a multitude of novel targeting strategies.

What was the impact on other disciplines?
The data provides novel insight into the pathology of malaria and how the malaria parasite using VAR2CSA binds to the placental receptor.

What was the impact on technology transfer?
Nothing to report

What was the impact on society beyond science and technology?
The project demonstrates how basic research into malaria pathology can provide novel tools against cancer, highlighting the societal importance of basic research.

5. CHANGES/PROBLEMS

Changes in approach and reasons for change
Due to time constraints caused by the shift from saporin to a more clinical relevant toxin we changed the animal model from an induced model to a xenograft model.

Actual or anticipated problems or delays and actions or plans to resolve them
Nothing to report.

Changes that had a significant impact on expenditures
Nothing to report.

Significant changes in use or care of human subjects, vertebrate animals, biohazards, and/or select agents
Nothing to report.

Significant changes in use or care of human subjects
Nothing to report.

Significant changes in use or care of vertebrate animals
Instead of running the DMBA induced model we used a xenograft mouse model.

Significant changes in use of biohazards and/or select agents
Nothing to report.

6. PRODUCTS

Publications, conference papers, and presentations
Journal publications
1) Ali Salanti, Thomas M Clausen, Mette Ø Agerbæk, Nader Al Nakouzi, Madeleine Dahlbäck2, Htoo Z Oo, Sherry Lee, Tobias Gustavsson, Jamie R Rich, Bradley J Hedberg, Yang Mao, Line Barington, Marina A Pereira, Janine LoBello, Makoto Endo, Ladan Fazli, Jo Soden, Chris K Wang, Adam F Sander, Robert Dagil, Susan Thrane, Peter J Holst, Le Meng, Francesco Favero, Glen J Weiss, Morten A Nielsen, Jim Freeth, Torsten O Nielsen1, Joseph Zaia, Nhan L Tran, Jeff Trent, John S Babcook, Thor G Theander, Poul H Sorensen and **Mads Daugaard**. *Targeting human cancer by a glycosaminoglycan binding malaria protein.* **Cancer Cell. 2015 Oct 12;28(4):500-14**

2) Clausen TM, Pereira MA, Oo HZ, Resende M, Gustavson T, Mao Y, Sugiura N, Liew J, Fazli L, Theander TG, **Daugaard M**, Salanti A. *Real-time and label free determination of ligand binding-kinetics to primary cancer tissue specimens; a novel tool for the assessment of biomarker targeting.* **Sens Biosensing Res. 2016 Jul;9:23-30.**

3) Thomas Mandel Clausen, Marina Ayres Pereira, Nader Al Nakouzi, Htoo Zarni Oo, Mette 1 Agerbæk, Sherry Lee, Maj Sofie 1rum-Madsen, Anders Riis Kristensen, Amal El-Naggar, Paul M. Grandgenett, Jean L. Grem, Michael A. Hollingsworth, Peter J. Holst, Thor Theander, Poul H. Sorensen, **Mads Daugaard**, Ali Salanti. *Oncofetal Chondroitin Sulfate Glycosaminoglycans Are Key Players in Integrin Signaling and Tumor Cell Motility*. **Mol Cancer Res; 14(12); 1–12. 2016 AACR.**

Books or other non-periodical, one-time publications
Nothing to report.

Other publications, conference papers, and presentations
2015 The 10th Tuscany Retreat on Cancer Research. Tuscany, Italy. August 6, 2015. Invited speaker: Dr. Mads Daugaard. Title: Glycosaminoglycans are novel cancer targets
2015 Canadian Cancer Research Conference 2015. Montreal, Quebec, Canada. November 9, 2015. Invited speaker: Dr. Mads Daugaard. Title: Targeting glycosaminoglycans via recombinant malaria proteins
2016 BCCA research seminar series. January 11, 2016. Invited speaker: Dr. Mads Daugaard
Title: Targeting glycosaminoglycans via recombinant malaria proteins
2016 Beatson Institute, Glasgow, Scotland, UK. June 28, 2016. Invited speaker: Dr. Mads Daugaard. Title: Targeting post-translational glycan modifications in cancer
2016 Gordon Conference on Cell Death, Girona, Spain. July 4, 2016. Speaker: Mads Daugaard
Title: Targeting post-translational glycan modifications in cancer

Website(s) or other Internet site(s)
Nothing to report.

Technologies or techniques
We have established a technique for realtime label-free kinetics measurements in primary tissue.

Inventions, patent applications, and/or licenses
The research builds upon patents that we submitted prior to the initiation of the grant.

Other Products
Nothing to report.

7. PARTICIPANTS & OTHER COLLABORATING ORGANIZATIONS

What individuals have worked on the project?

Name:	Mads Daugaard (UBC)
Person months:	6
Role:	PI
Support:	DoD, UBC, PCC

Name:	Ali Salanti (UCPH)
Person months:	6
Role:	PI
Support:	DoD, UCPH, ERC

Name:	Reza Safaee (UBC)
Person months:	4
Role:	Post doc
Support:	DoD, UBC,

Name:	Elham Alijazaeri (UCPH)
Person months:	12
Role:	Lab tech
Support:	DoD, UCPH,

Name:	Dulguun Battsogt (UBC)
Person months:	12
Role:	Research Assistant
Support:	DoD, PCC

Name:	Adam Sander (UCPH)
Person months:	3
Role:	Post doc
Support:	DoD, UCPH,

Has there been a change in the active other support of the PD/PI(s) or senior/key personnel since the last reporting period?

Nothing to report.

What other organizations were involved as partners?

Nothing to report.

8. SPECIAL REPORTING REQUIREMENTS

COLLABORATIVE AWARDS

The report covers all work performed at University of British Columbia and University of Copenhagen under the partnering PI mechanism.

QUAD CHARTS

Nothing to report.

9. APPENDICES

Attached are two articles describing the data presented in this report. Figure references in report text point to figures in these articles as indicated.

1 Salanti, A. *et al.* Targeting Human Cancer by a Glycosaminoglycan Binding Malaria Protein. *Cancer Cell* 28, 500-514, doi:10.1016/j.ccell.2015.09.003 (2015).

2 Clausen, T. M. *et al.* Real-time and label free determination of ligand binding-kinetics to primary cancer tissue specimens; a novel tool for the assessment of biomarker targeting. *Sens Biosensing Res* 9, 23-30, doi:10.1016/j.sbsr.2016.05.003 (2016).

3 Clausen, T. M. *et al.* Oncofetal Chondroitin Sulfate Glycosaminoglycans are Key Players in Integrin Signaling and Tumor Cell Motility. *Molecular cancer research : MCR*, doi:10.1158/1541-7786.MCR-16-0103 (2016).

Article

Cancer Cell

Targeting Human Cancer by a Glycosaminoglycan Binding Malaria Protein

Graphical Abstract

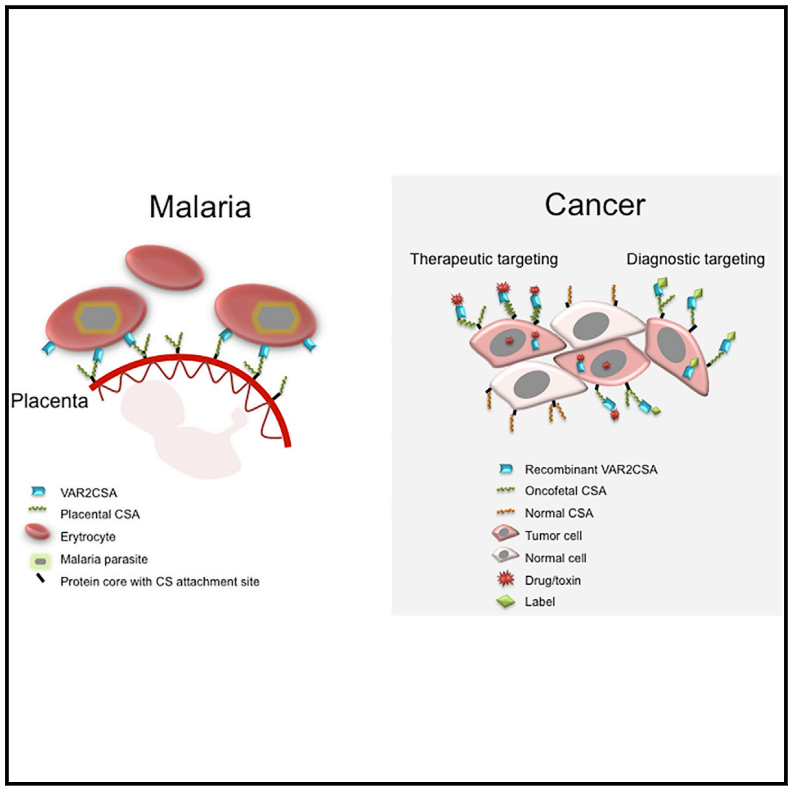

Authors

Ali Salanti, Thomas M. Clausen, Mette Ø. Agerbæk, ..., Thor G. Theander, Poul H. Sorensen, Mads Daugaard

Correspondence

salanti@sund.ku.dk (A.S.), mads.daugaard@ubc.ca (M.D.)

In Brief

The malarial protein VAR2CSA binds a placenta-specific chondroitin sulfate (CS). Salanti et al. show that the same CS is present in high fractions of cancer cells of many cancer types and that recombinant VAR2CSA conjugated with therapeutics strongly inhibit in vivo tumor growth.

Highlights

- The placenta and cancer express a similar type of oncofetal chondroitin sulfate
- Oncofetal chondroitin sulfate is displayed on proteoglycans in cancer
- Recombinant VAR2CSA proteins detect oncofetal chondroitin modifications
- Human cancer can be broadly targeted by malarial VAR2CSA drug conjugates in vivo

Salanti et al., 2015, Cancer Cell *28*, 500–514
October 12, 2015
http://dx.doi.org/10.1016/j.ccell.2015.09.003

CellPress

CellPress

Cancer Cell
Article

Targeting Human Cancer by a Glycosaminoglycan Binding Malaria Protein

Ali Salanti,[1,2,17,*] Thomas M. Clausen,[1,2,3,4,5,17] Mette Ø. Agerbæk,[1,2,3,4] Nader Al Nakouzi,[3,4] Madeleine Dahlbäck,[1,2] Htoo Z. Oo,[3,4] Sherry Lee,[3] Tobias Gustavsson,[1,2] Jamie R. Rich,[6,7] Bradley J. Hedberg,[6,7] Yang Mao,[8] Line Barington,[1,2] Marina A. Pereira,[1,2] Janine LoBello,[9] Makoto Endo,[10,11,12,13] Ladan Fazli,[3] Jo Soden,[14] Chris K. Wang,[3] Adam F. Sander,[1,2] Robert Dagil,[1,2] Susan Thrane,[1,2] Peter J. Holst,[1,2] Le Meng,[8] Francesco Favero,[15] Glen J. Weiss,[9,16] Morten A. Nielsen,[1,2] Jim Freeth,[14] Torsten O. Nielsen,[10,11] Joseph Zaia,[8] Nhan L. Tran,[9] Jeff Trent,[9] John S. Babcook,[6,7] Thor G. Theander,[1,2] Poul H. Sorensen,[5,18] and Mads Daugaard[3,4,18,*]

[1]Department of Immunology and Microbiology, Centre for Medical Parasitology, University of Copenhagen, 1014 Copenhagen, Denmark
[2]Department of Infectious Diseases, Copenhagen University Hospital, 2100 Copenhagen, Denmark
[3]Vancouver Prostate Centre, Vancouver, BC V6H 3Z6, Canada
[4]Department of Urologic Sciences, University of British Columbia, Vancouver, BC V5Z 1M9, Canada
[5]Department of Molecular Oncology, British Columbia Cancer Research Centre, Vancouver, BC V5Z 1L3, Canada
[6]Kairos Therapeutics, Inc., Vancouver, BC V6T 1Z3, Canada
[7]Centre for Drug Research and Development, Vancouver, BC V6T 1Z3, Canada
[8]Department of Biochemistry, Boston University School of Medicine, Boston, MA 02118, USA
[9]Translational Genomics Research Institute (TGen), Phoenix, AZ 85004, USA
[10]Genetic Pathology Evaluation Centre, University of British Columbia, Vancouver, BC V6H 3Z6, Canada
[11]Department of Pathology and Laboratory Medicine, University of British Columbia, Vancouver, BC V6T 2B5, Canada
[12]Department of Anatomic Pathology, Kyushu University, Fukuoka 812-8582, Japan
[13]Department of Orthopaedic Surgery, Kyushu University, Fukuoka 819-0395, Japan
[14]Retrogenix Ltd., Crown House, Bingswood Estate, Whaley Bridge, High Peak SK23 7LY, UK
[15]Centre for Biological Sequence Analysis, Technical University of Denmark, Lyngby 2800, Denmark
[16]Cancer Treatment Centers of America, Goodyear, AZ 85338, USA
[17]Co-first author
[18]Co-senior author
*Correspondence: salanti@sund.ku.dk (A.S.), mads.daugaard@ubc.ca (M.D.)
http://dx.doi.org/10.1016/j.ccell.2015.09.003

SUMMARY

Plasmodium falciparum engineer infected erythrocytes to present the malarial protein, VAR2CSA, which binds a distinct type chondroitin sulfate (CS) exclusively expressed in the placenta. Here, we show that the same CS modification is present on a high proportion of malignant cells and that it can be specifically targeted by recombinant VAR2CSA (rVAR2). In tumors, placental-like CS chains are linked to a limited repertoire of cancer-associated proteoglycans including CD44 and CSPG4. The rVAR2 protein localizes to tumors in vivo and rVAR2 fused to diphtheria toxin or conjugated to hemiasterlin compounds strongly inhibits in vivo tumor cell growth and metastasis. Our data demonstrate how an evolutionarily refined parasite-derived protein can be exploited to target a common, but complex, malignancy-associated glycosaminoglycan modification.

INTRODUCTION

When the malaria parasite, *Plasmodium falciparum,* replicates within infected erythrocytes, the latter become susceptible to clearance through the spleen. To avoid host clearance, the parasite expresses adhesion proteins on the surface of infected erythrocytes, which effectively anchor these cells to specific receptors in the host vasculature (Baruch et al., 1995). The anchor protein, VAR2CSA, mediates binding of infected erythrocytes to placental syncytiotrophoblasts (Salanti et al., 2003, 2004). This is

Significance

For decades researchers have sought to identify characteristics shared between placental or fetal development and cancer. This is based on the hypothesis that cancer cells, as part of their return to a less differentiated state, re-express genes involved in rapid growth and invasion during tissue development to facilitate cellular transformation and tumor progression. Using a specific placental glycan-binding malaria protein, we demonstrate that placental-like glycans are widely expressed in human tumors, with absent-to-low expression in normal tissues other than placenta. Furthermore, by conjugation of cytotoxic compounds to this protein, we demonstrate its capacity to specifically target cancer cells and block tumor growth in vivo.

the key event underlying placental malaria pathogenesis. In the placenta, VAR2CSA binds a distinct type of chondroitin sulfate (CS) glycosaminoglycan (GAG) chain called CS A (CSA) (Fried and Duffy, 1996). The minimal CS binding region of VAR2CSA consists of the Duffy Binding Ligand-like (DBL) 2X domain with flanking interdomain (ID) regions. This domain binds CS with remarkably high specificity and affinity (K_D ~15 nM) (Clausen et al., 2012; Dahlbäck et al., 2011).

CS is comprised of long linear polymers of repeated N-acetyl-D-galactosamine (GalNAc) and glucuronic acid (GluA) residues. These are present as modifications to proteoglycans (CSPGs) in the extracellular matrix (ECM) and in the cell plasma membrane. CSA chains are characterized by the presence of 4-*O*-sulfations (C4S) on the majority of the GalNAc residues of a given CS chain. Individual CSA chains show considerable variability with respect to the number of sulfated GalNAc residues, the density of sulfation modifications along the chain, as well as the chain length (Gama et al., 2006; Igarashi et al., 2013). *P. falciparum*-infected erythrocytes have been reported to bind CS oligosaccharides with 4-*O*-sulfated character (Alkhalil et al., 2000; Beeson et al., 2007). VAR2CSA expressing parasites only adhere in the placenta and do not bind to CS expressed elsewhere in the body (Fried and Duffy, 1996; Salanti et al., 2004). This suggests that placental CS, although incompletely resolved, is a distinct CS subtype expressed exclusively in the placenta. The function of placental-like CS (pl-CS) chains is not fully understood, but they are associated with the ability of trophoblasts to invade the uterine tissue and promote rapid cell proliferation as part of the normal placental implantation process (Baston-Büst et al., 2010). As proliferation and invasion are features shared with tumor cells, we hypothesized that placenta and cancer might express a similar type of CS. We explored the feasibility of using recombinant produced VAR2CSA proteins to target human cancer cells.

RESULTS

Recombinant Malarial VAR2CSA Detects a Distinct Placental-type CS

To examine the interaction between *P. falciparum*-infected erythrocytes and CS in the placenta, we developed an immunohistochemistry assay relying on the interaction between V5-tagged recombinant VAR2CSA (rVAR2) or control protein (rContr) (Figure 1A) and human tissue specimens. The rVAR2 protein efficiently bound both human and murine placental tissue, producing a grid-like staining pattern characteristic of plasma membrane binding, with no staining detected in normal tonsil control tissue (Figures 1B and S1A). Binding to placental tissues was completely inhibited by competition with purified CSA or by enzymatic removal of CS chains using chondroitinase AC, indicating that rVAR2 detects only pl-CS (Figure 1B). The majority of pl-CS was detected in the syncytiotrophoblast layer (Figure 1C, red arrows), with some staining in the underlying stromal cell compartment (Figures 1B and 1C). Staining with anti-C4S (2B6) revealed that CSA is abundant in most tissues despite the lack of rVAR2 staining. This confirms the tissue specificity of pl-CS (Figures 1D, S1B, and S1C). To evaluate the specific expression of pl-CS in other human tissues, we analyzed 20 different normal tissue types for their ability to bind rVAR2. While all tissues analyzed (other than placenta) displayed minimal to absent rVAR2 staining (Figure 1E), some tissues exhibited weak focal stromal staining not associated with cellular plasma membranes (Figure S1D). The choriocarcinoma cell line BeWo has been extensively used as a model for villous trophoblast function (Orendi et al., 2011). As expected, *P. falciparum*-infected human erythrocytes expressing VAR2CSA efficiently adhered to BeWo cells (Figure 1F, red arrows). Moreover, rVAR2 displayed strong binding to BeWo cells as measured by flow cytometry (Figure 1G), while primary endothelial, mesothelial, and embryonic kidney cells displayed low to absent binding of rVAR2 even at high concentrations (200 nM) (Figure 1H). Thus, in line with the fact that *P. falciparum*-infected VAR2CSA-expressing erythrocytes only sequester to the placenta, these data demonstrate that rVAR2 detects a distinct form of pl-CS expressed exclusively in the placenta and not on other normal cells or tissues.

pl-CS Is Expressed on Most Human Cancer Cells

The CSPG component of the placenta has been associated with the ability of the placental cells to maintain high proliferation rates and the capacity of the villous trophoblasts to invade into uterine tissue during implantation (Baston-Büst et al., 2010; Van Sinderen et al., 2013). Invasion and enhanced proliferation are phenotypes shared with cancer cells. We therefore hypothesized that the placental- and malignant compartments display a common CS signature that binds malarial VAR2CSA. Accordingly, we first showed that VAR2CSA expressing *P. falciparum*-infected erythrocytes displayed binding to human cancer cell lines in vitro, while no binding was observed to normal primary cells (Figure 2A). We next tested binding of rVAR2 to cancer cell lines and found that rVAR2 reacted with 95% (106/111) of patient-derived human cancer cell lines of hematopoietic, epithelial, and mesenchymal origin (Figures 2B–2E; Table S1). The interaction was rVAR2-concentration dependent and could be blocked by competition with soluble CSA (Figures 2B–2E and S2A). Furthermore, the affinity of rVAR2 binding to C32 melanoma cells was high and occurred with a K_D-value of 13 nM (Figure 2F). Also, VAR2CSA expressing *P. falciparum*-infected erythrocytes adhered to C32 cells and this interaction could be completely blocked by purified CSA (Figure 2G).

We next determined the specificity of the rVAR2-CSA interaction using ELISA as well as a flow cytometry-based competition assay on C32 cells. While all batches of rVAR2 (rVAR2-1, 2, and 3) efficiently bound immobilized CSPG molecules, no binding was observed to heparin sulfate PG (HSPG) or BSA as measured by ELISA (Figure S2B). Furthermore, pre-treating C32 cells with chondroitinase ABC reduced the rVAR2 binding to background levels (rContr) (Figures 2H–2J). The rVAR2-C32 interaction was also inhibited by purified free CSA in a dose-dependent manner (Figure 2H), whereas competition with the structurally similar 6-*O*-sulfated CS C (CSC) (Figure 2I) or highly charged heparan sulfate (HS) (Figure 2J) had limited effect on rVAR2 binding. Furthermore, while rVAR2 bound to the HS deficient CHO-pgsD-677, no binding was observed to CHO-S745A cells that have been selected for low xylosyltransferase activity and therefore low overall GAG content (Esko et al., 1985) (Figures S2C–S2E). Thus, human cancer and placental trophoblast cells express a common

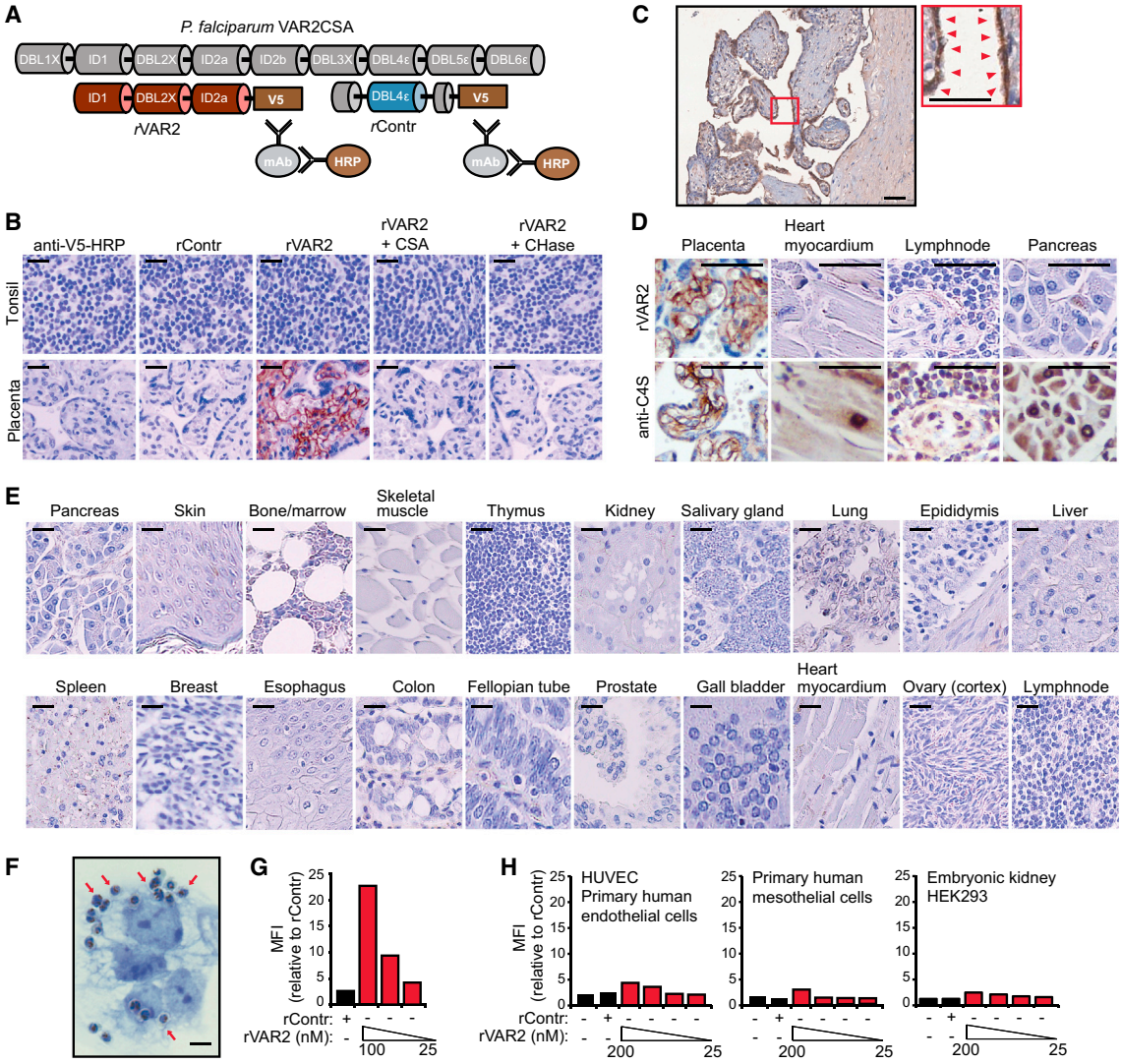

Figure 1. rVAR2 Detects a Distinct CS Modification in Human Placenta

(A) Schematic illustration of full-length *P. falciparum* VAR2CSA (gray), recombinant minimal CS-binding region (red), and recombinant non-CS binding region rContr (blue). The antibodies toward the C-terminal V5 tag are used to detect rVAR2.

(B) Representative images of indicated tissue specimens incubated with anti-V5 + anti-mouse-HRP alone (anti-V5-HRP) or in combination with recombinant rContr or rVAR2 with or without chondroitinase ABC (CHase ABC) or purified CSA. The scale bar represents 20 μm.

(C) Human placenta tissue stained as in (B), red arrows indicate pl-CS on the syncytium. The scale bars represent 10 μm.

(D) The denoted tissues stained for total CSA using enzymatic GAG end-processing and anti-C4S (2B6) antibody or for CS detected by rVAR2 as in (B). The scale bar represents 10 μm.

(E) A selection of 20 normal tissues stained as in (B). The scale bar represents 20 μm.

(F) Representative image of *P. falciparum*-infected, VAR2CSA-expressing erythrocytes bound to the plasma membrane (red arrows) of trophoblastic BeWo cells. The scale bar represents 1 μm.

(G) Relative mean fluorescence intensity (MFI) of trophoblastic BeWo cells incubated with recombinant rContr or rVAR2 as indicated and detected by flow cytometry using anti-V5-FITC.

(H) HUVECs, human primary mesothelial cells, and human embryonic kidney cells (HEK293) analyzed as in (G).

See also Figure S1.

and distinct form of CS, which can be specifically recognized by recombinant malarial VAR2CSA.

De novo CSA synthesis involves several enzymes (Sugahara et al., 2003). While B3GAT1 is required for synthesis of the basal GlcA-Gal-Gal-Xyl-Ser linker tetrasaccharide common to all GAGs, CSGALNACT1 commits the GAG to the CS pathway. Within the CS maturation pathway, CHST11 mediates CSA-specific 4-*O*-sulfation of the GalNAc residues of the CS chain (Figure 2K). Furthermore, the sulfation level of CSA is balanced by the 4-*O*-sulfatase ARSB, which removes C4S from the CSA chains (Litjens et al., 1989). RNAi-mediated knock down of B3GAT1, CSGALNACT1, and CHST11 expression inhibited the

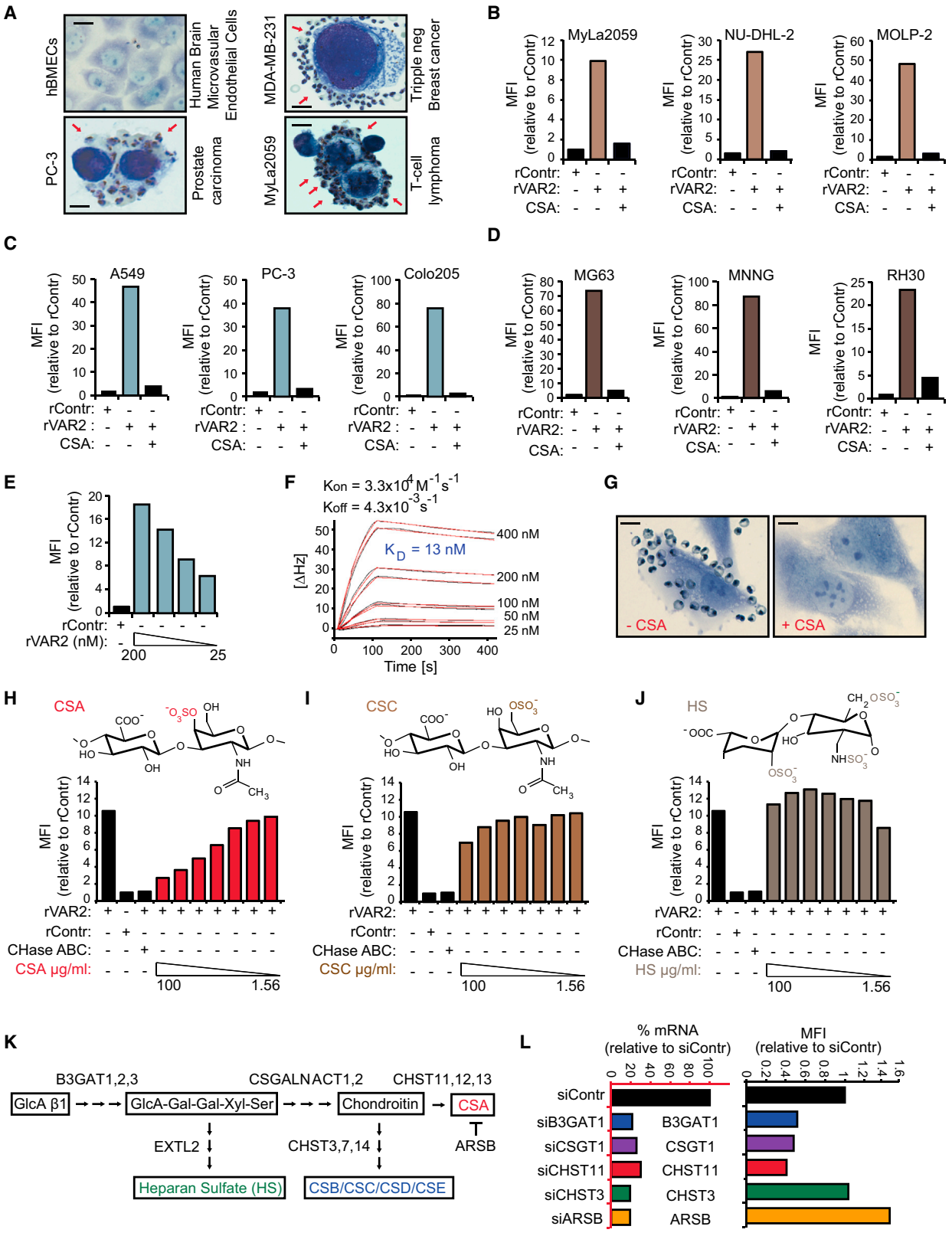

Figure 2. rVAR2 Detects pl-CS on Cancer Cells

(A) Representative images of indicated normal primary cells (hBMECs) and tumor cells (PC-3, MDA-MB-231, and MyLa2059) with adherence *P. falciparum*-infected, VAR2CSA-expressing human erythrocytes (red arrows). The scale bar represents 1 μm.

(legend continued on next page)

binding of rVAR2 to U2OS cells, while knock down of CHST3, an enzyme involved in 6-*O*-GalNAc sulfation, had no effect on binding (Figure 2L). Knock down of ARSB increased the binding of rVAR2 (Figure 2L), indicating that 4-*O*-sulfated CS residues constitute an important component of the pl-CS GAG chain.

To confirm the clinical relevance of CS expression, we analyzed available expression data from lung cancer patients linked to therapeutic outcome for expression of the key enzymes involved in CSA synthesis (B3GAT1, CSGALNACT1, and CHST11). While the expression pattern of enzymes required for synthesis of the CS GAG backbone (B3GAT1 and CSGALNACT1) had no predictive value in lung cancer, high expression of the enzyme specifically required for CSA 4-*O*-sulfation (CHST11) significantly correlated with poor relapse-free survival in three independent lung cancer cohorts (Figure S2F). The same pattern was observed for breast and colon cancer (Figure S2F). Together, these data indicate that major human cancers induce expression of a CS chain, which likely consists predominantly of GalNAc residues.

pl-CS Is Widely Expressed in Primary Human Cancer

To extend these findings to human tumor specimens, we examined a panel of human epithelial tumors for rVAR2 binding as compared to adjacent normal tissue from the same patients, using the same methods as in Figures 1B–1E. Although differences in pl-CS staining intensity were observed among the different subtypes and tumor stages, all tumors displayed strong rVAR2 binding and only weak staining in matched normal tissue (Figure 3A). The staining pattern indicates that pl-CS may be expressed on both epithelial tumor cells and tumor-associated stromal cells. Binding of rVAR2 to primary human tumors could be completely inhibited by competing with soluble CSA chains or by enzymatic removal of CS from the tissue (Figure 3B). Moreover, pl-CS was not restricted to epithelial tumors, as rVAR2 also strongly reacted with mesenchymal soft-tissue and bone sarcomas (Figure 3C).

We then analyzed 676 malignant tumors from patients with localized stage I–III invasive ductal breast carcinoma (n = 124), stage IIb bone sarcomas (n = 20), and stage I–III soft-tissue sarcomas (n = 532). Ranking the staining-intensity on a 0–3 scale (where 2 equals the staining intensity of the placenta) revealed that ~90% of the breast tumors, ~80% of the bone sarcomas, and ~85% of soft-tissue sarcoma specimens studied showed positive staining for pl-CS on the plasma membrane or in the tumor stroma (Figures 3D, S3A, and S3B). Of all the sarcoma subtypes investigated, only Ewing sarcomas showed weak or absent binding of rVAR2 in the majority of cases (Figure 3D). To investigate whether the weak binding of rVAR2 to Ewing sarcomas was due to a general lack of CS chains or a specific lack of pl-CS, we analyzed a tissue microarray (TMA) of 47 Ewing sarcoma specimens in triplicates from adult and pediatric patients. The TMA was subjected to staining with three different CS reagents, rVAR2, 2B6 (binding C4S following Chondroitinase ABC treatment), and CS56 (binding C4S and C6S) (Figures S3C–S3E). This analysis showed that 80.6% of all Ewing sarcoma cases were positive for at least one of the three reagents, while rVAR2 stained ~39% of the Ewing specimens (Figure S3F). These data suggest that Ewing sarcomas display a broad selection of CS chains, but only a fraction of these are placental-type CS that can be bound by rVAR2. Moreover, while many low-risk mesenchymal neoplasms (including lipoma, fibromatosis, neurofibroma, Schwannoma, and pigmented villonodular synovitis) displayed absent or low-to-moderate staining for pl-CS, the majority of malignant lesions showed strong staining (Figure S3G).

With a tool to broadly target pl-CS chains in primary human cancer, we next analyzed whether this malignancy-associated CS alteration was linked to progression or outcome of malignant disease. We analyzed an available melanoma progression TMA (n = 159) for expression of pl-CS. While the majority of benign nevi displayed an absent or low pl-CS expression, the presence of pl-CS in the tumor microenvironment increased significantly in Clark 2–5 staged melanoma ($p = 0.000056$) and in metastatic/recurrent disease ($p = 0.000058$) (Figure 3E; Table S2). These data suggest that pl-CS is a candidate marker for disease progression in melanoma. We subsequently investigated whether pl-CS detected by rVAR2 was associated with outcome in human non-small cell lung cancer. Analysis of a TMA comprised of 165 primary tumors linked to outcome demonstrated that high expression of pl-CS correlated with poor relapse-free survival of the patients ($p = 0.016$) (Figures S3H and S3I). Collectively, these data demonstrate that highly diverse human malignant tumor types originating from distinct germ layers display a common distinct pl-CS signature that predicts disease progression and outcome (summarized in Figure 3F).

Molecular Characterization and Expression of Placenta-like CS

To better define the rVAR2 binding of CS from cancer cells, we extracted GAGs from different cancer cell types followed

(B–D) Relative mean fluorescence intensity (MFI) of representative hematological (B), epithelial (C), or mesenchymal (D) lineage human cancer cell lines incubated with recombinant rContr or rVAR2 in combination with soluble CSA as indicated and detected by flow cytometry using anti-V5-FITC.

(E) C32 human melanoma cells incubated with recombinant rContr or indicated concentrations of recombinant rVAR2 analyzed as in (B).

(F) Sensorgram showing binding between recombinant VAR2CSA and immobilized C32 cells measured in delta Hertz [ΔHz] as a function of time (s) using the indicated concentrations of recombinant protein. The black lines represent data and the red lines represent fitted curves attained by a 1:1 binding model. The affinity is given as K_D values calculated from K_{on} and K_{off}.

(G) Representative images of C32 melanoma cells flushed over with *P. falciparum*-infected human erythrocytes in absence ($^-$CSA) or presence ($^+$CSA) of soluble CSA. The scale bar represents 1 μm.

(H–J) Relative mean fluorescence intensity (MFI) of C32 melanoma cells incubated with recombinant rContr or rVAR2 in combination with chondroitinase ABC (CHase ABC), soluble CSA, (H), CSC (I), or HS (J) as indicated and detected by flow cytometry using anti-V5-FITC.

(K) Schematic illustration of key enzymatic events in the CS synthesis pathway.

(L) rVAR2 binding (black bars, right) and RT-PCR readout of mRNA levels (blue bars, left) of U2OS cells transfected with control (C), B3GAT1 (B3), CSGALNACT1 (CSG), CHST11 (C11), CHST3 (C3), or ARSB (AB) siRNAs.

See also Figure S2 and Table S1.

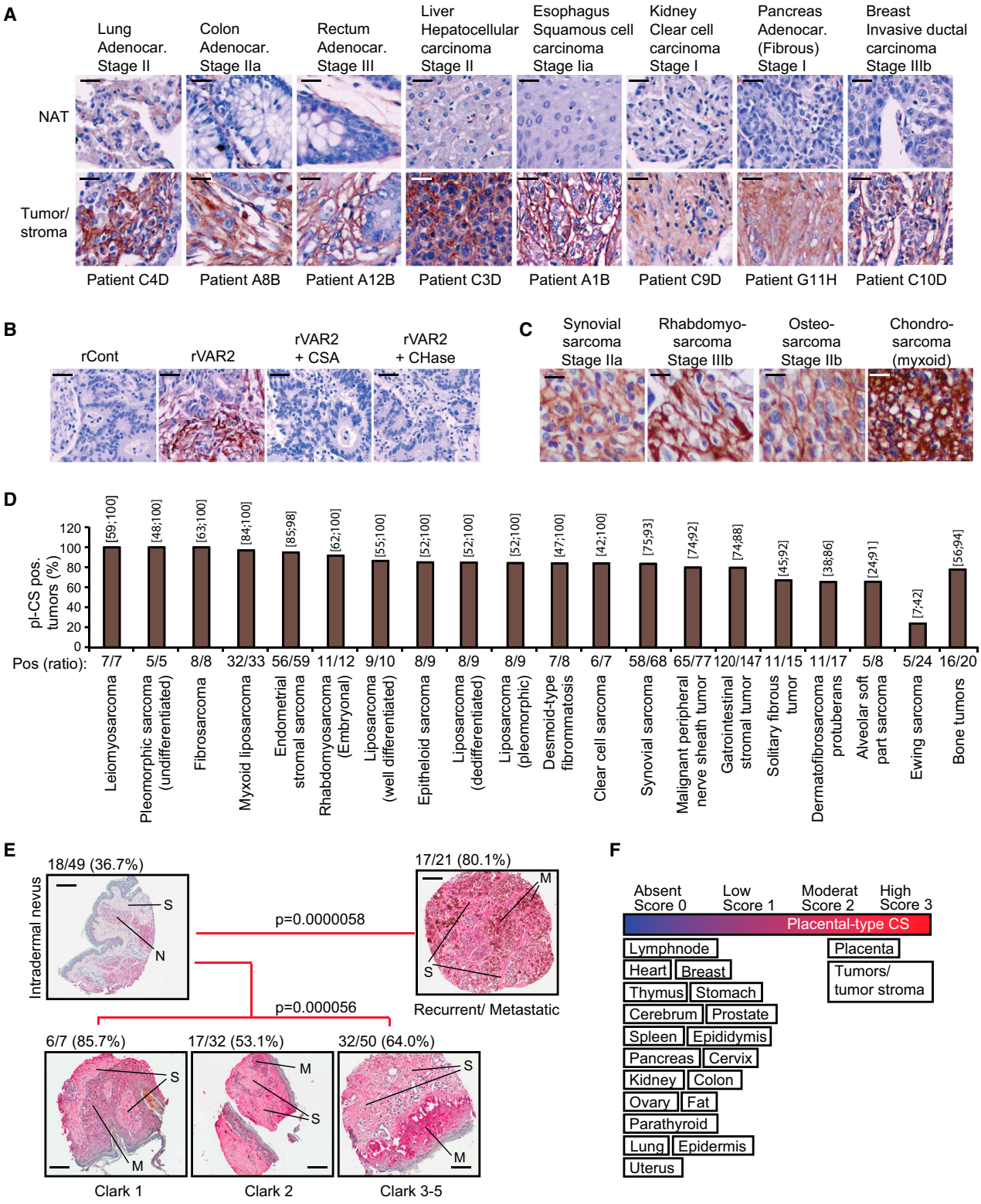

Figure 3. Diverse Types of Human Cancer Express pl-CS

(A) Representative images of indicated patient-matched primary tumor and normal adjacent tissue (NAT) specimens stained with rVAR2-V5 and detected by anti-V5-HRP. The scale bar represents 10 μm.

(B) Representative images of stage IIa breast tumors stained with rContr or rVAR2 as in (A) with or without soluble CSA or chondroitinase ABC (CHase ABC). The scale bar represents 10 μm.

(legend continued on next page)

by rVAR2 affinity purification, structural analysis using tandem mass spectrometry (tandem-MS), and affinity analysis using Attana's biosensor technology and flow cytometry. MS of GAG extracts showed that bovine trachea CSA (BT-CSA) was 10% un-sulfated and 90% mono-sulfated (no di-sulfation detected), whereas cancer-associated CS was 98% mono-sulfated (Figure 4; Table S3). Furthermore, tandem-MS revealed that BT-CSA mono-sulfated population contained 79.6% C4S and 20.4% of C6S, while CS from Myla2059 lymphoma cells contained 69.8% C4S and 30.2% C6S (Figure 4B, left). Although rVAR2 binding to cancer cells and tissue was outcompeted by BT-CSA, high amounts (100–400 μg/ml) were required to fully disrupt the rVAR2-cancer cell interaction (Figures 2B–2D). This indicated that rVAR2 only bound a fraction of the CSA chains present in the crude BT-CSA preparation. To investigate this, we affinity purified BT-CSA and MyLa2059 CS extract on an rVAR2 column (Figure 4B, right) and characterized it by MS. BT-CSA affinity purification on rVAR2 resulted in mono-sulfated CS that was enriched (90%) for C4S (Figure 4B; Table S3). Compared to bulk BT-CSA, the BT-CSA eluted from the column was considerably more effective in competitively inhibiting the binding between rVAR2 and C32 melanoma cells as measured by flow cytometry (Figure 4C), as well as the binding of rVAR2 to immobilized CSPG measured by the biosensor (Figure 4D). CS from MyLa2059 cells affinity purified on rVAR2 columns inhibited binding of rVAR2 to immobilized CSPG with an IC_{50} of 0.033 μg/ml compared to 0.063 μg/ml for placenta CS and 0.79 μg/ml for BT-CSA (Figures 4D and S4A–S4C; Table S4).

Placental cells, human melanoma cells, and some breast cancer and glioma cells have been found to express high levels of the CSA-modified proteoglycan, CSPG4 (Van Sinderen et al., 2013; Wang et al., 2010). To test whether CSPG4 carries pl-CS that can be bound by rVAR2, we analyzed co-localization and direct interaction between rVAR2 and CSPG4 on C32 melanoma cells. The rVAR2 stain co-localized with CSPG4 (Figure 4E) and specifically pulled down CS-conjugated CSPG4 from C32 melanoma cells (Figure 4F). However, rVAR2 could also bind tumor cells negative for CSPG4 expression (compare Figures 4G and 2B–2E), suggesting that pl-CS can be displayed on other CPSG protein cores. To identify these, we transfected non-malignant HEK293 cells (which do not bind rVAR2) with 3,500 different human plasma membrane proteins (Figure 4H). Following validation with CSA competition and enzymatic removal of CS chains by chondroitinase treatment, it was evident that 17 of the 3,500 proteins facilitated binding to rVAR2 (Figure 4H). Thus, in addition to CSPG4 (not included in the screen), at least 17 proteins including CD44, carbonic anhydrase IX (CA9), syndecan 1 (SDC1), or tomoregulins (TMEFF1 and -2) can carry pl-CS when overexpressed in HEK cells. Further studies are required to investigate if all of the proteoglycans can be modified with CS in vivo. Interestingly, ten of these proteins have previously been described as being conditional CS-conjugated and 15 have been directly associated with human malignant disease (Table S5). To investigate the inter-tumor diversity in expression of proteoglycans able to display pl-CS, we analyzed 1,555 primary human tumor specimens representing 17 major types of human cancers using the Bittner array (Rhodes et al., 2004) and the Riker melanoma array (Riker et al., 2008). This analysis showed that the proteoglycans associated with pl-CS were differentially, but complementarily, expressed in each of the 17 major cancer groups tested (Figures 4I and S4D). Accordingly, we validated the interaction of rVAR2 with the CS-modified form of CD44 in C32 melanoma cells (Figure 4J). Moreover, rVAR2 efficiently pulled down glycosylated CD44 from C32 melanoma protein lysates (Figure 4K). Together, these data suggest that rVAR2 can be utilized to broadly target pl-CS chains in human malignancies with different proteoglycan expression profiles.

Internalization and In Vivo Localization of rVAR2

The specific presence of a pl-CS modification in malignant tumors suggests that VAR2CSA may be utilized to deliver cytotoxic payloads directly to the tumor microenvironment. We first investigated if rVAR2 is internalized upon binding to tumor cells. Alexa488-labeled rVAR2 (rVAR2-A488) (Figure 5A) rapidly bound to human colon cancer cells (Colo205) and was efficiently internalized within 30 min (Figures 5B and 5C). Similar internalization dynamics were observed with three other cancer cell lines (Figure 5D). We then investigated if rVAR2 was able to sequester to tumors in vivo. To visualize rVAR2 tumor sequestration, we conjugated an Alexa750 near-infra red (NIR) fluorescent probe to rVAR2 (rVAR2-NIR) (Figure 5E, top). The rVAR2-NIR was administrated IV into PC-3 tumor bearing mice and a NIR signal from the tumor region was observed after 10 min in vivo and ex vivo (Figure 5E, bottom). Moreover, ex vivo analysis of fixed PC-3 xenografts confirmed strong rVAR2 reactivity in the tumors as measured by immunohistochemistry (Figure 5F). Similarly, we injected the rVAR2-NIR IV into B16-tumor bearing mice and followed the rVAR2-NIR signal for 48 hr. As in the PC3 xenograft, rVAR2 rapidly located to the tumor and the signal was detectable 48 hr after injection (Figures 5G and 5H). Together, these data suggest that rVAR2 can be utilized to facilitate intracellular delivery of cytotoxic compounds to pl-CS expressing cells in vivo.

Targeting Tumors through the rVAR2 pl-CS Signature

To test whether rVAR2 could be used as a pl-CS-specific tumor targeting system, we genetically fused the cytotoxic domain of Diphtheria toxin (DT388) to rVAR2, creating a recombinant rDT388-VAR2 (rVAR2-DT) fusion protein (Figure 6A). In vitro, the rVAR2-DT protein efficiently killed tumor cell lines of both

(C) Representative images of indicated soft-tissue and bone sarcomas stained with rContr or rVAR2 as in (A). The scale bar represents 5 μm.
(D) Column graph representation of pl-CS staining intensity in the indicated soft-tissue and bone sarcoma subtypes (n = 552) processed as in (A) and scored (0–3) for binding to recombinant VAR2CSA. The columns show the percentage and exact binomial 95% confidence interval of pl-CS positive (score 2–3) tumors.
(E) Representative images of a melanoma progression TMA stained with anti-V5-HRP in combination with recombinant rVAR2 and scored (0–3). The fraction of score 2–3 (moderate/high) pl-CS (pl-CS) positive tumors was identified and p values were generated by the Goodman-Kruskal-Gamma test (Nevus, N; Stroma, S; and Melanoma cells, M). The scale bar represents 40 μm.
(F) Schematic representation of pl-CS expression in the indicated tissue categories.
See also Figure S3 and Table S2.

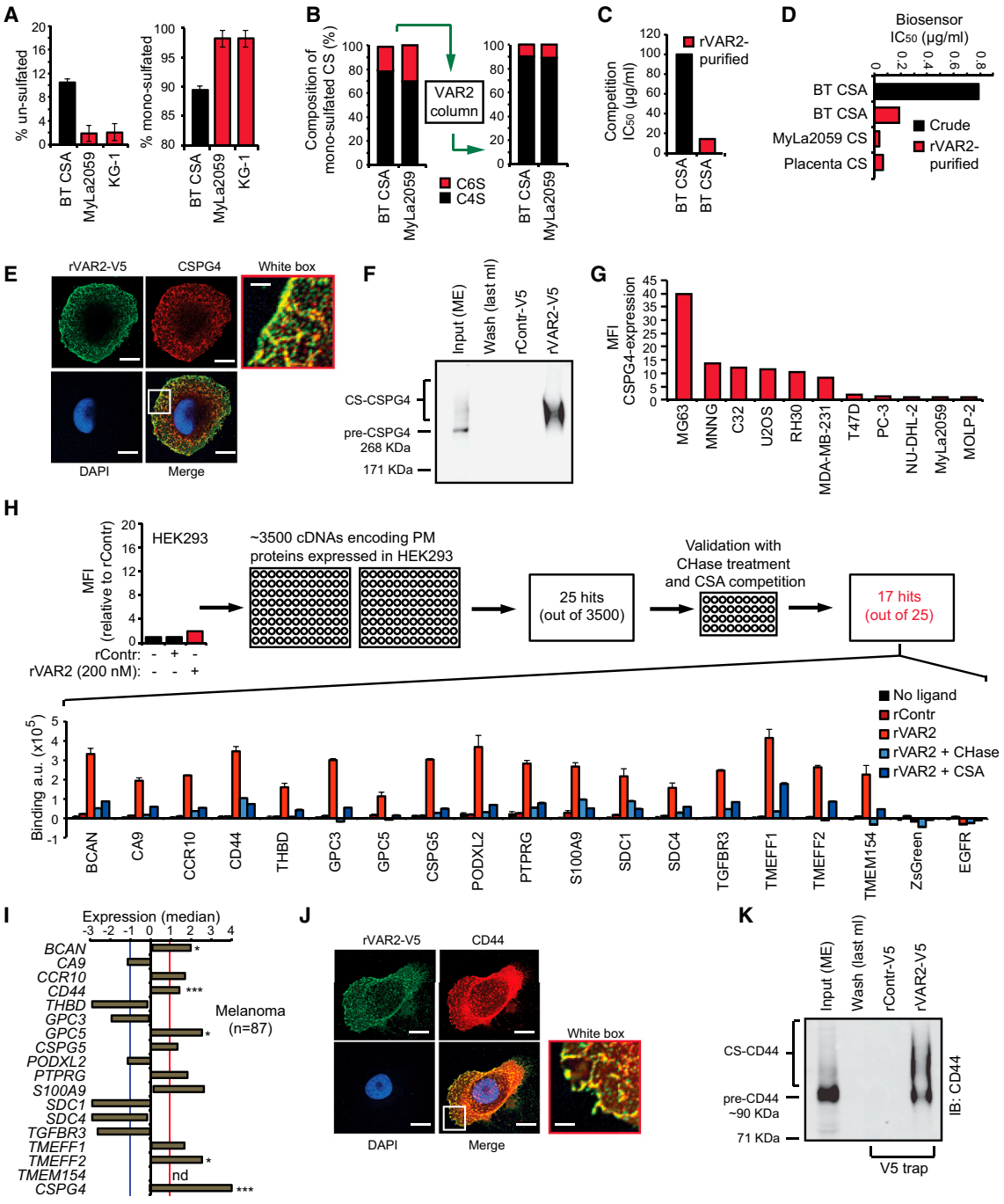

Figure 4. Defining the rVAR2 CS Epitope

(A) Level of un-sulfated (left) and mono-sulfated (right) disaccharides of extracted CS from Sigma BT-CSA, T cell lymphoma (MyLa2059), and myeloid leukemia (KG-1) determined by liquid chromatography MS analysis. The values are given as a percentage of the total CS in the sample.

(B) BT-CSA and MyLa2059 CSA were affinity purified on a custom made rVAR2 column and eluted in a NaCl gradient. The composition of the mono-sulfated CS was analyzed by tandem MS before (left) and after (right) affinity purification.

(C) Binding inhibition capacity of BT-CSA before and after rVAR2 affinity purification is shown as the concentration needed to block 50% of the binding (IC_{50} values) between rVAR2 and the cells as measured by flow cytometry.

(D) Biosensor analyses of the capacity of BT-CSA (before and after rVAR2 affinity purification) and rVAR2 affinity-purified Myla2059 and placental CS, to inhibit rVAR2 binding to immobilized CSPG. The binding inhibition is shown as the concentration needed to block 50% of the binding (IC_{50} values) between rVAR2 and the cells.

(E) Representative picture of a C32 human melanoma cell co-stained for CS using rVAR2-V5 (green) and CSPG4 (red). The co-localization was analyzed by confocal microscopy. The scale bar represents 0.5 μm.

(legend continued on next page)

epithelial and mesenchymal origin (Figures 6B and 6C) with low IC_{50} values (from 0.8 nM to 12.2 nM). The rVAR2-DT toxin had no effect on normal primary human endothelial cells (HUVEC) (Figure 6C), and competition with CSA abolished the cytotoxic effect of rVAR2-DT on cancer cells (Figure 6B). Moreover, small interfering (si)RNAs targeting C4S-sulfotransferase CHST11 or the CS backbone-conjugation enzyme CSGALNACT1 prevented the cytotoxic effects of rVAR2-DT in prostate cancer PC-3 cells (Figures 6D and 6E). These data demonstrate that the C4S conjugation machinery is required for rVAR2 to deliver a cytotoxic payload to tumor cells.

Prostate cancer is a leading cause of morbidity and death among men in the Western world, and the prognosis for advanced castration resistant prostate cancer (CRPC) is poor (Kirby et al., 2011). We therefore tested the efficacy of rVAR2-DT in a mouse tumor xenograft model based on the metastatic CRPC cell line, PC-3. As few as three doses of rVAR2-DT were able to significantly inhibit growth of PC-3 CRPC tumors in vivo (Figure 6F). We next performed independent experiments to assess the longer-term effect of three doses of rVAR2-DT on CRPC growth in vivo. The rVAR2-DT treated group was monitored for tumor growth for up to 20 days after the first dose. Similar to the first setup (Figure 6F), we observed a strong inhibition of tumor growth in the rVAR2-DT treated group (Figure 6G). Interestingly, the inhibitory effect of rVAR2-DT on tumor growth persisted 14 days after first dose (10 days after last dose), before slow re-growth of the tumor was observed (day 14, blue arrows) (Figure 6G). The PC-3 cells used in the study expressed luciferase, allowing us to monitor the impact of rVAR2-DT on PC-3 xenografts by IVIS. Scanning of the mice at day 3 and day 13 after the initial dose fully corroborated the results from Figures 6F and 6G and showed marked inhibition of chemiluminiscence within the treated group (Figure 6H). Histopathology analysis revealed dramatic differences between rVAR2-DT treated and un-treated tumors. While the vehicle control displayed intact and dense tumor architecture with little necrosis (Figure 6I), rVAR2-DT treated tumors showed massive necrosis (Figure 6J), similar to what is seen in the liver after wild-type DT delivery (Saito et al., 2001). Furthermore, rVAR2-DT treated xenografts were also positive for TUNEL staining indicative of apoptosis (Figure 6K). Examination of kidney and liver tissues from the rVAR2-DT treated animals showed normal tissue architecture and no morphologic signs of toxicity (Figures 6L and 6M). These data demonstrate that rVAR2 can facilitate efficacious CS-dependent delivery of a cytotoxic compound to CRPC tumors in vivo with no morphologic evidence of adverse effects on normal tissues.

Development and Efficacy of an rVAR2-Hemiasterlin Drug Conjugate

From the human clinical trials with DT fusions, it is apparent that high drug concentrations are not well tolerated. We therefore chemically conjugated a hemiasterlin analog (KT886) to rVAR2 via a protease cleavable linker (Figure S5), utilizing free cysteines in the recombinant protein (Figures 7A and 7B). The rVAR2-KT886 drug conjugate (VDC886) carried an average of three toxins per rVAR2 molecule (Figure 7B). ELISA, biosensor, and flow cytometry confirmed the affinity and specificity of VDC886 to pl-CS. A total of 33 cancer cell lines of different origin were tested for sensitivity to VDC886. All lines were effectively killed in vitro by the VDC886, with IC_{50} values ranging from 0.2 pM to 30 nM (Figure 7C). We performed a dose escalation study of VDC886 in healthy female CD-1 mice, increasing the dose up to 15 mg/kg. The maximum tested dose of 15 mg/kg was well tolerated, and the animals did not display any signs of morbidity or physical distress. Histopathology examination of different organs did not show any evidence of adverse cytotoxic effects (Figure 7D). Importantly, the pl-CS modification was present in the murine placenta (Figure S1), as well as on murine tumor cells (Figures 5D, 5G, 7H, and 7K), indicating that the absence of adverse effects was not due to lack of pl-CS expression capability in the murine system. We subsequently tested the efficacy of the VDC886 in vivo using two different human xenograft mouse models of non-Hodgkin's lymphoma (Karpas299) and prostate cancer (PC-3). VDC886 treatment significantly inhibited growth of both Karpas299 (Figure 7E) and PC-3 (Figure 7F) tumors as compared to the control groups. Remarkably, two out of six mice in the VDC886-treated PC-3 tumor group showed complete remission 32 days after the first treatment (Figure 7G). These data demonstrate that VDC886 can target diverse human tumor types in vivo. To further analyze the anti-tumor effects of pl-CS targeting in vivo, we made use of a highly aggressive syngeneic (immunocompetent) mouse model of metastatic murine breast cancer cells. 4T1 breast cancer cells were efficiently

(F) Extracted membrane proteins (Input ME) from C32 melanoma cells were subjected to an on-column pulldown on a HiTrap NHS column coupled with rVAR2-V5 or rControl-V5. The figure shows Input (ME), last 1 ml of wash of the rVAR2-V5 column, and the 0.5 M NaCl elution following concentration. The samples were analyzed for precipitation of precursor (pre-CSPG4) and CSA-conjugated CSPG4 by immunoblotting (IB:CSPG4) as indicated.

(G) Relative mean fluorescence intensity (MFI) of indicated cell lines incubated with anti-CSPG4 antibody and detected by flow cytometry.

(H) Relative mean fluorescence intensity (MFI) of HEK293 cells incubated with recombinant rContr or rVAR2 as indicated and detected by flow cytometry using anti-V5-FITC. The HEK293 cells were transfected with 3,500 cDNAs encoding known tumor-associated plasma membrane proteins inserted in a ZsGreen expression system and analyzed for their ability to facilitate binding to recombinant rVAR2 detected by anti-V5-Alexa647. The column graph displays quantified anti-V5-Alexa647 detection (arbitrary units, a.u.) in HEK293 cells transfected with the indicated plasma membrane proteins and left un-treated (no ligand), or treated with recombinant rContr, rVAR2 alone, or in combination with chondroitinase ABC (rVAR2 + CHase) or purified CSA (rVAR2 + CSA).

(I) Median expression compared to overall average of the genes encoding the 17 proteins from (H) plus CSPG4 in primary melanoma (n = 87) patient specimens extracted from the Oncomine Riken melanoma array (*$p < 0.05$ and ***$p < 0.001$) (not determined: nd) (missing probe). The red and blue cross-lines designate the threshold for up and downregulated.

(J) Representative picture of a C32 human melanoma cell co-stained for CS using rVAR2-V5 (green) and CD44 (red). The co-localization was observed by confocal microscopy. The scale bar represents 0.5 μm.

(K) Extracted membrane proteins (Input ME) from C32 melanoma cells were subjected to an on-column pulldown on a HiTrap NHS column coupled with rVAR2-V5 or rControl-V5. The figure shows Input (ME), last 1 ml of wash of the rVAR2-V5 column, and the 0.5 M NaCl elution following up-concentration. The samples were analyzed for precipitation of precursor (pre-CD44) and CS-conjugated CD44 by immunoblotting (IB:CD44) as indicated. The error bars indicate ± SD.
See also Figure S4 and Tables S3–S5.

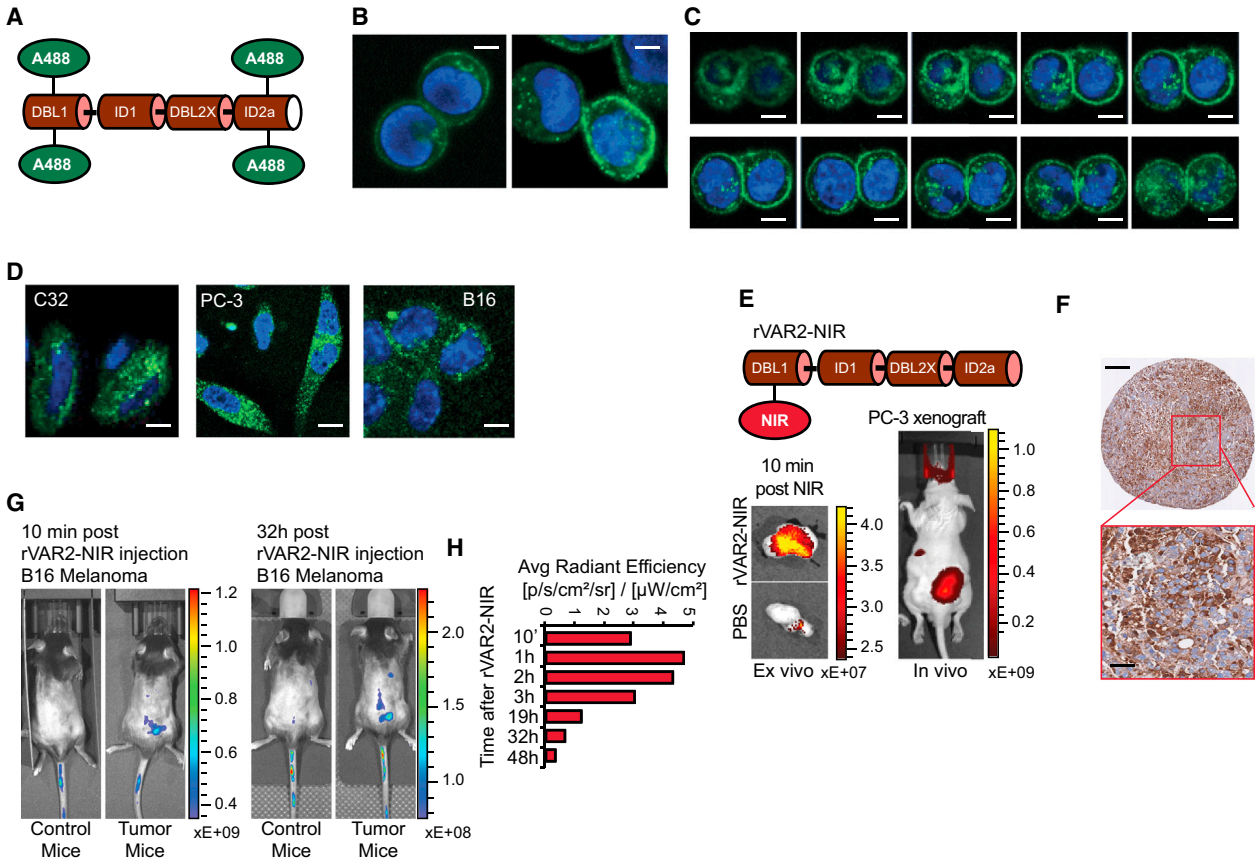

Figure 5. rVAR2 Internalization and In Vivo Tumor Localization

(A) Schematic illustration of rVAR2 conjugated with Alexa-488 (rVAR2-A488).

(B) Colo205 colon carcinoma cells analyzed by confocal microscopy 5 (left) and 30 (right) min after addition of rVAR2-FITC (green) and DAPI (blue). The scale bar represents 0.5 μm.

(C) Confocal microscopy analysis of Colo205 cells as in (B) displayed as vertical depth at 30 min after addition of rVAR2-FITC. The scale bar represents 0.5 μm.

(D) C32 melanoma, PC-3 prostate adenocarcinoma, and B16 murine melanoma cells analyzed as in (B) 30 min after addition of rVAR2-FITC. The scale bar represents 0.5 μm.

(E) Schematic illustration of rVAR2 conjugated with NIR Alexa-750 (rVAR2-NIR) probe (upper) and in vivo (right) and ex vivo (left) detection of NIR signal in PC-3 tumor xenografts 10 min post-rVAR2-NIR injection in tail vein.

(F) IHC of PC-3 tumor xenografts stained with rVAR2-V5 and detected by anti-V5-HRP. The scale bar represents 40 μm.

(G) C57BL/6 mice with no tumors (Control mice) or carrying established B16 murine melanoma tumors (Tumor mice) were injected with rVAR2-NIR in the tail vein at day 10 and scanned in an IVIS Spectrum CT scanner.

(H) Quantification of IVIS signal from a subcutaneous B16 tumor (right flank) after rVAR2-NIR injection at different time intervals from 10 min to 48 hr. The right flank signal is considered as background and is *subtracted from the initial signal*.

bound by rVAR2 in a concentration and CSA-dependent manner (Figure 7H). Moreover, VDC886 demonstrated strong cytotoxicity in 4T1 cells in vitro, which could be completely rescued by competition with soluble CSA (Figure 7I). Injection of luciferase-4T1 cells in the left ventricle of the heart of C57BL/6 mice resulted in aggressive bone metastasis with an overall penetrance of 50%–60% (Figure 7J). The bone metastases invaded into adjacent muscle and showed strong pl-CS expression as analyzed by rVAR2-based immunohistochemistry (IHC) (Figure 7K). Notably, of the mice with 4T1 bone metastases, five out of six mice in the VDC886-treated group were still alive at the end of the study (day 54) with no detectable metastases, while all control-treated mice died with metastatic disease ($p = 0.0196$; Figures 7L and 7M). Indeed, VDC886-treatment significantly increased survival of mice with 4T1 bone metastasis as compared to control-treated mice. Collectively, these data provide compelling evidence that diverse human and murine tumor types can be effectively targeted in vivo using an rVAR2 drug conjugate.

DISCUSSION

The placenta is a fast-growing organ in which cells display high mitotic rates, the ability to invade the uterine tissue, and the capacity to establish an elaborate vasculature. These are features shared with cancer, and hence researchers have for decades attempted to identify molecules shared between the placental and malignant compartments (Holtan et al., 2009). We have demonstrated that recombinant versions of the evolutionarily refined malaria protein VAR2CSA can broadly

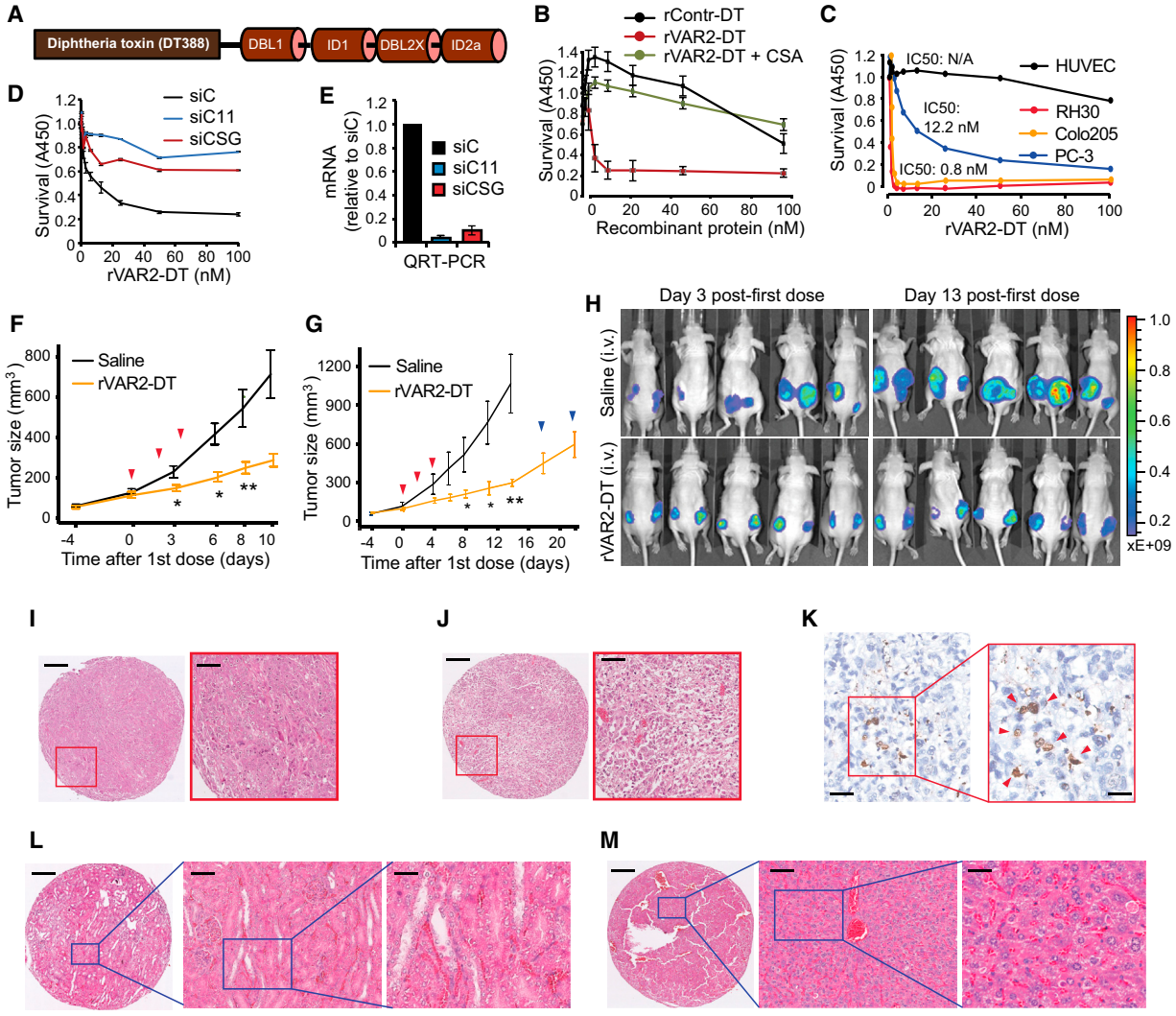

Figure 6. In Vivo Cancer Targeting Using rVAR2 Fusion Construct rVAR2-DT388

(A) Schematic figure showing the architecture of the rVAR2-DT388 fusion protein.

(B) Survival of B16 melanoma cells treated with increasing concentrations (0–100 nM) of a DT-fused (rContr-DT) or rVAR2-DT with or without CSA competition as indicated and analyzed for WST1 staining 96 hr post-treatment. The error bars indicate ± SD.

(C) Survival of indicated cell lines treated with increasing concentrations (0–100 nM) of rVAR2-DT.

(D) PC-3 cells were transfected with control siRNA (siC) or siRNAs targeting CHST11 (siC11) or CSGALNACT1 (siCSG) and treated with the indicated concentrations (0–100 nM) of rVAR2-DT for 96 hr before analyzed for survival using methylene blue staining assay. The error bars indicate ± SD.

(E) Quantitative RT-PCR of indicated mRNA levels in PC-3 cells after 72 hr post-transfection with control siRNA (siC), CSGALNACT1 siRNA (siCSG), and CHST11 siRNA (siC11). The error bars indicate ± SD.

(F and G) Quantification of tumor volume over 10 days (Experiment 1, F) and 20 days (Experiment 2, G) in Foxn1^{nu} mice xenotransplated with PC-3 cells and treated on day 0, 2, and 4 (red arrows) with either saline (black line) or 0.6 mg/kg rVAR2-DT (yellow line) (*$p < 0.05$ and **$p < 0.01$). The error bars indicate ± SEM.

(H) IVIS analysis of PC-3 tumor growth in mice (from G) on day 3 and 13 post-first dose treatment with saline or rVAR2-DT as indicated.

(I and J) Representative hematoxylin and eosin (H&E) images as indicated of PC-3 xenograft tumor after treatment with saline (I) or rVAR2-DT (J). The scale bar represents 40 μm.

(K) Representative image of PC-3 xenograft tumor stained with TUNEL reagent (in 20× and 40× magnification as indicated). The scale bar represents 10 μm (left) and 5 μm (right).

(L and M) Representative H&E images as indicated of kidney (L) and liver (M) extracted from rVAR2-DT treated mice in (G). The scale bar represents 40 μm.

detect pl-CS on trophoblastic cells as well as in human tumors.

The broad targeting potential of rVAR2 is likely facilitated by the redundant presentation of pl-CS chains on several different cancer-associated PGs such as CSPG4 and CD44. Several of the PGs that carry an rVAR2-reactive CS chain are currently being, or have been, tested as targets in clinical trials (Casucci et al., 2013; Wang et al., 2011). We propose that targeting the common CS chain present on different cancer-associated PGs may potentially offer a broad cancer targeting strategy.

Since rVAR2 is efficiently internalized into pl-CS expressing cells, rVAR2 could potentially facilitate the delivery of anti-cancer

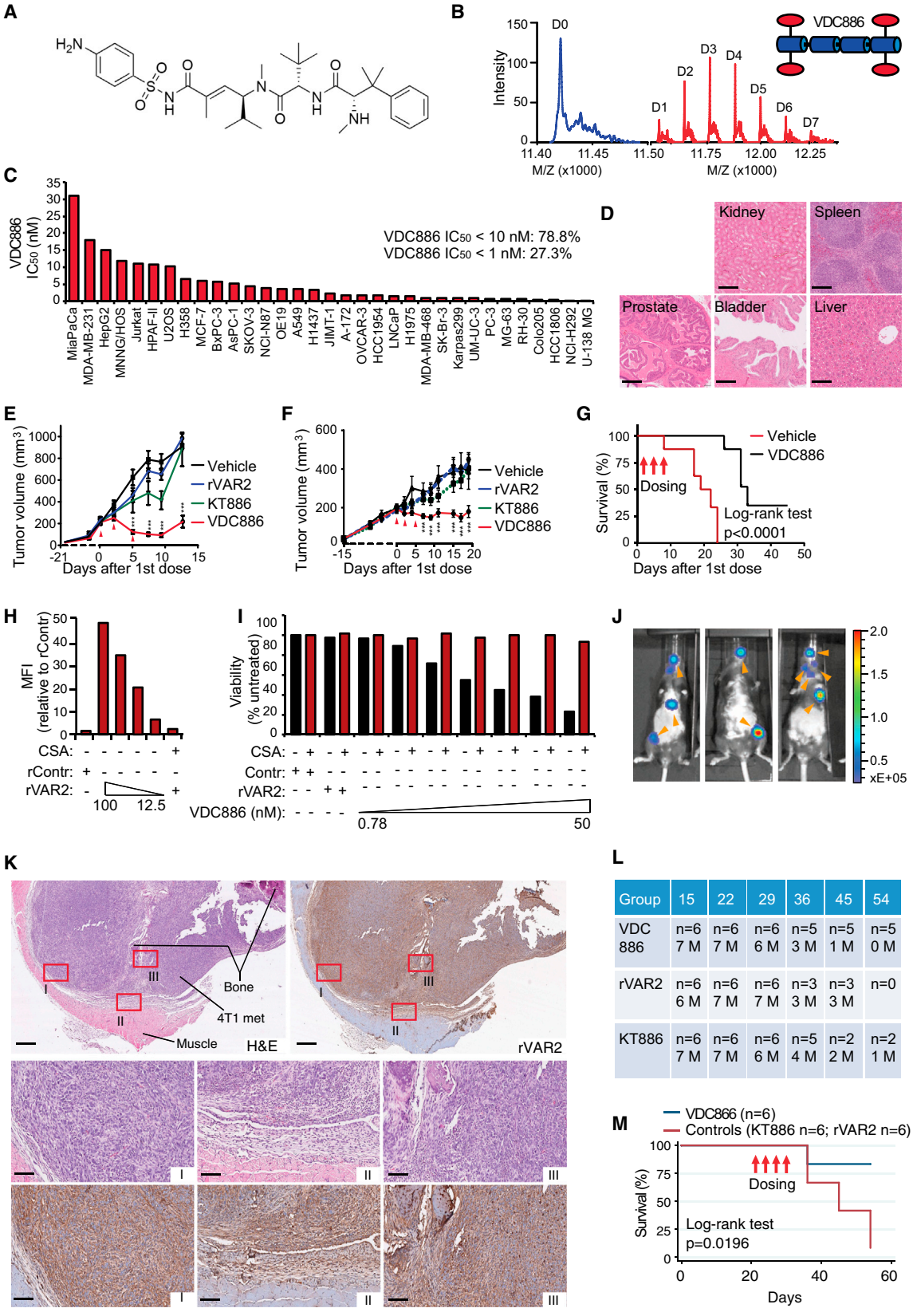

Group	15	22	29	36	45	54
VDC 886	n=6 7 M	n=6 7 M	n=6 6 M	n=5 3 M	n=5 1 M	n=5 0 M
rVAR2	n=6 6 M	n=6 7 M	n=6 7 M	n=3 3 M	n=3 3 M	n=0
KT886	n=6 7 M	n=6 7 M	n=6 6 M	n=5 4 M	n=2 2 M	n=2 1 M

(legend on next page)

compounds directly into the tumor environment. This notion was supported by our in vivo and ex vivo imaging experiments. We subsequently demonstrated the therapeutic potential of targeting pl-CS on human tumors by two different approaches. First, rVAR2 genetically fused to a part of the diphtheria toxin (rVAR2-DT), efficiently killed tumor cells in vitro and in vivo in a CS-dependent manner. Second, chemical conjugation of a hemiasterlin toxin to rVAR2 created a highly potent VDC886 that specifically targeted pl-CS on diverse tumor cells in vitro and in vivo. Notably, non-pregnant mice injected with rVAR2-DT or VDC886 showed no adverse treatment effects, suggesting that pl-CS is expressed below rVAR2–based detection levels in non-malignant tissue in mammals. This is supported by the observation that *P. falciparum*-infected erythrocytes cannot bind anywhere in vascularized tissue compartments, except in the placenta.

Our data promote pl-CS as a candidate target for broad rVAR2-based anti-cancer therapies, as well as a progression marker for selected human tumor types such as melanoma. rVAR2 provides an example of how evolutionarily refined host-pathogen anchor molecules can be conveniently exploited to access and target cancer associated glycans.

EXPERIMENTAL PROCEDURES

Reagents and Cell Culture

The recombinant proteins were expressed in SHuffle T7 Express Competent *E. coli* (NEB) and purified using HisTrap from GE Healthcare, followed by size exclusion chromatography. Purified CSA, HS, and chondroitinase ABC were obtained from Sigma. CSC was obtained from Seikagaku, and Monoclonal anti-V5 and anti-V5-FITC antibodies were obtained from Invitrogen. Cells were transfected with siRNAs (QIAGEN) (10 nM final) against B3GAT1, CSGALNACT1, CHST11, CHST3, or ARSN using RNAiMAX (Invitrogen) and analyzed for rVAR2 binding by flow cytometry and for mRNA expression by RT-PCR.

IHC

Using the Ventana Discovery platform, sectioned paraffin-embedded tissue samples were stained with 500 picomolar V5-tagged rVAR2 without antigen retrieval, followed by 1:700 monoclonal anti-V5 step and a anti-mouse-HRP detection step. For a detailed description, please see Supplemental Information.

Flow Cytometry

Cells were grown to 70%–80% confluency in appropriate growth media and harvested in an EDTA detachment solution (Cellstripper). Cells were incubated with protein (200–25 nM) in PBS containing 2% fetal bovine serum (FBS) for 30 min at 4°C and binding was analyzed in a FACSCalibur (BD Biosciences) after a secondary incubation with an anti-V5-FITC antibody. For inhibition studies, protein was co-incubated with indicated concentration of GAGs (CSA, CSC, and HS).

Binding Kinetics Analysis

A quartz crystal microbalance biosensor (Attana Cell A200, Attana AB) was used for the kinetic analyses. Cells were seeded onto cell compatible sensor chips and incubated 24 hr at 37°C. Cells were then fixed in 3.7% formaldehyde and visualized using DAPI. The data, including k_{on}, k_{off}, and the calculated K_D, were presented as sensorgrams showing VAR2CSA fragments binding to cells as response (in Hertz) as a function of time (s). Curve fitting was performed in the Attache evaluation software (Attana AB).

Immunocytochemistry

Internalization Assay

rVAR2 protein was conjugated with the Alexa488 fluorophore according to the manufacturer's instructions. C32 cells were seeded to coverslips and grown to 60% confluency. There were 200 nM rVAR2-488 that were incubated with the cells for 1 hr at 4°C and then washed once to allow internalization of only surface-bound protein at either 10 min or 60 min at 37°C. Cells were subsequently washed with PBS prior to fixation with 4% paraformaldehylde for 15 min at room temperature. Coverslips were mounted in mounting media containing DAPI and analyzed by laser-scanning confocal microscopy.

Co-localization

C32 melanoma cells were grown on glass cover slides. Cells were fixed in 4% paraformaldehyde (PFA), blocked in 1% BSA/ 5% FBS, and stained for CS

Figure 7. In Vivo Cancer Targeting Using VDC886

(A) Structure of the hemiasterlin analog KT886.

(B) MS readout confirming KT886 loading on rVAR2 through a toxin-linker functionalized with a maleimide group to enable conjugation to protein-thiols. The D0 (blue) represents un-conjugated rVAR2 and D1-7 (red) designates the number of KT886 loaded. The VDC886 carries 3.5 KT886 toxins on average.

(C) Indicated human cancer cell lines were seeded in 96-well plates and treated with VDC886 in concentrations ranging from 0.01 pM to 1 μM. The column graph displays IC_{50} kill-values of VDC886 performance.

(D) Representative H&E images as indicated of kidney, spleen, prostate, bladder, and liver extracted from mice subjected to three doses of VDC886 on alternating days (15 mg/kg). The scale bar represents 10 μm.

(E) Female C.B-17/IcrHsd-Prkdc scid mice engrafted with Karpas299 non-Hodgkin's lymphoma cells on the back were treated with 1× PBS (vehicle), naked rVAR2 (rVAR2), KT886 alone (KT886), or VDC886. The treatments were administered intravenously on day 0, 2, and 5 (red arrows) as indicated.

(F) Male Foxn1^{nu} mice were implanted subcutaneously on the back with the PC3 prostate cancer cell line in 100 μl of Matrigel (in both right and left flanks). The test articles, as in (E), were administered intravenously on day 0, 2, and 5 (red arrows) as indicated. The animals remained on study until their combined tumor burden reached 1,000 mm^3 in size or they otherwise required euthanasia due to distress (humane endpoint).

(G) Kaplan-Meier curve of Vehicle and VDC886 treated mice from (F). There were two of the six mice on study in the VDC886 treated group that had complete re-mission of disease (***$p < 0.001$).

(H) 4T1 murine breast cancer cells were analyzed by flow cytometry for binding to the indicated concentrations of rVAR2 or 100 nM rContr in the absence or presence of soluble CSA.

(I) The indicated concentration range of VDC886 was tested on 4T1 murine mammary cancer cells in the absence or presence of soluble CSA as indicated.

(J) Detection of bone metastasis detectable by IVIS (orange arrows) in C57BL/6 mice 2–3 weeks after injected with luciferase-expressing 4T1 cells from (H) and (I) in the left ventricle of the heart.

(K) Extracted bone metastasis from (J) subjected to matched H&E staining and immunohistochemical pl-CS staining using rVAR2-V5 + anti-V5-HRP as indicated. The lower image displays the sections within red boxes (from upper). The scale bar represents 1 mm (upper) and 50 μm (lower).

(L) Mice as in (J) with bone metastasis visible in the same IVIS detection range (n = 18) were randomized into three groups with six mice per group (n = 6) and subjected to four doses of VDC886 (15 mg/kg), rVAR2 alone (rVAR2), or KT886 alone (KT886) in equivalent molar ratios to VDC886 on day 21, 24, 27, and 30. All groups were monitored on day 15, 22, 29, 36, 45, and 54 as indicated for number of mice (n) and number of visible metastasis (M).

(M) Kaplan-Meier survival plot of (L), comparing the two control groups (rVAR2 and KT886) combined with VDC886 treated mice. The mice were sacrificed when reaching their humane endpoint. The red arrows designate dosing days. The p value was calculated with Chi2 log-rank test. The error bars represent ± SEM. See also Figure S5.

using rVAR2-V5 and CSPG4 (LHM2, Abcam) or CD44 (2C5, RnD Systems) overnight at 4°C. rVAR2 was detected by anti-V5 (Rabbit) and anti-Rabbit-Alexa488. CSPG4 and CD44 antibodies were detected with anti-mouse-Alexa568. Nuclei were stained with DAPI. Slides were analyzed by laser-scanning confocal microscopy.

CS Extraction from Cancer Cells

Myla-2059 T cell lymphoma and KG-1 leukemia cells were grown to 1 × 10^6 cells/ml in supplemented RPMI-1620. A total of 500 × 10^6 cells (Myla-2059 and KG-1) were pelleted and the pellet was treated with Trypsin-EDTA (Lonza), containing 1 mM NaSO4, for 30 min at 37°C. The supernatant was cleared of cells and the GAGs were extracted by ion exchange chromatography. Briefly, the supernatant was loaded onto a Q FF sepharose column (GE), the column was washed in 200 mM NaCl, and finally the GAGs were eluted in 1.5 M NaCl. The GAG's were precipitated overnight (O/N) at 4°C in two volumes of ethanol and the precipitate was collected by centrifugation.

Purification of CS on a VAR2 Column

There were 1.5 mg rVAR2 (DBL1-ID2a) that were immobilized onto a Hitrap NHS HP Column (GE). The column was inactivated with ethanolamine and washed in PBS. Sigma CSA or Myla-2059 GAG extract was adjusted to 1 × PBS and loaded onto the column in five passages. The column was washed in PBS and the bound GAG eluted at 0.25 M NaCl, 0.5 M NaCl, 1 M NaCl, and 2 M NaCl in succession. The eluted GAGs were precipitated in ethanol O/N at 4°C in two volumes of ethanol and the precipitate was collected by centrifugation. The eluted fractions were tested for their ability to inhibit rVAR2 binding to CSPG (Attana) and C32 cancer cells (Flow Cytometry, see above).

Disaccharide Analysis of CS

The disaccharide compositions of CS samples were analyzed using chondroitinase ABC and size exclusion chromatography-MS (SEC-MS) as previously described (Shi and Zaia, 2009). Each type of CS disaccharides was extracted from the total ion chromatogram (TIC), integrated, and quantified by comparing with an external standard containing known amount of CS disaccharides. The sulfation position for the monoly-sulfated disaccharides was determined by tandem-MS experiments using previously established methods (Shao et al., 2013). The diagnostic fragment ions for the 4-*O*-sulfated disaccharide (Y_1, *m/z* 300.0484) and for 6-*O*-sulfated disaccharide (Z_1, *m/z* 282.0362) were extracted from the TIC, counted, and compared with a standard curve generated using commercial standards.

Biosensor Affinity Analysis

The analysis of the purified GAG species was performed on a quartz crystal microbalance biosensor (Attana A100, Attana AB). CSPG (Decorin, Sigma) was coupled to a LNB carboxyl chip using EDC and Sulfo-NHS. The chip was inactivated with ethanolamine. The sensor chips were inserted into the machine and allowed to stabilize in PBS running buffer, at 25°C using a flow rate of 25 μl per min. rVAR2 (30 nM) was mixed with a titration of inhibitor and injected onto the surface. Control rVAR2 was run repeatedly during analysis to account for changes in the binding surface. The binding surface was re-generated after each test injection with injections of 0.25% SDS in PBS. Peak response levels were recorded using the Attester Evaluation software (Attana AB) and presented as a ratio to the nearest rVAR2 injection. IC_{50} values were calculated in Excel.

IVIS In Vivo Imaging

rVAR2 was NIR labeled through available amines with an Alexa750 Succinimidyl ester (Invitrogen). This was done with an excess of NIR probe (10× molar) according to the manufacturer's instructions. The coupled protein was injected (4 mg/kg) IV in the tail vein of healthy and tumor bearing mice 10 days post-establishment of a subcutaneous B16 melanoma tumor in the right flank. The mice were scanned using an IVIS spectrum CT scanner (Perkin Elmer). Scanning was done at time intervals ranging from 10 min to 48 hr. In vivo tumor signal quantification is presented as an absolute signal in reference to the signal of the flank of the healthy control mouse. Data analysis was performed using the Living Image Software (Caliper Life Sciences).

Patient Material

All human specimens were collected under full consent and according to the guidelines set forth and approved by the University of British Columbia (UBC) human ethics committee.

In Vivo Studies

The methodologies described were re-viewed and approved by the Institutional Animal Care Committee (IACC) at the University of British Columbia and the animal experiments inspectorate at the University of Copenhagen prior to conducting the study. During the study the care, housing, and use of animals was performed in accordance with the Canadian Council on Animal Care Guidelines and the Danish animal experiments inspectorate guidelines. For a detailed description of the in vivo studies and tolerability studies please see the Supplemental Information section.

SUPPLEMENTAL INFORMATION

Supplemental Information includes Supplemental Experimental Procedures, five figures, and five tables and can be found with this article online at http://dx.doi.org/10.1016/j.ccell.2015.09.003.

AUTHOR CONTRIBUTIONS

M.D., A.S., T.G.T., T.M.C., J.S.B., and P.H.B.S. designed the research; T.M.C., M.Dahlbäck, M.Ø.A., T.G., N.A.N., C.K.W., S.L., H.Z.O., L.F., M.E., J.S., L.B., F.F., M.A.N., J.F., Y.M., L.M., J.L., R.D., S.T., M.A.P., J.R.R., and B.J.H. performed the experiments; T.O.N., N.L.T., J.T., G.J.W., J.Z., P.J.H., and A.F.S. provided useful reagents and helpful discussions; and A.S., P.H.B.S., T.G.T., T.M.C., and M.D. wrote the manuscript.

ACKNOWLEDGMENTS

The authors are thankful to Dr. Chao Sima at TGen, Phoenix, AZ, for assistance with TMA-related bioinformatics; Dr. Jeffrey Allen formerly of University of Tennessee Health Science Center, Memphis, TN, currently at Humboldt Medical Specialists, Eureka, CA for lung cancer tissue access and assistance with clinical annotation; Birita Fritleifsdottir for help with B16 xenograft model; and Monika Stints and Thomas Lavstsen for hBMEC cells. We would like to acknowledge the contributions of Geoffery Winters, Alex Mandel, Tom Hseih, Peter Bergqvist, Lawrence Amankwa, Siobhan O'Brien, Faisal Pany, Eric Cruz, and Natalia Neverova for their work on the rVAR2 drug conjugate at The Centre for Drug Research and Development.

The work was supported by funds from the Novo Nordisk Foundation; the Danish Cancer Society; and Stand Up To Cancer – St. Baldrick's Pediatric Dream Team Translational Research Grant (SU2C-AACR-DT1113). Stand Up To Cancer is a program of the Entertainment Industry Foundation administered by the American Association for Cancer Research; Augustinus Foundation; U.S. Department of Defense (DoD); the Harboe Foundation; the European Research Councils (ERC) through the MalOnco program; The Danish Innovation Foundation; VAR2 Pharmaceuticals; Kairos Therapeutics; the Spar Nord Foundation; Team Finn and other riders in the Ride to Conquer Cancer; Safeway; and the Prostate Cancer Canada (PCC) Foundation. A.S., M.D., T.G.T., and P.H.S. are shareholders of VAR2 Pharmaceuticals ApS and members of the board of directors. J.R., B.H., and J.B. are employees of Kairos Therapeutics, Inc. J.F. and J.S. are employees of Retrogenix Ltd.

Received: June 12, 2015
Revised: July 31, 2015
Accepted: September 8, 2015
Published: October 12, 2015

REFERENCES

Alkhalil, A., Achur, R.N., Valiyaveettil, M., Ockenhouse, C.F., and Gowda, D.C. (2000). Structural requirements for the adherence of Plasmodium falciparum-infected erythrocytes to chondroitin sulfate proteoglycans of human placenta. J. Biol. Chem. *275*, 40357–40364.

Baruch, D.I., Pasloske, B.L., Singh, H.B., Bi, X., Ma, X.C., Feldman, M., Taraschi, T.F., and Howard, R.J. (1995). Cloning the P. falciparum gene encoding PfEMP1, a malarial variant antigen and adherence receptor on the surface of parasitized human erythrocytes. Cell *82*, 77–87.

Baston-Büst, D.M., Götte, M., Janni, W., Krüssel, J.S., and Hess, A.P. (2010). Syndecan-1 knock-down in decidualized human endometrial stromal cells leads to significant changes in cytokine and angiogenic factor expression patterns. Reprod. Biol. Endocrinol. *8*, 133.

Beeson, J.G., Andrews, K.T., Boyle, M., Duffy, M.F., Choong, E.K., Byrne, T.J., Chesson, J.M., Lawson, A.M., and Chai, W. (2007). Structural basis for binding of Plasmodium falciparum erythrocyte membrane protein 1 to chondroitin sulfate and placental tissue and the influence of protein polymorphisms on binding specificity. J. Biol. Chem. *282*, 22426–22436.

Casucci, M., Nicolis di Robilant, B., Falcone, L., Camisa, B., Norelli, M., Genovese, P., Gentner, B., Gullotta, F., Ponzoni, M., Bernardi, M., et al. (2013). CD44v6-targeted T cells mediate potent antitumor effects against acute myeloid leukemia and multiple myeloma. Blood *122*, 3461–3472.

Clausen, T.M., Christoffersen, S., Dahlbäck, M., Langkilde, A.E., Jensen, K.E., Resende, M., Agerbæk, M.O., Andersen, D., Berisha, B., Ditlev, S.B., et al. (2012). Structural and functional insight into how the Plasmodium falciparum VAR2CSA protein mediates binding to chondroitin sulfate A in placental malaria. J. Biol. Chem. *287*, 23332–23345.

Dahlbäck, M., Jørgensen, L.M., Nielsen, M.A., Clausen, T.M., Ditlev, S.B., Resende, M., Pinto, V.V., Arnot, D.E., Theander, T.G., and Salanti, A. (2011). The chondroitin sulfate A-binding site of the VAR2CSA protein involves multiple N-terminal domains. J. Biol. Chem. *286*, 15908–15917.

Esko, J.D., Stewart, T.E., and Taylor, W.H. (1985). Animal cell mutants defective in glycosaminoglycan biosynthesis. Proc. Natl. Acad. Sci. USA *82*, 3197–3201.

Fried, M., and Duffy, P.E. (1996). Adherence of Plasmodium falciparum to chondroitin sulfate A in the human placenta. Science *272*, 1502–1504.

Gama, C.I., Tully, S.E., Sotogaku, N., Clark, P.M., Rawat, M., Vaidehi, N., Goddard, W.A., 3rd, Nishi, A., and Hsieh-Wilson, L.C. (2006). Sulfation patterns of glycosaminoglycans encode molecular recognition and activity. Nat. Chem. Biol. *2*, 467–473.

Holtan, S.G., Creedon, D.J., Haluska, P., and Markovic, S.N. (2009). Cancer and pregnancy: parallels in growth, invasion, and immune modulation and implications for cancer therapeutic agents. Mayo Clin. Proc. *84*, 985–1000.

Igarashi, N., Takeguchi, A., Sakai, S., Akiyama, H., Higashi, K., and Toida, T. (2013). Effect of molecular sizes of chondroitin sulfate on interaction with L-selectin. Int. J. Carbohydr. Chem. *2013*, 9.

Kirby, M., Hirst, C., and Crawford, E.D. (2011). Characterising the castration-resistant prostate cancer population: a systematic review. Int. J. Clin. Pract. *65*, 1180–1192.

Litjens, T., Baker, E.G., Beckmann, K.R., Morris, C.P., Hopwood, J.J., and Callen, D.F. (1989). Chromosomal localization of ARSB, the gene for human N-acetylgalactosamine-4-sulphatase. Hum. Genet. *82*, 67–68.

Orendi, K., Kivity, V., Sammar, M., Grimpel, Y., Gonen, R., Meiri, H., Lubzens, E., and Huppertz, B. (2011). Placental and trophoblastic in vitro models to study preventive and therapeutic agents for preeclampsia. Placenta *32* (*Suppl*), S49–S54.

Rhodes, D.R., Yu, J., Shanker, K., Deshpande, N., Varambally, R., Ghosh, D., Barrette, T., Pandey, A., and Chinnaiyan, A.M. (2004). ONCOMINE: a cancer microarray database and integrated data-mining platform. Neoplasia *6*, 1–6.

Riker, A.I., Enkemann, S.A., Fodstad, O., Liu, S., Ren, S., Morris, C., Xi, Y., Howell, P., Metge, B., Samant, R.S., et al. (2008). The gene expression profiles of primary and metastatic melanoma yields a transition point of tumor progression and metastasis. BMC Med. Genomics *1*, 13.

Saito, M., Iwawaki, T., Taya, C., Yonekawa, H., Noda, M., Inui, Y., Mekada, E., Kimata, Y., Tsuru, A., and Kohno, K. (2001). Diphtheria toxin receptor-mediated conditional and targeted cell ablation in transgenic mice. Nat. Biotechnol. *19*, 746–750.

Salanti, A., Staalsoe, T., Lavstsen, T., Jensen, A.T., Sowa, M.P., Arnot, D.E., Hviid, L., and Theander, T.G. (2003). Selective upregulation of a single distinctly structured var gene in chondroitin sulphate A-adhering Plasmodium falciparum involved in pregnancy-associated malaria. Mol. Microbiol. *49*, 179–191.

Salanti, A., Dahlbäck, M., Turner, L., Nielsen, M.A., Barfod, L., Magistrado, P., Jensen, A.T., Lavstsen, T., Ofori, M.F., Marsh, K., et al. (2004). Evidence for the involvement of VAR2CSA in pregnancy-associated malaria. J. Exp. Med. *200*, 1197–1203.

Shao, C., Shi, X., White, M., Huang, Y., Hartshorn, K., and Zaia, J. (2013). Comparative glycomics of leukocyte glycosaminoglycans. FEBS J. *280*, 2447–2461.

Shi, X., and Zaia, J. (2009). Organ-specific heparan sulfate structural phenotypes. J. Biol. Chem. *284*, 11806–11814.

Sugahara, K., Mikami, T., Uyama, T., Mizuguchi, S., Nomura, K., and Kitagawa, H. (2003). Recent advances in the structural biology of chondroitin sulfate and dermatan sulfate. Curr. Opin. Struct. Biol. *13*, 612–620.

Van Sinderen, M., Cuman, C., Winship, A., Menkhorst, E., and Dimitriadis, E. (2013). The chrondroitin sulfate proteoglycan (CSPG4) regulates human trophoblast function. Placenta *34*, 907–912.

Wang, X., Wang, Y., Yu, L., Sakakura, K., Visus, C., Schwab, J.H., Ferrone, C.R., Favoino, E., Koya, Y., Campoli, M.R., et al. (2010). CSPG4 in cancer: multiple roles. Curr. Mol. Med. *10*, 419–429.

Wang, X., Katayama, A., Wang, Y., Yu, L., Favoino, E., Sakakura, K., Favole, A., Tsuchikawa, T., Silver, S., Watkins, S.C., et al. (2011). Functional characterization of an scFv-Fc antibody that immunotherapeutically targets the common cancer cell surface proteoglycan CSPG4. Cancer Res. *71*, 7410–7422.

SUPPLEMENTAL DATA

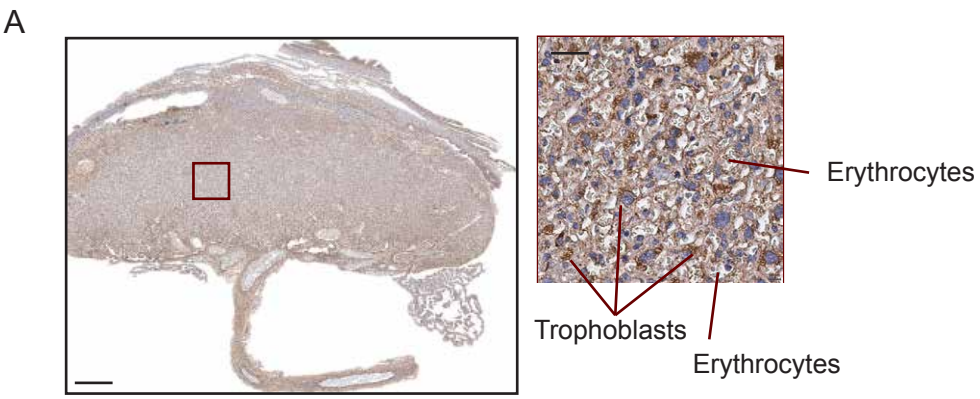

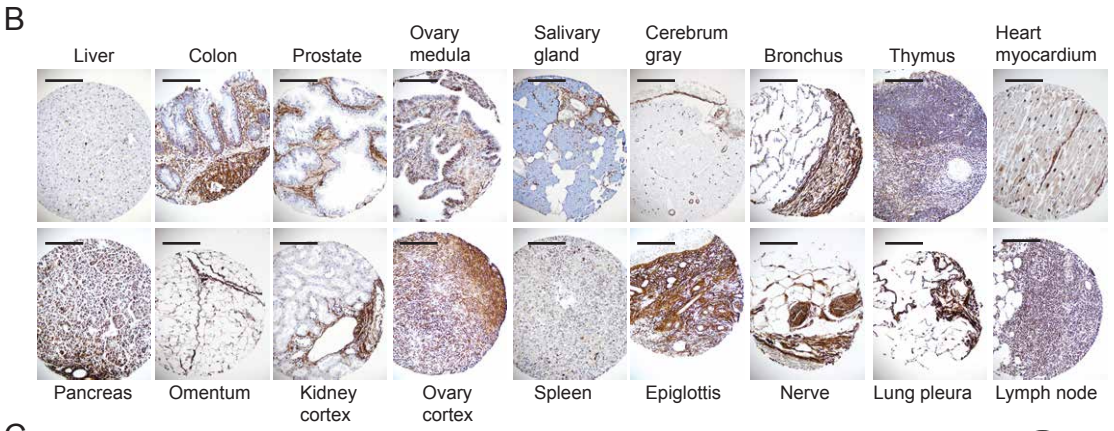

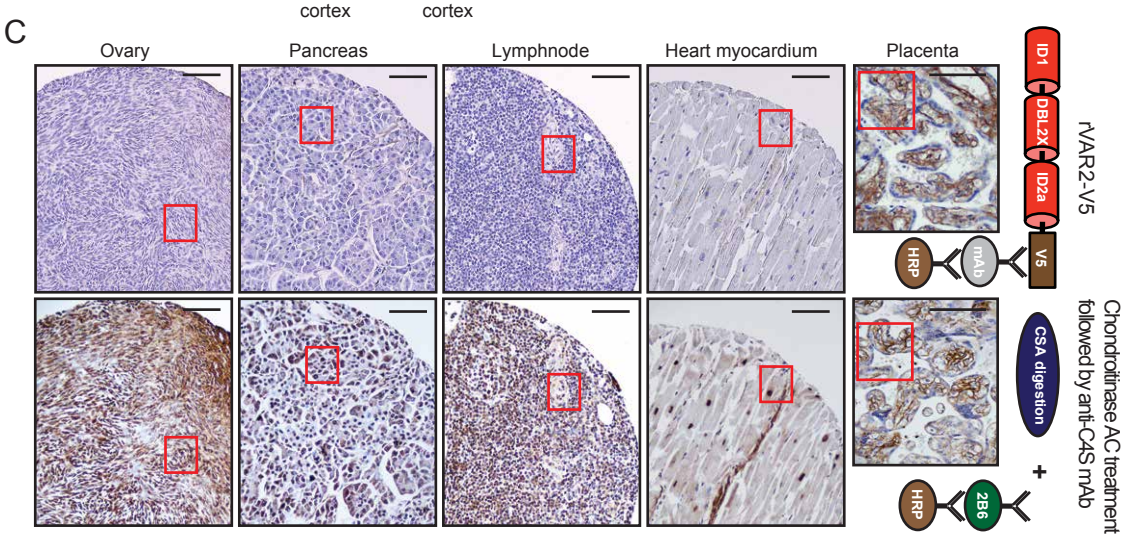

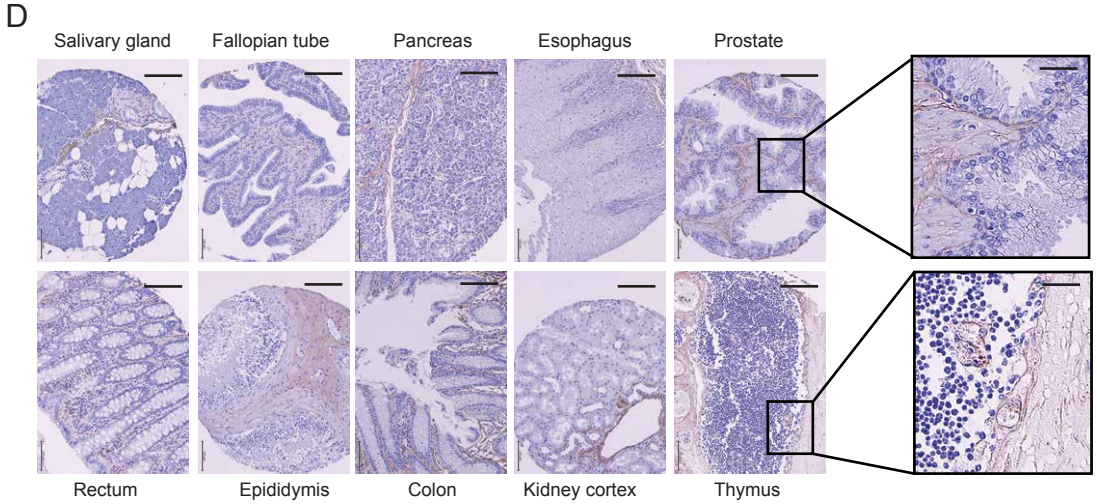

Figure S1, related to Figure 1

(**A**) 4x (left - scale bar 1 mm) and 40x (right - scale bar 150 µm) magnified images of murine placenta incubated with 500 picomolar rVAR2 and 1:700 anti-V5-HRP. Red box represents magnifications of the indicated area.
(**B**) Representative 10x (scale bar 300 µm) magnified images of indicated normal tissue cores incubated with 1 U/ml Chondroitinase AC followed by 1:20 dilution of anti-C4S (2B6) antibody.
(**C**) Representative images of indicated normal tissue specimens stained with 500 picomolar recombinant VAR2CSA and 1:700 anti-V5-HRP (upper panel) or as describe in **C** (lower panel) (Scale bar 200 µm). Red boxes represents areas presented in **Figure 1E**.
(**D**) Representative 10x (Scale bar 250 µm) magnified images of indicated normal tissue specimens incubated with 500 picomolar rVAR2 and 1:700 anti-V5-HRP. Black boxes represent magnifications of the indicated areas (Scale bar 100 µm).

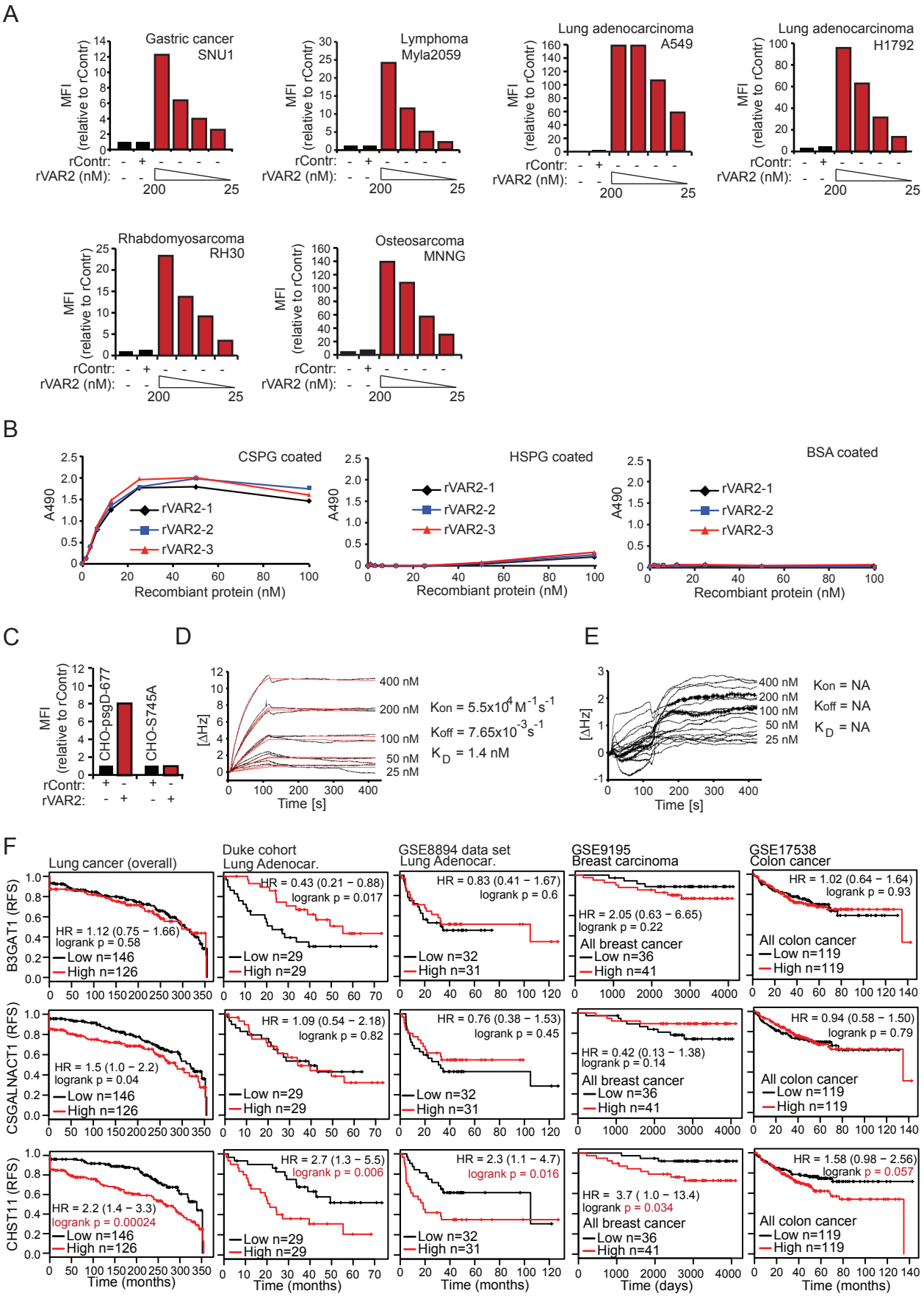
A
Gastric cancer
SNU1
Lymphoma
Myla2059
Lung adenocarcinoma
A549
Lung adenocarcinoma
H1792
Rhabdomyosarcoma
RH30
Osteosarcoma
MNNG
MFI (relative to rContr)
rContr:
rVAR2 (nM):
200
25
B
CSPG coated
HSPG coated
BSA coated
A490
rVAR2-1
rVAR2-2
rVAR2-3
Recombiant protein (nM)
C
CHO-psgD-677
CHO-S745A
rVAR2:
D
[ΔHz]
400 nM
200 nM
100 nM
50 nM
25 nM
Kon = 5.5x10^4 M^-1s^-1
Koff = 7.65x10^-3s^-1
K_D = 1.4 nM
Time [s]
E
Kon = NA
Koff = NA
K_D = NA
F
Lung cancer (overall)
Duke cohort
Lung Adenocar.
GSE8894 data set
Lung Adenocar.
GSE9195
Breast carcinoma
GSE17538
Colon cancer
B3GAT1 (RFS)
CSGALNACT1 (RFS)
CHST11 (RFS)
HR = 1.12 (0.75 − 1.66)
logrank p = 0.58
Low n=146
High n=126
HR = 0.43 (0.21 − 0.88)
logrank p = 0.017
Low n=29
High n=29
HR = 0.83 (0.41 − 1.67)
logrank p = 0.6
Low n=32
High n=31
HR = 2.05 (0.63 − 6.65)
logrank p = 0.22
All breast cancer
Low n=36
High n=41
HR = 1.02 (0.64 − 1.64)
logrank p = 0.93
All colon cancer
Low n=119
High n=119
HR = 1.5 (1.0 − 2.2)
logrank p = 0.04
HR = 1.09 (0.54 − 2.18)
logrank p = 0.82
HR = 0.76 (0.38 − 1.53)
logrank p = 0.45
HR = 0.42 (0.13 − 1.38)
logrank p = 0.14
HR = 0.94 (0.58 − 1.50)
logrank p = 0.79
HR = 2.2 (1.4 − 3.3)
logrank p = 0.00024
HR = 2.7 (1.3 − 5.5)
logrank p = 0.006
HR = 2.3 (1.1 − 4.7)
logrank p = 0.016
HR = 3.7 (1.0 − 13.4)
logrank p = 0.034
HR = 1.58 (0.98 − 2.56)
logrank p = 0.057
Time (months)
Time (days)

Figure S2, related to Figure 2

(**A**) Relative mean fluorescence intensity (MFI) of the denoted cell lines incubated with recombinant control protein (rContr) or VAR2CSA (rVAR2) as indicated and detected by flow cytometry using anti-V5-FITC.
(B) Enzyme-linked immunosorbent assay (ELISA) showing concentration dependent rVAR2 binding of three independently synthesized protein batches (rVAR2-1,2,3) to immobilized CSPG (left), HSPG (middle), and BSA (right). (**C**) Relative mean fluorescence intensity (MFI) of Immortalized CHO-psgD-677 and CHO-S745A cells incubated with recombinant control protein (rContr) or VAR2CSA (rVAR2) as indicated and detected by flow cytometry using anti-V5-FITC.
(**D-E**) Sensorgram showing binding between recombinant VAR2CSA and immobilized CHO-psgD-677 (D) and CHO-S745A (E) cells measured in delta Hertz [ΔHz] as a function of time (in seconds) using the indicated concentrations of recombinant protein. Black lines represent data, and red lines represent fitted curves attained by a 1:1 binding model. Black box summarizes K_{on}, K_{off}, and the calculated K_D value.
(F) Kaplan-Meier plots of the expression of key CS enzymes CHST11, B3GAT1 and CSGALNACT1 linked to overall survival or recurrence free survival (RFS) in indicated datasets of overall lung cancer, the Duke and GSE8894 cohort of lung adenocarcinoma, the GSE9195 breast cancer cohort and the GSE17538 colon cancer cohort. High and low expression was defined as using the median value of the selected gene as separation point. Hazard ratio (HR) was calculated using Cox proportional hazards regression, and p value was calculated using the logrank test.

Table S1, Related to Figure 2 [1]

Cancer of epithelial lineage		
A549	Lung adenocarcinoma	++
H1792	Lung adenocarcinoma	+++
BeWo	Placenta choriocarcinoma	++
C32	Melanoma	++
LCC6	Melanoma	++
Colo 205	Colorectal adenocarcinoma	+++
ES-2	Ovarian clear cell carcinoma	++
LNCap	Prostate adenocarcinoma	++
PC-3	Prostate adenocarcinoma	+++
MDA-MB-231	Breast adenocarcinoma	++
T47D	Breast ductal carcinoma	+
SNU-1	Gastric carcinoma	++
T24	Bladder transitional cell carcinoma	++
UM-UC-6	Bladder transitional cell carcinoma	+++
Cancer of mesenchymal lineage		
CW9019	Rhabdomyosarcoma	+
RH30	Rhabdomyosarcoma	++
MG63	Osteosarcoma	++
MNNG	Osteosarcoma	+++

U2os	Osteosarcoma	++
TC32	Ewing sarcoma	+
TC71	Ewing sarcoma	++
Cancer of hematopoietic lineage		
FARAGE	Diffuse Large B-cell lymphoma	0
SU-DHL-8	Diffuse Large B-cell lymphoma	+
KG-1	Acute Myelogenous Leukemia	+++
MOLP-2	Multiple Myeloma	++
MyLa 2059	Cutaneous T cell lymphoma	++
NALM-6	B cell precursor acute lymphoblastic leukemia	++
NU-DHL-1	B cell lymhphoma	++

[1] Patient-derived cancer cell lines bound by rVAR2 sorted according to cancer type. 0: no binding; +: low binding; ++: medium binding; +++: high binding. In total, 111 cancer cell lines were tested in flow cytometry of which 106 (95%) cells were positive for VAR2 binding.

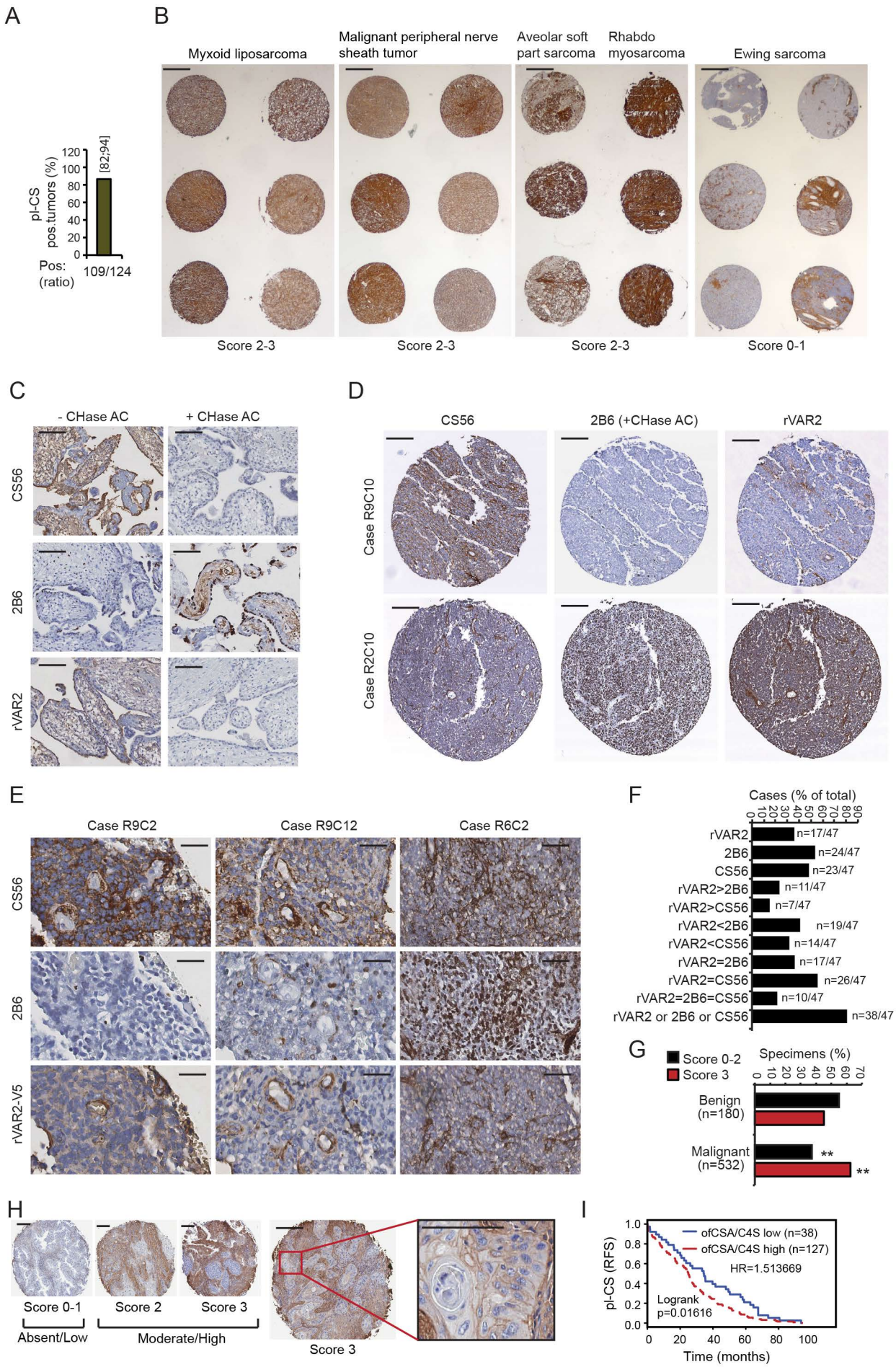
A
pl-CS pos.tumors (%)
120
100
80
60
40
20
0
[82;94]
Pos: (ratio)
109/124
B
Myxoid liposarcoma
Malignant peripheral nerve sheath tumor
Aveolar soft part sarcoma
Rhabdo myosarcoma
Ewing sarcoma
Score 2-3
Score 2-3
Score 2-3
Score 0-1
C
- CHase AC
+ CHase AC
CS56
2B6
rVAR2
D
CS56
2B6 (+CHase AC)
rVAR2
Case R9C10
Case R2C10
E
Case R9C2
Case R9C12
Case R6C2
CS56
2B6
rVAR2-V5
F
Cases (% of total)
0 10 20 30 40 50 60 70 80 90
rVAR2 n=17/47
2B6 n=24/47
CS56 n=23/47
rVAR2>2B6 n=11/47
rVAR2>CS56 n=7/47
rVAR2<2B6 n=19/47
rVAR2<CS56 n=14/47
rVAR2=2B6 n=17/47
rVAR2=CS56 n=26/47
rVAR2=2B6=CS56 n=10/47
rVAR2 or 2B6 or CS56 n=38/47
G
Score 0-2
Score 3
Specimens (%)
0 10 20 30 40 50 60 70
Benign (n=180)
Malignant (n=532)
**
**
H
Score 0-1
Score 2
Score 3
Absent/Low
Moderate/High
Score 3
I
pl-CS (RFS)
1.0
0.8
0.6
0.4
0.2
0.0
ofCSA/C4S low (n=38)
ofCSA/C4S high (n=127)
HR=1.513669
Logrank p=0.01616
0 20 40 60 80 100
Time (months)

Figure S3, related to Figure 3

(**A**) Column graph representation of placental-like CS (pl-CS) staining intensity of mixed breast cancer subtypes (n=124) scored (0-3) for binding to recombinant VAR2CSA. Column shows percentage and exact binomial 95% confidence interval of placental-like CS positive (score 2-3) tumors.
(**B**) Representative 2x (Scale bar 500 μm) magnified overview images of the soft tissue mesenchymal tumor tissue microarray (Fig. 3G) incubated with recombinant VAR2CSA (rVAR2-V5) and anti-V5-HRP and scored on a 0-3 scale for plasma membrane staining intensity where score 2 equals that of placenta.
(**C**) Representative images of human placenta specimens stained for CS expression with CS56 antibody, 2B6 antibody, and rVAR2 protein (Scale bar 100 μm). When indicated, specimens were pre-treated with chondroitinase AC to depolymerize the C4S and C6S chains down to 1 single CS unit (stub), which if C4S creates an epitope for the 2B6 antibody while removing binding of the CS56 and rVAR2 (control for binding specificity to CS).
(**D**) Representative images (4x magnification - scale bar 125 μm) of 2 (out of 47) tissue micro arrayed cases of mixed adulthood and pediatric Ewing's sarcoma treated and stained as in **C**.
(**E**) Three cases of Ewing sarcoma tissue specimens stained with CS56, 2B6 or rVAR2 as in **C** (Scale bar 150 μm).
(**F**) Ewing's sarcoma TMA (n=47) stained with the 3 reagents (CS56, 2B6, and rVAR2) where analyzed for relative staining intensity as follows **i**) rVAR2 (score 2-3) vs. 2B6 (score 0-1) (rVAR2>2B6); **ii**) rVAR2 (score 2-3) vs. CS56 (score 0-1) (rVAR2>CS56); **iii**) rVAR2 (score 0-1) vs. 2B6 (score 2-3) (rVAR2<2B6); **iv**) rVAR2 (score 0-1) vs. CS56 (score 2-3) (rVAR2<CS56); **v**) rVAR2 and 2B6 same score (rVAR2=2B6); **vi**) rVAR2 and CS56 same score (rVAR2=CS56); rVAR2 and 2B6 and CS56 same score (rVAR2=2B6=CS56); **vii**) at least one of the reagents with a score 2-3 (rVAR2 or 2B6 or CS56).
(**G**) Column graph representation of the distribution in staining intensity between benign vs. malignant soft-tissue lesions. **:p<0.0001.
(**H**) Representative images of a (n=165) non-small cell lung cancer TMA stained with recombinant VAR2CSA (rVAR2). Red box marks the amplified area of a score 3 squamous cell carcinoma. (Scale bar 250 μm).
(**I**) Kaplan-Meier plot of non-small cell lung tumor TMA stained for placental-like CSA showing recurrence free survival (RFS) of patients with low (score 0-1, n=38) or high (score 2-3, n=127) expressing tumors. Hazard ratio (HR) was calculated using Cox proportional hazards regression, and p value was calculated using the logrank test.

Table S2, related to Figure 3

Melanoma	Score 0	Score 1	Score 2	Score 3
Benign	14/49 (28.6%)	17/49 (34.7%)	17/49 (34.7%)	1/49 (2.0%)
Clark 1	0/7 (0.0%)	1/7 (14.3%)	2/7 (28.6%)	4/7 (57.1%)
Clark 2	5/32 (15.7%)	10/32 (31.3%)	8/32 (25.0%)	9/32 (28.1%)
Clark 3	2/24 (8.3%)	6/24 (25.0%)	12/24 (50.0%)	4/24 (16.7%)
Clark 4	3/23 (13.0%)	6/23 (26.1%)	8/23 (34.8%)	6/23 (26.1%)
Clark 5	0/3 (0.0%)	1/3 (33.3%)	0/3 (0.0%)	2/3 (66.7%)
Recurrent/ Metastatic	3/21 (14.3%)	1/21 (4.8%)	8/21 (38.1%)	9/21 (42.9%)

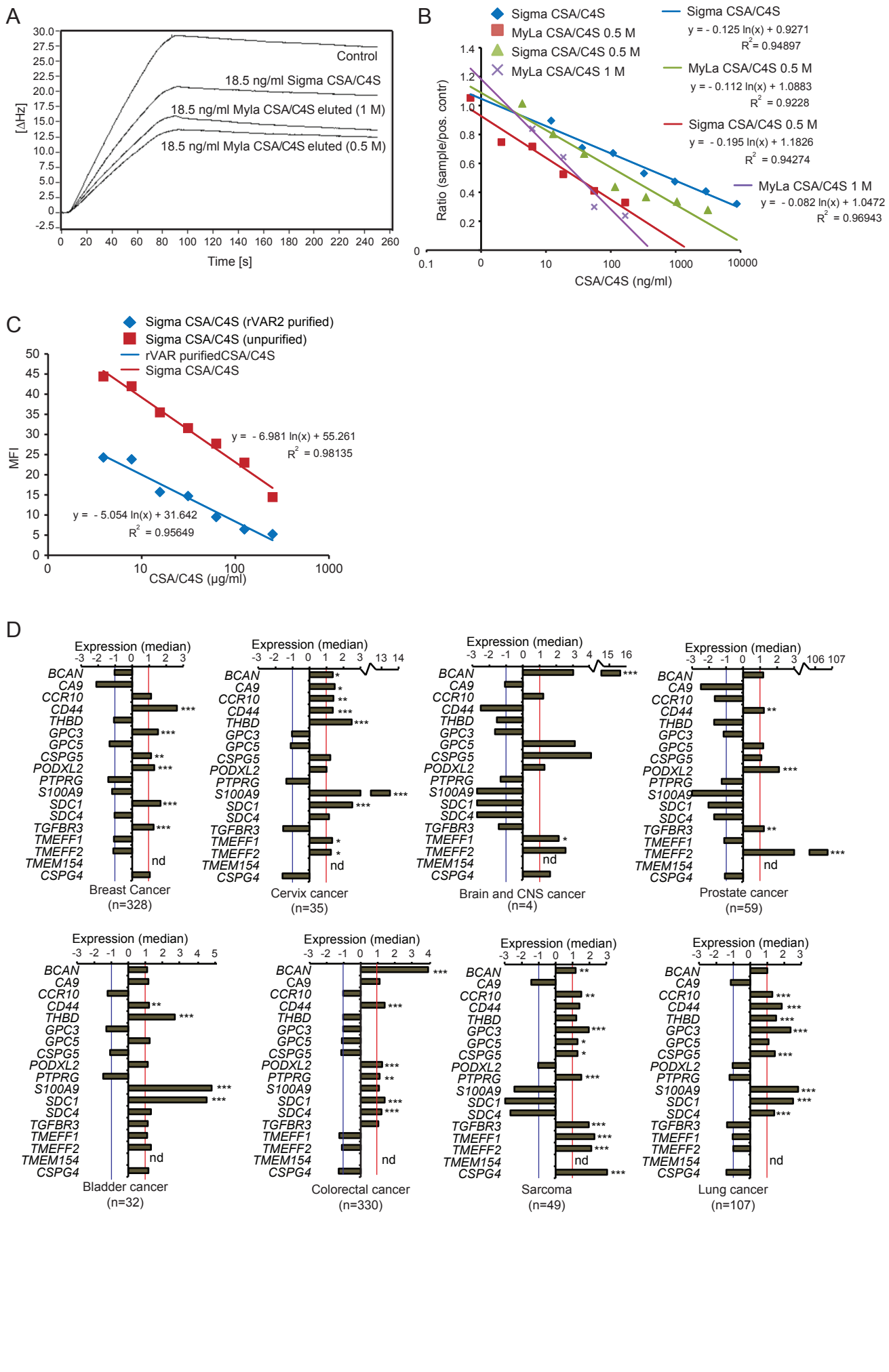
A
Control
18.5 ng/ml Sigma CSA/C4S
18.5 ng/ml Myla CSA/C4S eluted (1 M)
18.5 ng/ml Myla CSA/C4S eluted (0.5 M)
[ΔHz]
Time [s]
B
Sigma CSA/C4S
MyLa CSA/C4S 0.5 M
Sigma CSA/C4S 0.5 M
MyLa CSA/C4S 1 M
Sigma CSA/C4S
y = - 0.125 ln(x) + 0.9271
R2 = 0.94897
MyLa CSA/C4S 0.5 M
y = - 0.112 ln(x) + 1.0883
R2 = 0.9228
Sigma CSA/C4S 0.5 M
y = - 0.195 ln(x) + 1.1826
R2 = 0.94274
MyLa CSA/C4S 1 M
y = - 0.082 ln(x) + 1.0472
R2 = 0.96943
Ratio (sample/pos. contr)
CSA/C4S (ng/ml)
C
Sigma CSA/C4S (rVAR2 purified)
Sigma CSA/C4S (unpurified)
rVAR purifiedCSA/C4S
Sigma CSA/C4S
y = - 6.981 ln(x) + 55.261
R2 = 0.98135
y = - 5.054 ln(x) + 31.642
R2 = 0.95649
MFI
CSA/C4S (µg/ml)
D
Expression (median)
BCAN
CA9
CCR10
CD44
THBD
GPC3
GPC5
CSPG5
PODXL2
PTPRG
S100A9
SDC1
SDC4
TGFBR3
TMEFF1
TMEFF2
TMEM154
CSPG4
nd
Breast Cancer
(n=328)
Cervix cancer
(n=35)
Brain and CNS cancer
(n=4)
Prostate cancer
(n=59)
Bladder cancer
(n=32)
Colorectal cancer
(n=330)
Sarcoma
(n=49)
Lung cancer
(n=107)

Figure S4, related to Figure 4

(**A**) Representative sensorgram from the binding analysis (IC_{50} values) of high- and low affinity rVAR2-bound CS purified from crude bulk trachea CSA (Sigma) and from MyLa 2059 T-cell Lymphoma cells. Binding of 30 nM rVAR2 pre-incubated with the indicated CS concentrations is measured as delta Hertz [ΔHz] as a function of time (seconds). Inhibitory capacity was assessed as a decrease in peak response levels compared to the positive control.

(**B-C**) IC_{50} values were calculated from the biosensor (**B**) and FACS (**C**) analysis using linear regression. Concentration of CS is plotted against rVAR2 binding given as a ratio to the nearest positive control (B) or MFI (C). Linear regression was performed in Excel. The equations and corresponding R2 values are given in the plots, while the resulting IC_{50} values are shown in table S4.

(D) Expression of the indicated genes encoding VAR2CSA plasma membrane binding placental-like CS-modified proteoglycans Figure 4H in the indicated patient specimens extracted from the Oncomine Bitner array and divided into cancer groups. Blue and red lines represent median cut-off for average expression across the entire dataset. *p<0.05, **p<0.01, ***p<0.001. nd: not determined (missing probe).

Table S3, related to Figure 4 [1]

	Myla2059		KG-1	
Composition	Input	rVAR2 purified	Input	rVAR2 purified
Non-sulfated	1.9±1.4%	0%	2.1±1.5%	0%
Mono-sulfated	98.1±1.4%	100%	98.1±1.4%	100%
C4S	93.9%	95.8%	95.1%	95.5%
C6S	6.1%	4.2%	4.9%	4.5%
Di-sulfated	0%	0%	0%	0%

[1] Compositional analysis of extracted CS species before and after rVAR2 affinity purification. Table shows degree of sulfation as determined by LC-MS and ratio of C4S versus C6S as determined by tandem MS. Selected data is summarized graphically in Fig 5B-E.

Table S4, related to Figure 4 [1]

	Sigma CSA/C4S	Sigma CSA/C4S	MyLa2059 CSA/C4S	Placenta CSA/C4S
Affinity	Input	rVAR2 purified	rVAR2 purified	rVAR2 purified
IC_{50} µg/ml (Biosensor)	0.79	0.19	0.033	0.063
IC_{50} µg/ml (Cancer cell flow cytometry)	99.6	14.7	n.d.	n.d.
Composition				
Non-sulfated	10.5±0.5%	1.4±1.1%	0%	
Mono-sulfated	89.5±0.5%	98.6±1.1%	100%	
C4S	79.6%	90.3%	95.8%	
C6S	20.4%	9.7%	4.2%	
Di-sulfated	0%	0%	0%	

[1] Summary of the analysis of the capacity of BT-CSA, before and after rVAR2 affinity purification, and rVAR2 affinity purified Myla2059 CS and placental CS, to inhibit rVAR2 binding to immobilized CSPG in the Attana biosensor and binding to cancer cells in FACS. The composition of the different sources of CS (as in table S2) is listed below. N.d. means that experiment could not be performed due to insufficient amounts of material. Binding inhibition is shown as the concentration needed to block 50% of the binding (IC_{50} values) between rVAR2 and the cells measured by biosensor. Data is summarized in Fig 5F-G.

Table S5, related to Figure 4[1].

Gene symbol	Protein	Presence of CSA chain(s)	Known function in Cancer
BCAN	Brevican	Yes	Cell adhesion and motility. Isoforms highly expressed on cell surface in glioma (Theocharis et al., 2010)
CA9	Carbonic anhydrase IX	Proteoglycan but not previously shown to be CSA conjugated.	Involved in cell proliferation and transformation, and solid tumor acidification. Expressed in all clear-cell renal cell carcinoma, but is not detected in normal kidney (Takacova et al., 2013). Also expressed in various other tumours including breast cancers.
CCR10	Chemokine receptor 10	Not known	Chemokine receptor. Overexpressed in lymphoma, cutaneous squamous cell carcinoma (Kai et al., 2011) and melanoma. Suggested to be involved in metastasis (Murakami et al., 2004).
CD44	CD44 molecule	Yes on splicevariants	Cell adhesion and migration. Associated with a wide range of cancers and cancer stem cells (Naor et al., 1997)
THBD	Thrombomodulin	Yes	Binds thrombin. Differently expressed in a wide range of cancers including carcinoma, adenocarcinoma and glioma. Loss of TM expression correlates with certain cancer progressions. Progression of cancer correlates with serum levels of TM and high expression promotes angiogenesis and

			metastasis (Hanly et al., 2005).
GPC3	Glypican 3	HS proteoglycan but not previously shown to present CSA	Binds ECM proteins and growth factors. Has been described as an oncofetal antigen in hepatocellular carcinoma (Iozzo and Sanderson, 2011).
GPC5	Glypican 5	Yes	Binds ECM proteins and growth factors. Overexpressed in several tumors. Has been demonstrated to increase tumour proliferation in rhabdomyosarcomas by potentiating the action of FGF-2, HGF and Wnt1A (Williamson et al., 2007).
CSPG5	Neuroglycan	Yes	ND
PODXL2	Podocalyxin-like 2	Yes	Cell adhesion. Overexpressed in several tumors including breast and prostate cancer, malignant brain tumours, testicular, hepatocellular and renal cell carcinoma Overexpression has been shown to be an independent predictor of prognosis in breast, renal and colorectal cancers (Larsson et al., 2011).
PTPRG	Protein tyrosin phosphatase, receptor type, G	Proteoglycan with CS acceptor site	Enzyme involved in cell growth, differentiation, mitotic cycle, and transformation by oncogenes. Gene methylation and protein activity is associated with tumor suppression (Della Peruta et al., 2010).

S100A9	S100 calcium binding protein A9	No	A calcium- and zinc-binding protein important in the regulation of inflammatory processes and immune response. Upregulated in various cancers including hepatocellular carcinoma (HCC) (Wu et al., 2013).
SDC1 **&** ***SDC4***	Syndecan 1 & Syndecan 4	Yes	Regulates cell proliferation, differentiation, adhesion and migration. In particular Syndecan-4 is a focal adhesion component in a range of cell types and mediates breast cancer cell adhesion and spreading. Overexpressed in many cancers including prostate and breast and is key to spread of cancer. Expression correlations with tumor recurrence and poor prognosis (Theocharis et al., 2010).
TGFBR3	Transforming growth factor, beta receptor III. Also called Betaglycan	Yes (Part time)	Binds TGF. Plays a role in multiple cancers. Has been shown to decrease cancer cell motility (Mythreye and Blobe, 2009).
TMEFF1/TENB1	Transmembrane protein with EGF-like and two follistin-like domain 1 also called Tomoregulin-1	Proteoglycan with unknown modification but has several putative CS acceptor sites	Associated with prostate cancer as well as gastric cancer (Uchida et al., 1999).
TMEFF2/TENB2	Transmembrane protein with EGF-like and two follistin-like domain 1 Tomoregulin-2	Yes	Diagnostic marker for prostate cancer (Zhao et al., 2008).
TMEM154	Transmembrane protein 154	Not known but has	ND

		putative CS acceptor site	

[1]VAR2SCA plasma membrane binding-proteins identified by a functional gain-of-binding Retrogenix
screen. ND: No data available.

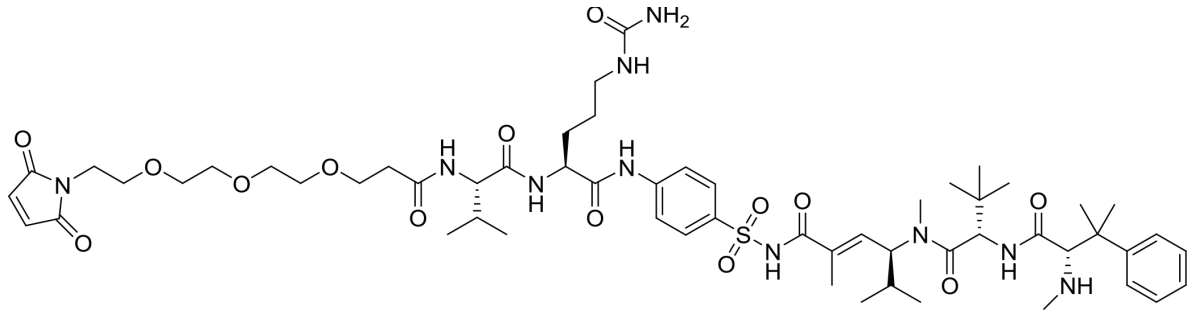

Figure S5, related to Figure 7
Structure of the protease cleavable linker-molecule MTvc886 used to conjugate KT886 to rVAR2.

SUPPLEMENTAL EXPERIMENTAL PROCEDURES

Cell lines

Human Cancer cell lines BxPC-3‡, NCI-N87‡, HCC1954‡, HCT-15‡, Capan-2‡, AsPC-1‡, Jurkat‡, MiaPaCa-2‡, OVCAR-3‡, Karpas299†, H1975◦, NCI-H358‡, SK-BR-3‡, MCF-7‡, DLD-1‡, NCI-H1437◦, HPAF-II‡, Colo205◦, MG63◦, PC-3‡, T47D‡, MDA-MB-231‡, MDA-MB-468‡, A549‡, 253J B-V◦, UM-UC-3‡, K562*, Rh30◦, U2OS◦ ,U138MG‡, A172‡, MNNG/HOS◦, JIMT-1◦, OE19†, DU145‡, HepG2‡, SKOV-3‡, KG1a‡, H292‡, and HCC1806‡ were obtained from ATCC‡, Sigma-Aldrich†, the University of Copenhagen*, or the Vancouver Prostate Centre/British Columbia Cancer Agency◦ and were cultured as instructed by the supplier. The Myla2059 Lymphoma cell lines were graciously donated by Niels Ødum at the University of Copenhagen. FARAGE, SU-DHL-8, KG-1 and NALM-6 were a kind gift from Karen Dybkaer, Aalborg University Hospital, Denmark.

Enzyme-linked immunosorbent assay (ELISA)

Plastic wells were coated with either Chondroitin Sulfate Proteoglycan (CSPG), Heparan Sulfate Proteoglycan (HSPG), or Bovine Serum Albumine (BSA) as indicated and binding of rVAR2 were detected using anti-his HRP antibody.

Immunohistochemistry

Normal tissue and clinico-pathological diagnosed tumor specimens from human patients were obtained from Origen and from tissue microarrays containing a wide variety of mesenchymal tumors (Pacheco and Nielsen, 2012). Lung cancer and melanoma samples

were obtained from patients who underwent total tumor resection. Specimen blocks chosen for the TMA met the criteria of nonnecrotic, nonirradiated, or chemo-treated lung cancer tissue. The TMA contains 231 NSCLC specimens (127 adenocarcinoma and 104 squamous cell carcinoma) and 159 mixed staged melanoma specimens. Samples were double punched 0.6 um diameter using an indexed manual arrayer with an attached stereomicroscope under the direction of a certified pathologist, who also reviewed and verified the tumor content. Test for association of CSA (low or high) with RFS in the lung TMA was performed using a one-tail Mann-Whitney test, and CSA scores with melanoma progression was performed using Goodman-Kruskal-Gamma test. $p < 0.05$ was considered significant. Using the Ventana Discovery platform, sectioned paraffin-embedded tissue samples were stained with 500 picomolar V5-tagged rVAR2 without antigen retrieval followed by 1:700 monoclonal anti-V5 step, and a anti-mouse-HRP detection step. Mounted and stained specimens were subsequently scored for membranous staining intensity on a 0-3 scale. Score 0-1 represented absent/weak staining and score 2-3 positive staining, where score 2 reflects a staining intensity equal to that of placenta (included as a positive control in each staining run). Within each cancer group the percentage and exact binomial 95% confidence interval was calculated using STATA 12 software.

Retrogenix Technology

Screening for VAR2CSA binding proteins was performed using the Retrogenix Cell Microarray technology (www.retrogenix.com). Initially 3550 expression vectors, each encoding a unique human plasma membrane protein and the fluorescent ZsGreen1 protein, were pre-spotted on glass slides. Human HEK293 cells were grown over the arrays and

reverse-transfected, resulting in the over-expression of each membrane protein and ZsGreen1. Slides were then incubated with 5 µg/ml V5-tagged VAR2 DBL1-ID2a followed by an AlexaFluor647-labeled anti-V5 antibody (AbD Serotec). VAR2CSA-binding proteins were identified by fluorescence imaging (ZsGreen1 and AlexaFluor647) and ImageQuant software (GE). For validation and specificity testing, expression vectors encoding the VAR2CSA binding proteins were re-spotted on new slides, and HEK293 cells were reverse-transfected. Slides were then treated with V5-tagged rVAR2 with or without 400 µg/ml CSA or following a 30 min chondroitinase ABC (CHase; Sigma) pre-treatment, or treated with rContr or with no ligand. Interactions were analysed using the AlexaFluor647-labeled anti-V5 antibody and fluorescence imaging. After fluorescence imaging of the slides, spot and background intensities were quantified from at least 6 high power field images representing at least 2 independent experiments using ImageQuant software (GE).

Bioinformatics

The Bittner multicancer dataset is available at http://www.oncomine.org/main/index.jsp (Rhodes et al., 2004). The dataset was analyzed for median expression of identified genes encoding VAR2CSA plasma-membrane binding proteins relative to a calculated average median expression across the entire dataset. Survival and microarray analysis were performed using the R statistical environment. Affymetrix microarray datasets linked to outcome were normalized using the Robust Multichip Array (RMA) method from affy package (Gautier et al., 2004) and optimal probe sets were selected with the Jetset package (Li et al., 2011). For the Duke and the Bild lung cancer datasets, survival analysis was

performed with the overall survival time. For all the others datasets the outcome variable is the time of recurrence free survival. Survival curves were calculated using the Kaplan-Meier method. High and low expression patients were divided using the median value of the selected gene as separation point. Hazard ratio was calculated using Cox proportional hazards regression, and p value was calculated using the logrank test.

Immunoprecipitation

Membrane proteins were extracted by lysing C32 cells with EBC lysis buffer (150 mM NaCl, 50 mM Tris-HCl, 2.5 mM MgCl2, 1 mM EDTA, 1% CHAPS and a protease inhibitor cocktail (Roche). The lysate was loaded onto a Hitrap NHS HP column (GE) containing immobilized rVAR2 or DBL4 control protein. The column was washed extensively in Lyses buffer as well as lysis buffer containing 250 mM NaCl. Bound protein was eluded with 0.5 M NaCl in lysis buffer and concentrated on a vivaspin column (MWCO 10.000 kDa). Protein samples and a high-molecular weight marker (LC5699, Life Technologies) were loaded onto a NuPAGE Tris-acetate gel (Life Technologies). Proteins were subsequently transferred to a nitrocellulose overnight at 4C at 75 mA. The membranes were stained with anti-CSPG4 antibody (LHM2, Abcam) or Anti-panCD44 (2C5, RnD systems).

Mass Spectrometry

Denaturing SEC-HRMS for intact mass analysis of recombinant VAR2 and VAR2 drug conjugates was performed on a Waters Acquity H Class UPLC with PDA detection at 280 nm utilizing an Acquity UPLC BEH 200 SEC column (1.7 uM, 4.6 mm x 150 cm).

High resolution mass spectrometry detection was achieved using a MicroMass Q-TOF Premier with a scan range from 250-4900 m/z. The analysis was performed using an isocratic elution at 0.25 ml/min over 11 min with 70/30 H20/ACN with 0.1% TFA and 0.1% FA. Data collection and analysis was done with MassLynx 4.1 with spectral deconvolution using MaxEnt1.

Subcutaneous PC3 and B16 tumor model

PC-3M-Luc-C6 cells ($2x10^6$ cells) were injected subcutaneously into the right flank of $Foxn1^{nu}$ mice on day -12. The mice were divided into 3 groups with 10 mice in each, and were treated with intravenous injections of vehicle (saline), a control DT388 fusion protein (rContr-DT), or an rVAR2 DT388 fusion protein (rVAR2-) respectively, on day 0, 2 and 6 at 0.6 mg/Kg doses. Tumor growth was monitored using a caliper-measuring tool, and the 3 longest perpendicular axes in the x/y/z plane of each tumor were measured. Tumor volume was calculated according to the standard formula: volume = xy^2*0.5236 (Janik et al., 1975). Saline and rVAR2-DT treated mice were also injected with luciferine and scanned for tumor chemiluminescence using IVIS at day 3 and 13 after 1^{st} dose (saline or rVAR2-DT). Control mice were given PBS or 0.33 mg/Kg rVAR2-NIR before sacrifice, and tumors were extracted and scanned by IVIS.

Karpas299 Xenograft Study

The in vivo efficacy study was performed at the Experimental Therapeutics & Animal Resource Centre at the BC Cancer Research Centre. Female C.B-17/IcrHsd-Prkdcscid mice (Harlan Laboratories) were anesthetized using isoflurane and were then implanted subcutaneously in the back with $1x10^6$ Karpas299 human T cell lymphoma tumour cells per mouse. Tumours were established over a period of 19 days, and test animals were then grouped according to tumour volume such that each group (n=7) had an equal distribution of tumour volumes. Dimensions of established tumours were measured with calipers. Tumour volumes were calculated according to the equation (Length x $Width^2$ /2) with the length (millimeters) being the longer axis of the tumour. The mean tumour volume on treatment day was greater than 150 mm^3. Intravenous test article administration began on Day 21, and continued every two to three days (total of three injections) at the doses indicated in the figure legend. Animals were injected based on individual body weights using a 28 G needle. Dilation of the lateral tail vein was achieved by holding the animals under a heating lamp for 1-2 min. The animals were briefly restrained (approximately 1 min) and injection was delivered into the lateral tail vein. Animal health was assessed acutely using Post Injection Clinical Observation Record (PICOR) forms. Body weights and tumour volumes were measured every Monday, Wednesday, and Friday. Animals remained on study until their tumours reached 800 mm^3 in size or they otherwise required euthanasia due to achieving a humane endpoint.

4T1 syngeneic bone metastasis model

Five to 6 weeks old C57black/6 female mice were maintained under isoflurane anesthesia and (5×10^5) 4T1-luciferase cells suspended in 100 µl of PBS solution were injected into the left ventricle under ultrasound guidance using a 30 gauge needle. The location of the tip of the needle in the left ventricle was confirmed by pulsatile blood flow in the hub of the needle. Animals were monitored until 8 weeks after injection using IVIS imaging system. Metastasis sites were collected at day of sacrifice and fixed in formalin for pathology studies.

Preparation of Drug Conjugate

To a solution of DBL1-ID2a (25.7 mg; 225 nmol) in ice cold PBS, pH 7.4 (34 ml) was added MTvc-KT886 (180 µl of a 10 mM dmso stock solution). The protein solution was mixed gently and allowed to stand on ice for a period of 70 min prior to concentration to a final volume of 12 ml by passage over an Amicon Ultra Centrifugal Filter (3000 xg; ~25 mins; 4°C; 50 kDa MWCO; Millipore product UFC905096). The concentrated protein solution was next purified over Zeba Spin Desalting Columns (40 kDa MWCO; 10 ml size; Thermo Scientific product 87772) preconditioned with sterile PBS. Concentration of the recovered materials was estimated by BCA assay using DBL1-ID2a as a standard. Composition and purity of the VDC were assessed by SDS-PAGE and SEC-UPLC-Esi-MS.

In vitro Cytotoxicity Assay of VAR2-Drug Conjugates using human Cancer Cell lines

Cells were removed from their culture vessel using Gibco® Trypsin-EDTA (Invitrogen # 25300-054). Detached cells were diluted in respective growth medium (Invitrogen #: 10313-021, A10491-01, 16600-082, 12561-056, 35050-061, 11415-064) + 10% Fetal bovine serum (Corning #: 35-015-CV) to 25000 cells/mL such that 100 µl/well will dispense 2500 cells/well. Cells were seeded into black walled, flat bottomed 96-well plates (Costar # 3904). Adherent cell lines cells were incubated for one night at 37 ^{0}C in a 5% CO2 atmosphere (No CO2 for MDA-MB-231) to allow the cells to attach to the microtitre plate surface, while suspension cells were seeded immediately before use. Test compounds were diluted directly in the appropriate cell growth medium at five-times the desired final concentration. These compounds were then titrated 1:3, over eight steps. A control with no test compound present (growth medium alone) was included on each microtiter plate in sextuplicate. 25 µl/well of the prepared titrations was added in triplicate to each cell line assayed. The cells and titrations were incubated at 37 ^{0}C / 5% CO2 for five nights. After the incubation, cell viability was measured using CellTiter-Glo® (Promega #G7572) reagent by adding thirty µl of prepared CellTiter-Glo® to each assay well. The mixtures were incubated for at least twenty min in the dark prior to measuring emitted luminescence using a microplate luminometer (500 ms integration time). The collected relative luminescence units (RLU) were converted to % cytotoxicity using the RLU values measured from the growth medium alone control as follows: % Cytotoxicity = 1 - [Well RLU/average medium alone control RLU]. Data (% Cytotoxicity vs. Concentration of

ADC (log10 [nM]) were plotted and were analyzed by non-linear regression methods using GraphPad Prism software v. 5.02 to obtain EC_{50} estimates.

***In vitro* toxicity assay using DT-VAR2**

The cells were seeded and incubated 3-5 days with toxin coupled rVAR2 or control protein. 400 µg/ml CSA was used as a specificity control. Following incubation, cells were washed in PBS and stained with Methylene Blue in Methanol or WST1 (Roche). Color was dissolved in 0.2 M Sodium Citrate in 50% Ethanol and quantified by absorbance at 450 nm. IC_{50} values were calculated as concentration of toxin at 50% survival. For a description of the in vitro tox assay using VCD886 please see supplementary methods.

Tolerability Study

Female CD-1 mice (Harlan Laboratories) were injected with the test articles and doses indicated in the figure legend using the housing/restraint/injection methods indicated above. Monitoring for acute toxicity effects was facilitated using the Post Injection Clinical Observation Record (PICOR) to assess morbidity and help determine humane endpoints. A PICOR was only completed for an animal in the event that a moribund animal was observed. Mice were monitored and weighed 3 times weekly for 12 days. Dose escalation occurred following favourable assessment of acute tolerability.

SUPPLEMENTAL REFERENCES

Della Peruta, M., Martinelli, G., Moratti, E., Pintani, D., Vezzalini, M., Mafficini, A., Grafone, T., Iacobucci, I., Soverini, S., Murineddu, M., et al. (2010). Protein tyrosine phosphatase receptor type {gamma} is a functional tumor suppressor gene specifically downregulated in chronic myeloid leukemia. Cancer research 70, 8896-8906.

Gautier, L., Cope, L., Bolstad, B.M., and Irizarry, R.A. (2004). affy--analysis of Affymetrix GeneChip data at the probe level. Bioinformatics 20, 307-315.

Hanly, A.M., Hayanga, A., Winter, D.C., and Bouchier-Hayes, D.J. (2005). Thrombomodulin: tumour biology and prognostic implications. Eur J Surg Oncol 31, 217-220.

Iozzo, R.V., and Sanderson, R.D. (2011). Proteoglycans in cancer biology, tumour microenvironment and angiogenesis. J Cell Mol Med 15, 1013-1031.

Janik, P., Briand, P., and Hartmann, N.R. (1975). The effect of estrone-progesterone treatment on cell proliferation kinetics of hormone-dependent GR mouse mammary tumors. Cancer Res 35, 3698-3704.

Kai, H., Kadono, T., Kakinuma, T., Tomita, M., Ohmatsu, H., Asano, Y., Tada, Y., Sugaya, M., and Sato, S. (2011). CCR10 and CCL27 are overexpressed in cutaneous squamous cell carcinoma. Pathol Res Pract 207, 43-48.

Larsson, A., Johansson, M.E., Wangefjord, S., Gaber, A., Nodin, B., Kucharzewska, P., Welinder, C., Belting, M., Eberhard, J., Johnsson, A., et al. (2011). Overexpression of podocalyxin-like protein is an independent factor of poor prognosis in colorectal cancer. Br J Cancer 105, 666-672.

Li, Q., Birkbak, N.J., Gyorffy, B., Szallasi, Z., and Eklund, A.C. (2011). Jetset: selecting the optimal microarray probe set to represent a gene. BMC Bioinformatics 12, 474.

Murakami, T., Cardones, A.R., and Hwang, S.T. (2004). Chemokine receptors and melanoma metastasis. J Dermatol Sci 36, 71-78.

Mythreye, K., and Blobe, G.C. (2009). Proteoglycan signaling co-receptors: roles in cell adhesion, migration and invasion. Cell Signal 21, 1548-1558.

Naor, D., Sionov, R.V., and Ish-Shalom, D. (1997). CD44: structure, function, and association with the malignant process. Adv Cancer Res 71, 241-319.

Pacheco, M., and Nielsen, T.O. (2012). Histone deacetylase 1 and 2 in mesenchymal tumors. Mod Pathol 25, 222-230.

Takacova, M., Bartosova, M., Skvarkova, L., Zatovicova, M., Vidlickova, I., Csaderova, L., Barathova, M., Breza, J., Jr., Bujdak, P., Pastorek, J., et al. (2013). Carbonic anhydrase IX is a clinically significant tissue and serum biomarker associated with renal cell carcinoma. Oncol Lett 5, 191-197.

Theocharis, A.D., Skandalis, S.S., Tzanakakis, G.N., and Karamanos, N.K. (2010). Proteoglycans in health and disease: novel roles for proteoglycans in malignancy and their pharmacological targeting. FEBS J 277, 3904-3923.

Uchida, T., Wada, K., Akamatsu, T., Yonezawa, M., Noguchi, H., Mizoguchi, A., Kasuga, M., and Sakamoto, C. (1999). A novel epidermal growth factor-like molecule containing two follistatin modules stimulates tyrosine phosphorylation of erbB-4 in MKN28 gastric cancer cells. Biochem Biophys Res Commun 266, 593-602.

Williamson, D., Selfe, J., Gordon, T., Lu, Y.J., Pritchard-Jones, K., Murai, K., Jones, P., Workman, P., and Shipley, J. (2007). Role for amplification and expression of glypican-5 in rhabdomyosarcoma. Cancer research 67, 57-65.

Wu, R., Duan, L., Ye, L., Wang, H., Yang, X., Zhang, Y., Chen, X., Weng, Y., Luo, J., Tang, M., et al. (2013). S100A9 promotes the proliferation and invasion of HepG2 hepatocellular carcinoma cells via the activation of the MAPK signaling pathway. Int J Oncol 42, 1001-1010.

Zhao, X.Y., Liu, H.L., Liu, B., Willuda, J., Siemeister, G., Mahmoudi, M., and Dinter, H. (2008). Tomoregulin internalization confers selective cytotoxicity of immunotoxins on prostate cancer cells. Transl Oncol 1, 102-109.

Sensing and Bio-Sensing Research 9 (2016) 23–30

Contents lists available at ScienceDirect

Sensing and Bio-Sensing Research

journal homepage: www.elsevier.com/locate/sbsr

Real-time and label free determination of ligand binding-kinetics to primary cancer tissue specimens; a novel tool for the assessment of biomarker targeting

Thomas Mandel Clausen [a,b,c,d,*], Marina Ayres Pereira [a,b], Htoo Zarni Oo [c,d,e], Mafalda Resende [a,b], Tobias Gustavson [a,b], Yang Mao [f,g], Nobuo Sugiura [h], Janet Liew [c,e], Ladan Fazli [c,e], Thor G. Theander [a,b], Mads Daugaard [c,d,e,**], Ali Salanti [a,b]

[a] Centre for Medical Parasitology at Department of Immunology and Microbiology, University of Copenhagen, Denmark
[b] Department of Infectious Diseases, Copenhagen University Hospital, Copenhagen, Denmark
[c] Vancouver Prostate Centre, Vancouver, BC V6H 3Z6, Canada
[d] Department of Urologic Sciences, University of British Columbia, Vancouver, BC, Canada
[e] Molecular Pathology and Cell Imaging Laboratory, Vancouver Prostate Centre, Vancouver, BC V6H 3Z6, Canada
[f] Copenhagen Center for Glycomics and Department of Cellular and Molecular Medicine, University of Copenhagen, Denmark
[g] Department of Biochemistry, Boston University School of Medicine, Boston, MA, USA
[h] Institute for Molecular Science of Medicine, Aichi Medical University, Japan

ARTICLE INFO

Article history:
Received 16 February 2016
Received in revised form 29 April 2016
Accepted 4 May 2016

Keywords:
Quartz crystal microscale
Biomarker
Biosensor
VAR2CSA
Cancer
Malaria

ABSTRACT

In clinical oncology, diagnosis and evaluation of optimal treatment strategies are mostly based on histopathological examination combined with immunohistochemical (IHC) expression analysis of cancer-associated antigens in formalin fixed paraffin-embedded (FFPE) tissue biopsies. However, informative IHC analysis depends on both the specificity and affinity of the binding reagent, which are inherently difficult to quantify *in situ*. Here we describe a label-free method that allows for the direct and real-time assessment of molecular binding kinetics *in situ* on FFPE tissue specimens using quartz crystal microbalance (QCM) enabled biosensor technology. We analysed the interaction between the rVAR2 protein and its placental-like chondroitin sulfate (pl-CS) receptor in primary human placenta tissue and in breast and prostate tumour specimens *in situ*. rVAR2 interacted with FFPE human placenta and cancer tissue with an affinity in the nanomolar range, and showed no detectable interaction with pl-CS negative normal tissue. We further validated the method by including analysis with the androgen receptor N-20 antibody (*anti*-AR). As the K_D value produced by this method is independent of the number of epitopes available, this readout offers a quantitative and unbiased readout for *in situ* binding-avidity and amount of binding epitopes. In summary, this method adds a new and important dimension to classical IHC-based molecular pathology by adding information about the binding characteristics in biologically relevant conditions. This can potentially be used to select optimal biologics for diagnostic and for therapeutic applications as well as guide the development of novel high affinity binding drugs.

1. Introduction

Cancer is a capital health problem in the modern world and therefore a major focus of modern medical research. Currently, diagnosis and disease management of most types of cancer is based on histopathological examination, combined with a molecular pathology analysis of primary tumour and potential metastatic lesions [3]. Classical molecular pathology analysis involves IHC evaluation of biomarkers that can inform on disease status and cancer subtype, as well as on molecular signatures able to guide therapy. The standard analysis is two-dimensional in the sense that the output only informs on expression intensity and pattern of the biomarker(s) in question. Nevertheless, molecular pathology assessment plays an important role in the diagnosis and disease management of several types of cancer. For example, IHC staining intensity and pattern of ErbB2/HER2 is widely used to guide treatment in human breast cancer [4,10,30]. In prostate cancer, the expression intensity and pattern of the androgen receptor (AR) is used

* Correspondence to: T.M. Clausen, Centre for Medical Parasitology, Bartholinsgade 2, 1356 Copenhagen, Denmark.
** Correspondence to: M. Daugaard, Vancouver Prostate Centre, Vancouver, BC V6H 3Z6, Canada.
E-mail addresses: tmc@sund.ku.dk (T.M. Clausen), mads.daugaard@ubc.ca (M. Daugaard).

http://dx.doi.org/10.1016/j.sbsr.2016.05.003

to predict the efficacy of *anti*-hormonal therapy [13]. However, the informative outcome of any molecular pathology analysis depends solely on the quality of the binding reagent and the avidity of the ligand-epitope interaction in *in situ*, which constitutes an inherent limitation of the method. Investigating the molecular characteristics of the interaction of a given targeting reagent with a biomarker could add extra information that would aid in disease diagnosis, patient stratification, as well as in evaluation for therapy [11].

Adding to the limited repertoire of informative tumour biomarkers, we have recently described a distinct chondroitin sulfate (CS) glycosaminoglycan (GAG) modification shared between the placental and malignant tissue compartments [27]. The observation was made in our work with placental malaria, in which infected erythrocytes express the VAR2CSA protein that allows them to anchor very specifically to a distinct type of CS in the placenta, thereby avoiding immune surveillance in the spleen [6,7,28]. Interestingly this distinct type of placental-like CS (pl-CS) is present on most cancer cells as well, while absent from normal tissue except placenta. This demonstrates the status of pl-CS as a cancer specific oncofetal antigen. pl-CS can be detected *in vitro*, *in vivo* and *in situ* using recombinant VAR2CSA proteins (rVAR2) [27]. The pl-CS modification is broadly present across multiple tumour types and the intensity of pl-CS tissue staining correlates with progression of malignant melanoma and predicts poor recurrence-free survival in non-small cell lung cancer patients [27]. Although a promising new cancer biomarker detection-reagent, rVAR2 is subject to the same limitations of standard molecular pathology analysis as any other established biomarker reagent, lacking important information on ligand-epitope binding avidity.

The Attana biosensor is an acoustic biosensor that measures changes in mass using the piezoelectric capacity of a quartz crystal (QCM technology) [17]. The change in mass per unit area on the crystal is directly proportional to the change in the crystals resonant frequency [29]. This allows for the use of the QCM technology as a microscale to measure small changes in mass, such as binding of an analyte to its immobilized ligand. More importantly, unlike surface plasmon resonance (SPR, Biacore [25,33]), which relies on the reflection of polarized light, the QCM platform is independent of the composition of the immobilized ligand. This technology therefore allows for the characterization of the binding and kinetic properties of a given analyte's interaction with a ligand in its native environment using fixed cells [18,23,24], and recently also live cells [16]. However, to date this has not been attempted for *in situ* FFPE tissue analysis of primary patient biopsies. Here, we present a method that adds a third dimension to classical two-dimensional molecular pathology assessment by incorporating a kinetic readout of analyte-ligand interactions *in situ* using QCM biosensor technology.

2. Materials and methods

2.1. Materials and reagents

Antibodies used for immunohistochemistry (IHC) and immunofluorescence (IF) were *anti*-AR rabbit polyclonal antibody (1:200, N-20, Santa Cruz, sc-816), *anti*-V5-FITC antibody (1:500, Life Technologies, 46–0308) and fluorescein *anti*-rabbit IgG antibody (1:500, Vector Laboratories, FI-1000).

2.2. Immunohistochemistry

Tissue stainings were performed using the Ventana Discovery platform. Sectioned paraffin embedded tissue samples were deparaffinized in EZ prep solution (Ventana) and stained with V5-tagged rVAR2 or *anti*-AR (N-20, Santa Cruz) antibody. In brief, tissue sections were incubated in Cell Conditioning 1 (CC1) or Cell Conditioning 2 (CC2) solution (Ventana) to retrieve antigen, followed by incubation with primary staining molecules. Bound rVAR2 was detected with an *anti*-V5 antibody, and an anti-mouse-HRP detection step. Bound antibodies were incubated with universal secondary antibody and visualized using Streptavidin-biotin peroxidase detection system and 3.3′-diaminobenzidine as chromogen.

2.3. Tissue immobilization

Attana COP-1 cartridges were disassembled to retrieve the COP-1 gold chip. The chip was coated in poly-L-lysine solution 5min at RT (Sigma) prior to tissue immobilization. The chip was rinsed in PBST and allowed to dry at RT for 2h. The FFPE tissue, tested positive for the given target in IHC, was macro-dissected at 5μm thickness on a microtome. The tissue was mounted on the chip and baked at 60°C for 1h.

2.4. Chip deparaffinization and antigen retrieval

The tissue chips were deparaffinized in EZ prep solution at 65°C in a water bath for 30min, and rinsed three times in PBS. Antigen retrieval was performed in 10mM sodium citrate, 0.05% Tween, pH 6 for 30min at 95°C. The chip was again rinsed three times in PBS. For AR experiments, the tissue was permeabilized in 0.5% saponin in PBS 10min at RT. For antibody experiments the chips were blocked in 1% BSA, 10% FBS in PBS for 1 h at RT. For rVAR2 experiments, the chips were blocked in Synblock (Immunochemistry Technologies) solution for 1h at RT. The treated tissue chips were mounted in the COP-1 cartridges, being very careful not to allow leakage of fluid to under the chip. In the optimization step the tissue was stained with ethidium bromide, and the integrity of the tissue was viewed in a top-down fluorescence microscope.

2.5. Cell chip preparation

Cells were seeded on COP-1 surfaces (Attana AB) at 80.000 cells in 700 uL of appropriate supplemented growth media. Following a 24h incubation at 37°C, 5% CO_2, the cells were fixed 10min in 4% PFA in PBS. The cells were washed in PBS and the cartridge was assembled, being careful of leakage. In the optimization step the cells were stained with ethidium bromide, and viewed in a top-down fluorescence microscope.

2.6. Purification of pl-CS from human placenta

5g of frozen placental tissue was minced and extensively washed with cold PBS. The tissue was then treated with 10mg collagenase type IV (Life Technologies) in 10mL PBS containing Ca^{2+} and Mg^{2+}, for 16h at 37°C. The resulting supernatant was cleared at 3000g for 10min. The pellet was further digested with Trypsin EDTA (Lonza) for 2h at 37°C. The resulting supernatant was cleared at 3000g for 10min. All the supernatants were combined and lyophilized. The dried extract was delipidated using a series of chloroform and methanol washes using 2:1, 1:1, 1:2 *v*/v ratios and dried at 55°C. The sample was then digested with 20mg Pronase (Roche) in 20mL 50mM Tris/HCl, pH7 and 5mM $CaCl_2$ for 16h at 50°C. After heat inactivation of the Pronase, 2mM $MgCl_2$ and 1000U Benzonase (Sigma-Aldrich) were added and the sample was incubated for 2h at 37°C. The sample was run on a DEAE column and eluded in 20mM NaOAc, pH 6, 1 M NaCl. The GAGs were precipitated in 3 volumes on ethanol 24h at 4°C. The precipitate was collected at 9000g for 30min and dried at 50°C. The dried sample was then resuspended in water and desalted using a PD-10 column (GE Healthcare). The sample was then treated with hyaluronidase from *Streptomyces hyalurolyticus* (Seikagaku Biobusiness Corporation, Japan), and A mixture of *Flavobacterium heparinum* heparin lyase I, II, and III in succession. The chondroitin sulfate was then precipitated in three volumes of ethanol, dried, and resuspended in water. The structure, purity and concentration was determined by MS.

2.7. Biotinylation of the pl-CS

Purified CS from the placenta was modified with an activated biotin reagent (sulfo-NHS-LC-biotin, Thermo-Pierce, Rockford, IL) at the amine group of the residual peptide left at the reducing end of CS chain after the trypsin digestion purification step. In Short the placental CS-peptide (100μg) in 50μL of 50mM phosphate buffer, pH 7.4, was mixed with the biotin reagent (1.0μmol) and incubated at room temperature for 2h. 5μL of 1M ethanolamine was then added to the mix and incubated at room temperature for 20min to terminate the reaction. The biotin-modified placental CS was purified on a Superose 12 HR 10/300 column (GE Healthcare, Piscataway, NJ) using 0.2M ammonium acetate as the eluent. The eluted product was finally freeze-dried three times. The placental CS-Biotin powder was resuspended in H_2O prior to use in experiments.

For immobilization of the purified biotinylated pl-CS on Biotin Chips a biotin chip (Attana AB) was allowed to stabilize in 10mM HEPES, 150mM NaCl, 0.005% Tween-20 at a flow rate of 100μL/min on the Attana Cell™ 200 instrument. The flow rate was lowered to 20μL/min and 100μg/mL streptavidin (Attana AB) was injected and allowed to interact with the surface. The pl-CS-biotin was then diluted to 50μg/ml and injected on the surface for immobilization.

2.8. Kinetic analysis

The chips were inserted in the Attana Cell 200 instrument (Attana AB) and allowed to stabilize in running buffer at 25μL/min (10μL/min for the AR experiments). The purified pl-CS experiment and tests of monoclonal antibodies were run in PBS. rVAR2 cell and tissue experiments were run in PBS containing Synblock diluted to 0.1× stock solution (Immunochemistry Technologies). Once stable, the baseline was verified with repeated injections of running buffer. The analyte to be tested was dissolved in the appropriate running buffer and diluted two-fold to yield the given concentration range. All injections were performed by the C-Fast autosampler (Attana AB). Baseline was checked between sample injections, by injections with running buffer. Blank injections were subtracted from the sample injections in the final analysis. The analytes were tested for reactivity against blank surfaces and against the given negative controls. The data was prepared using the Attana Attache software (Attana AB) and curve fitting was performed in the TraceDrawer software (Ridgeview Instruments) using the fit models given in Table 1. For some experiments a low level of background binding was accounted for by fitting a 1:2 model. Only the true high affinity values (K_D values) are listed in Table 1. For CSA inhibition, rVAR2 at a concentration of 100nM was pre-incubated with 400μg/mL bovine CSA (Sigma) and injected over the surface. For the verification of tissue adherence, rVAR2 was injected over the tissue surface until saturation. The lid on the COP-1 Cartridge was removed and the tissue incubated 30min with *anti*-V5-FITC (Invitrogen) at RT. The chip was washed and viewed under a top-down fluorescence microscope.

2.9. Immunofluorescence

The given cancer cell lines were seeded at a subconfluent concentration on glass slides and allowed to adhere at 37°C, 5% CO_2. The cells were then fixed in 4% PFA and washed in PBS. The cells were blocked for 1h at RT in 1% BSA, 5% FBS in PBS. The cells were then stained with V5 tagged rVAR2 or *anti*-AR (N-20, Santa Cruz) for 1h at RT in PBS containing 0.25% BSA. The cells were washed and incubated with *anti*-V5-FITC or anti-mouse-FITC in PBS containing 0.25% BSA. The slides were stained with DAPI, mounted, and viewed using confocal microscopy.

For the measurement of fluorescence intensity in the Attana chip rVAR2 detection on the prostate and tonsil tissues, 7 distinct areas of the tissue were selected and quantificated using the ImageJ software. Data is presented as Corrected Total Tissue Fluorescence (CTTF), for which the following formula was used, as described before: CTTF = Integrated density − (Area of selected region × Mean fluorescence of the background) [2,20]. Quantification shown represents one measured experiment.

2.10. Microscopy

A Nikon *C*1 confocal microscope with a 60× oil objective was used for imaging the IF cell stainings. A total of 5 representative pictures were taken per sample. Stainings were repeated twice. For analysis of the integrity of the immobilized tissue, a Leica DMLB with a Rolera-rx Fast 1394 camera and a 20× objective was used.

3. Results

3.1. Preparation of FFPE tissue specimens on QCM biosensor chips

Chips for the Attana QCM biosensor come with a wide variety of surfaces for the immobilization of different ligands to be analysed. Traditionally the kinetics of biomolecule interactions was studied with purified ligand immobilized on polystyrene or covalently linked through primary amines to reactive surfaces [22]. Recently, cells were grown on polystyrene chips optimized for cellular adherence (COP-1) and either fixed to the surface using PFA [8,23] or tested as live cells [16]. Our aim was to immobilize a piece of FFPE primary human tissue to the chip for subsequent binding analysis. The cell COP-1 chips are plasma-treated to become hydrophilic, which is optimal for cellular adherence. We macro-dissected a small circular piece of placental tissue, at a thickness of 5 μm and placed it in the middle of a COP-1 surface that was covered with Poly-L-Lysine prior to tissue immobilization (Fig. 1a).

The detection of protein targets in FFPE tissue requires removal of the paraffin matrix and often requires further treatment for the regeneration and availability of the target antigens. We performed deparaffinization in EZprep solution and antigen retrieval in 10mM sodium citrate, 0.05% tween, pH 6 [27]. The chips were visually inspected at each step to ensure the presence of the tissue on the chip.

Table 1
Curve fitting data for all QCM experiments. Listed is the tested analyte, the immobilized ligand, the model used for curve fitting in TraceDrawer, the obtained k_a, k_d, and K_D values, and the estimated error in that particular fit. NA depicts experiments for which no kinetic fit could be obtained due to no analyte binding. These are representative experiments of repeated setups.

	Sample	Fit model	K_a (1/M∗s)	K_d (1/s)	K_D (nM)	Est. Error (nM)
rVAR2	Placental tissue	1:2	9.2×10^4	3.9×10^{-4}	4.3	±0.01
	Prostate cancer tissue	1:1	12.7×10^4	11.3×10^{-4}	8.9	±0.06
	Tonsil tissue	NA	NA	NA	NA	NA
	Breast cancer tissue	1:2	7.9×10^4	5.3×10^{-4}	6.7	±0.3
	Purified placental CS	1:1	12.3×10^4	4.42×10^{-4}	3.6	0.05
	LNCap cells	1:2	9.4×10^4	5.2×10^{-4}	5.5	±0.0004
	SKBR3 cells	1:2	6.8×10^4	10.5×10^{-4}	15.6	±0.2
	CHO-s745A cells	NA	NA	NA	NA	NA
αAR	Prostate cancer tissue	1:2	13.0×10^4	13.1×10^{-4}	10	±0.04
	Placental tissue	NA	NA	NA	NA	NA
	LNCap cells	1:2	7.4×10^4	14.0×10^{-4}	18.9	±0.07
	PC3 cells	1:2	23.7×10^4	55.5×10^{-4}	23.5	±0.6

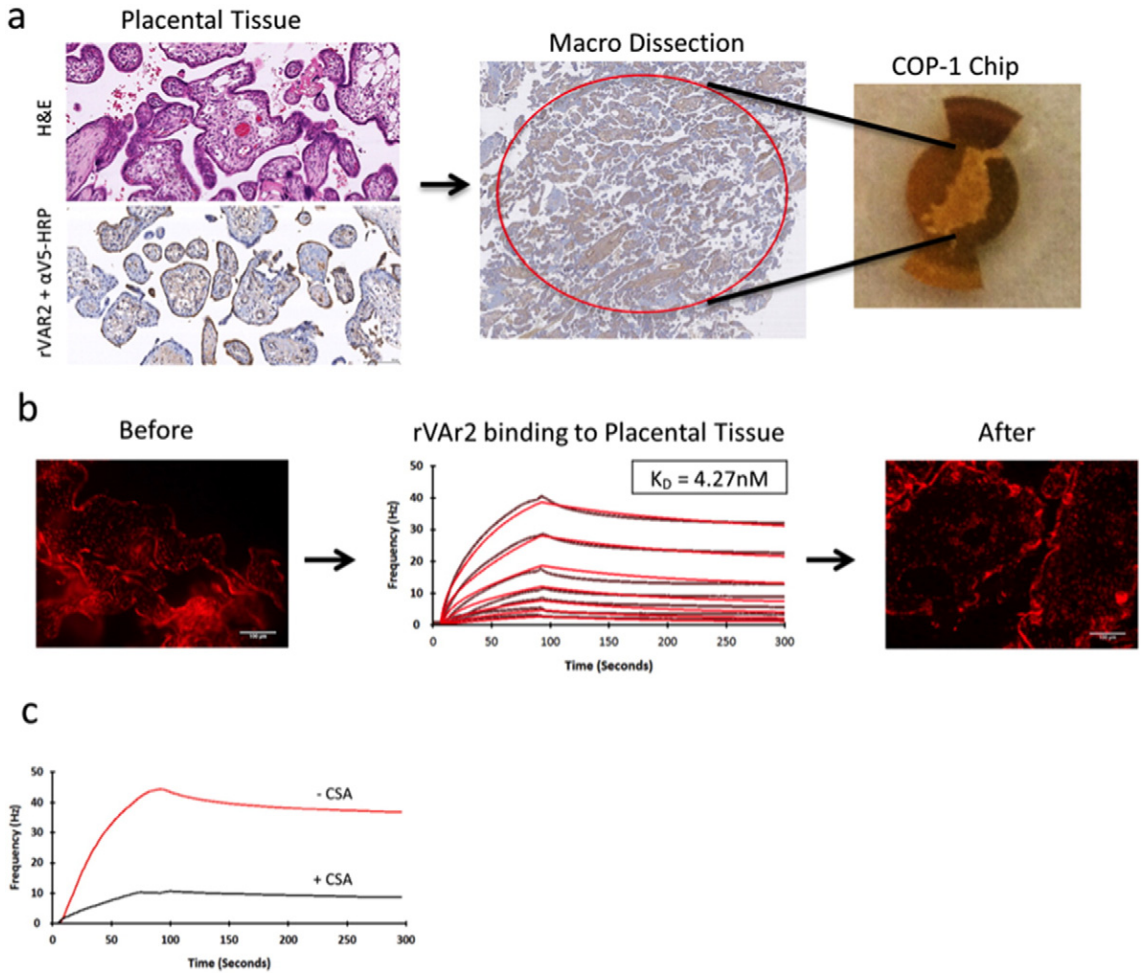

Fig. 1. Tissue immobilization, treatment, and initial test of rVAR2 binding. A) placental tissue tested positive for the presence of pl-CS using rVAR2 in IHC was cut and immobilized on a COP-1 chip. Both H&E staining and rVAR2 staining of matched tissue is shown B) Following tissue immobilization and treatment the placental tissue was tested for the interaction with rVAR2 (1:1 dilution 200nM–3.125 nM) in an Attana Cell 200 instrument. Curve fitting was performed in TraceDrawer. Black curve is original data, red is fitted data. The K_D value is listed. Tissue integrity was visualized with nuclear ethidium bromide staining before and after the experiment. C) rVAR2 was injected over an immobilized piece of placental tissue with and without pre-incubation with 400μg/mL soluble bovine CSA.

To test the availability of the pl-CS in the immobilized placental tissue we performed a binding experiment using a titration of rVAR2 protein (Fig. 1b). The integrity of the tissue was confirmed by visualizing the tissue with ethidium bromide DNA staining, before and after the binding experiment. rVAR2 highly interacted with the tissue with a K_D value of 4.3 nM. Furthermore, the interaction was CSA specific, as shown by the efficacy of inhibiting rVAR2 adhesion to the placental tissue with soluble CSA (Fig. 1c).

3.2. Affinity of the rVAR2:pl-CS interaction in primary tissue

We have shown that rVAR2 specifically interacts with pl-CS in the placenta and in most cancers, without binding CS on normal tissue [27]. This observation was mainly based on staining FFPE tissues with rVAR2 in IHC. We wanted to study the kinetics of the interactions and the relative abundance of pl-CS in patient-derived FFPE primary cancer tissue. For this purpose, we immobilized FFPE tissue from a prostate cancer and a breast cancer patient on COP-1 chips, and performed binding analysis with a titration of rVAR2 (Fig. 2a). A piece of tonsil tissue was used as the control for normal tissue. rVAR2 interacted to a high degree with both the prostate and breast cancer tissue with comparable K_D values (8.9 nM and 6.7 nM, respectively). As previously observed [27], rVAR2 staining of the tonsil tissue in IHC was very weak, with only a limited amount of focal staining (Fig. 2a). In accordance with this rVAR2 did not interact with the tonsil tissue immobilized on the chip, in real time. To confirm these results and verify that rVAR2 interacted with the tissue, we disassembled the prostate cancer and tonsil chips following an experiment and confirmed the presence and localization of rVAR2 binding using an *anti*-V5-FITC antibody (Fig. 2b and c). This showed an intense staining of the prostate cancer tissue with very limited signal seen on the tonsil chip.

To date, biosensor analysis has relied on the interaction between an analyte and an immobilized cell or purified receptor [5,8,16,22,23]. In line with this, we have previously investigated the interaction between several recombinant VAR2CSA proteins and immobilized bovine decorin [6,7], as well as the interaction of rVAR2 with a melanoma cell [27]. To verify the interaction between rVAR2 and the immobilized tissue, we performed the same analysis on purified placental-like CS and cancer cells of prostate and breast cancer origin (Fig. 3). We purified pl-CS from placenta, biotinylated it through the peptide remaining from protease treatment, and immobilized it on an Attana biotin chip. As with the tissue, rVAR2 interacted highly with the pl-CS on the surface in the same concentration range and with a comparable K_D value (3.6nM) (Fig. 3a). To further verify the interaction we cultured an AR positive prostate cancer cell line (LNCap), and a breast cancer cell line (SKBR3) on the surface of a COP-1 chip, fixed them in PFA, and subjected them to the same analysis. Both cell lines were shown positive for the presence of pl-CS by rVAR2 staining in IF (Fig. 3b). The interaction analysis was comparable between the two cells lines and the analysis performed on the tissues and the purified pl-CS (Fig. 3b). A CHO cell

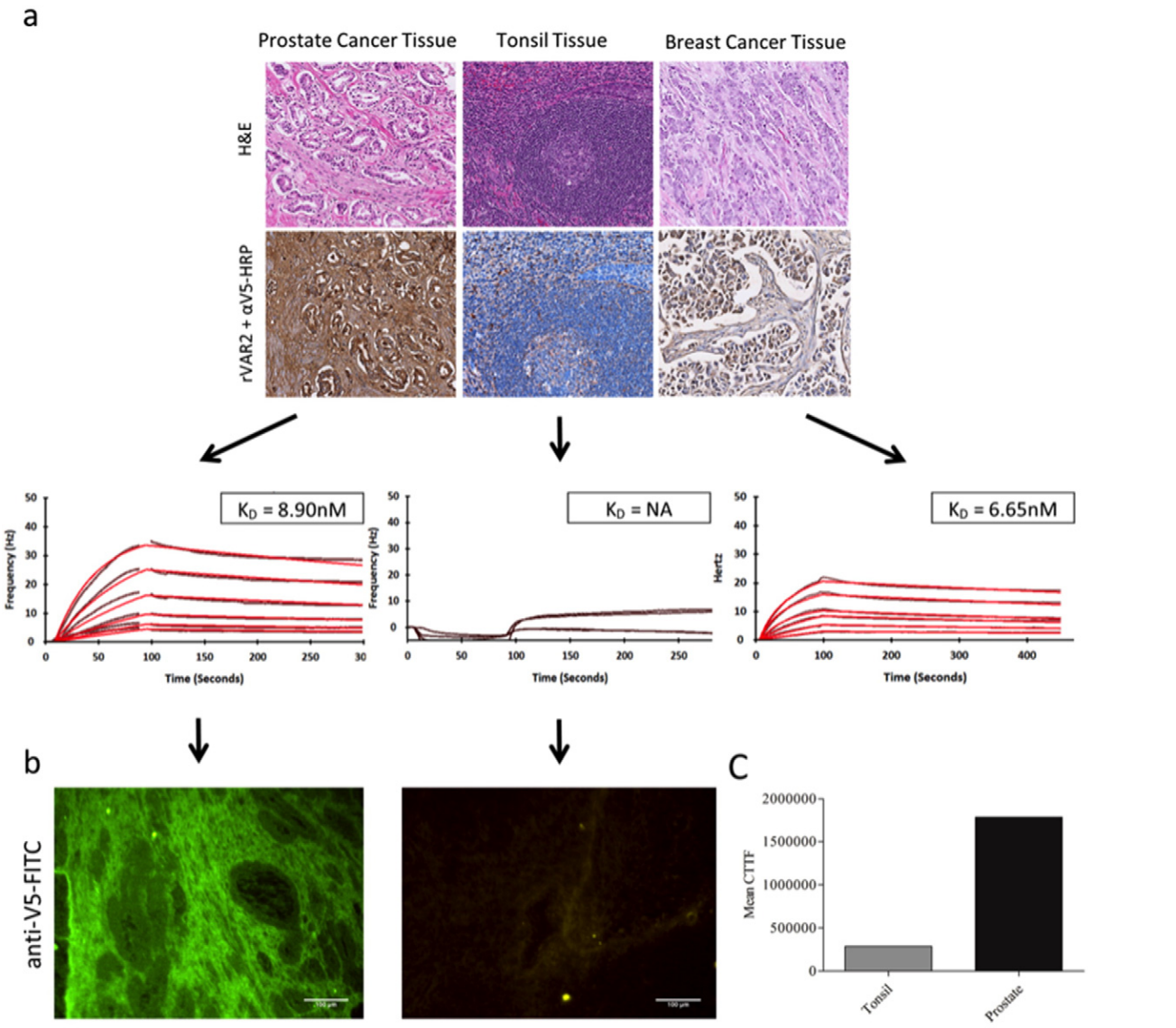

Fig. 2. Investigating the interaction between rVAR2 and pl-CS in cancer Tissue. A) Prostate cancer, breast cancer, and tonsil tissue were stained with rVAR2 in IHC. Both H&E staining and rVAR2 staining of matched tissue is shown. Matched tissue was immobilized on COP-1 surfaces and subjected to binding analysis with rVAR2 (1:1 dilution 200 nM–3.125 nM) in an Attana Cell 200 instrument. Curve fitting was performed in TraceDrawer. Black curve is original data, red is fitted data. The K_D value is listed. B) To further test the interaction a piece of prostate cancer or tonsil tissue, immobilized on a COP-1 chip, were saturated with rVAR2 in an Attana Cell 200 instrument. The chips were disassembled and the presence of v5 tagged rVAR2 was visualized with *anti*-V5-FITC. C) Quantification of fluorescence from 10 pictures taken of the chips in B).

selected for low xylotransferase activity (CHO-s745A) [9], and therefore low overall glycosaminoglycan (GAG) content, was used as the negative control for binding. This cell line was shown negative for the presence of pl-CS in IF, and was negative for the interaction with rVAR2 in the biosensor setup (Fig. 3b).

3.3. Affinity of an anti-AR antibody to prostate cancer tissue

To further extend the validation of the tissue biosensor setup, we selected a well-characterized cancer marker for which a validated monoclonal antibody is available. We analysed the interaction of the *anti*-Androgen Receptor (AR) N-20 antibody, used in the characterization of prostate cancer [13], with endogenous AR in cancer cells and in FFPE prostate cancer tissue. LNCap cells are known to express high levels of AR [21]. In accordance with this the LNCap cells was stained by anti-AR in IF and the anti-AR antibody interacted with the LNCap cells immobilized on a COP-1 surface, with a K_D value of 18.9 nM (Fig. 4a). Contrary to this PC3 cells, which are known to be androgen independent [32], showed very little AR staining in IF and a corresponding low level of interaction with the AR-antibody when immobilized on the biosensor chip (Fig. 4a). Having shown that the antibody worked in the biosensor setup, we selected an AR positive FFPE primary prostate cancer tissue biopsy, immobilized it on a COP-1 surface, and performed binding analysis on the Attana Cell 200. As with the rVAR2 analysis, interaction to the tissue was comparable to that of the immobilized AR positive cells (K_D value of 10 nM) (Fig. 4b). A piece of AR negative placental tissue showed no interaction with the AR antibody (Fig. 4c), confirming the target specificity. When comparing the peak responses measured in Hz between rVAR2 and *anti*-AR binding to the primary tissues it is evident that rVAR2 binding is up to 10 fold higher than the with the antibody.

4. Discussion

Discovery and characterization of cancer-associated markers effective in cancer diagnosis and treatment is a main focus in modern

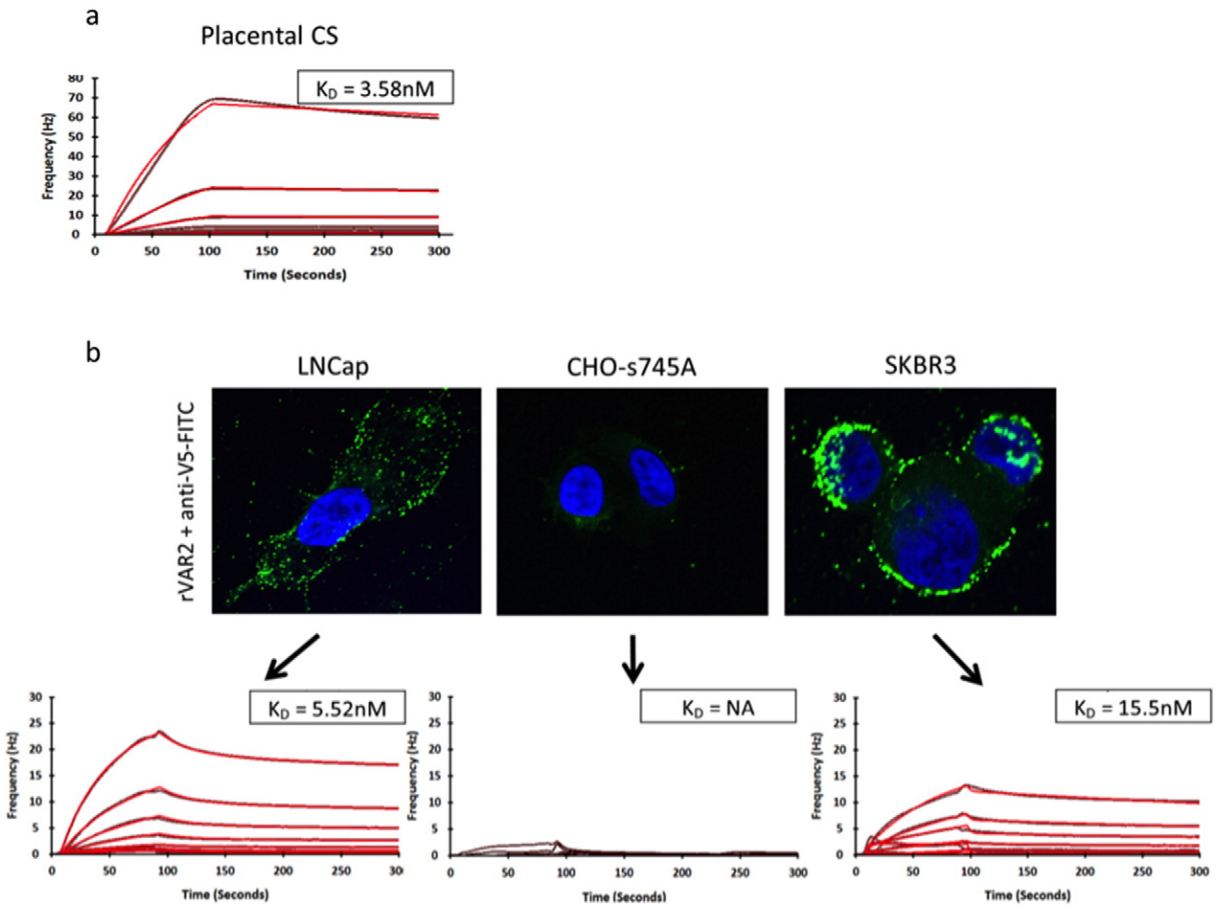

Fig. 3. Testing the interaction of rVAR2 with purified pl-CS and fixed cancer cell lines. A) pl-CS was purified from human placental tissue, biotinylated, and immobilized on an Attana biotin chip, and subjected to binding analysis with rVAR2 (1:1 dilution 200 nM–3.125 nM) in an Attana Cell 200 instrument. Curve fitting was performed in TraceDrawer. Black curve is original data, red is fitted data. The K_D value is listed. B) LNCap, SKBR3 and CHO-A745 cells were stained for pl-CS using V5 tagged rVAR2 in IF. The cells were then fixed on Attana COP-1 chips and subjected to binding analysis with rVAR2 (1:1 dilution 200 nM–3.125 nM) in an Attana Cell 200 instrument. Curve fitting was performed in TraceDrawer. Black curve is original data, red is fitted data. The K_D value is listed.

medicine. Several targets have been described [13,14]. Furthermore, we recently showed that the malarial VAR2CSA protein targets a specific type of placental-like chondroitin sulfate found in the placenta and on most cancer cells [27]. The field of medical science increasingly recognizes that a thorough molecular analysis of the biomarker recognition event is needed for full evaluation of a target for diagnostic and treatment purposes [11]. Such thorough analysis requires an in depth understanding of the molecular mechanism underlying the specific interaction as well as its kinetic properties. For this purpose scientists are utilizing a wide range of techniques including nuclear magnetic resonance (NMR) [12,26], mass-spectrometry (MS) [12], Enzyme-linked-immunosorbent-assay (ELISA), isothermal titration calorimetry (ITC) [15], and biosensor technology [1,5,19,22,24,31]. Common for these techniques is a requirement for the isolation and purification or recombinant expression of the target molecule. While these methods are valuable in describing a given biomarker and how to target it effectively, biomarker extraction is laborious and may interrupt key features only present in the biomarker's, or target's, native environment.

Current molecular pathology relies on the intensity and pattern of expression of the given biomarker using two-dimensional histopathological and IHC analysis. This work aims at adding an extra dimension of interaction time to classic pathology by performing kinetics of binding analysis directly on FFPE primary tissue specimens. We believe that this provides pathologists with a tool to evaluate disease specific targets not only by their presence and specific localization, but also by their molecular characteristics and how this relates to its direct interaction with a targeting molecule.

We macro-dissected out a small circular piece of paraffin-embedded tissue and put it on COP-1 Attana QCM chip surfaces. We then removed the paraffin and performed antigen retrieval. One problem was that the tissue did not stick sufficiently to non-treated COP-1 surfaces. A coating with poly-L-lysine was needed for proper immobilization. The antigen retrieval needed was optimized by IHC staining using the analytes in question. Subsequently, the tissue-coated chips were treated in an identical way, allowing for direct comparison. Since no light can go through the gold COP-1 surface, we visualized the immobilized tissue by a DNA stain and a fluorescent microscope before and after the experiments to ensure the integrity of the tissue. No change in morphology was seen, showing that the proposed method maintains proper tissue integrity for subsequent analysis. The exact epitope of recognition of the *anti*-AR (N-20) antibody and its molecular nature is not known. It is likely that antibody specific optimization on tissue treatments is needed to accommodate analysis of other antibodies, such as antibodies targeting conformational epitopes.

Having optimized the immobilization of the FFPE tissue, we performed binding experiments using rVAR2 and *Anti*-AR (N-20) monoclonal antibodies on tissues verified for the presence of the target antigen in question. All binding experiments were verified against appropriate cell lines, and in the case of rVAR2 also purified pl-CS. rVAR2 showed similar binding kinetics to purified placental-like CS, cell lines, and tissue. This confirms our strategy and supports the use of primary tissue for QCM experiments. It is common to evaluate specific binding in biosensor experiments by subtracting binding to a blank reference [25]. However, in working with immobilized cells and tissues we found

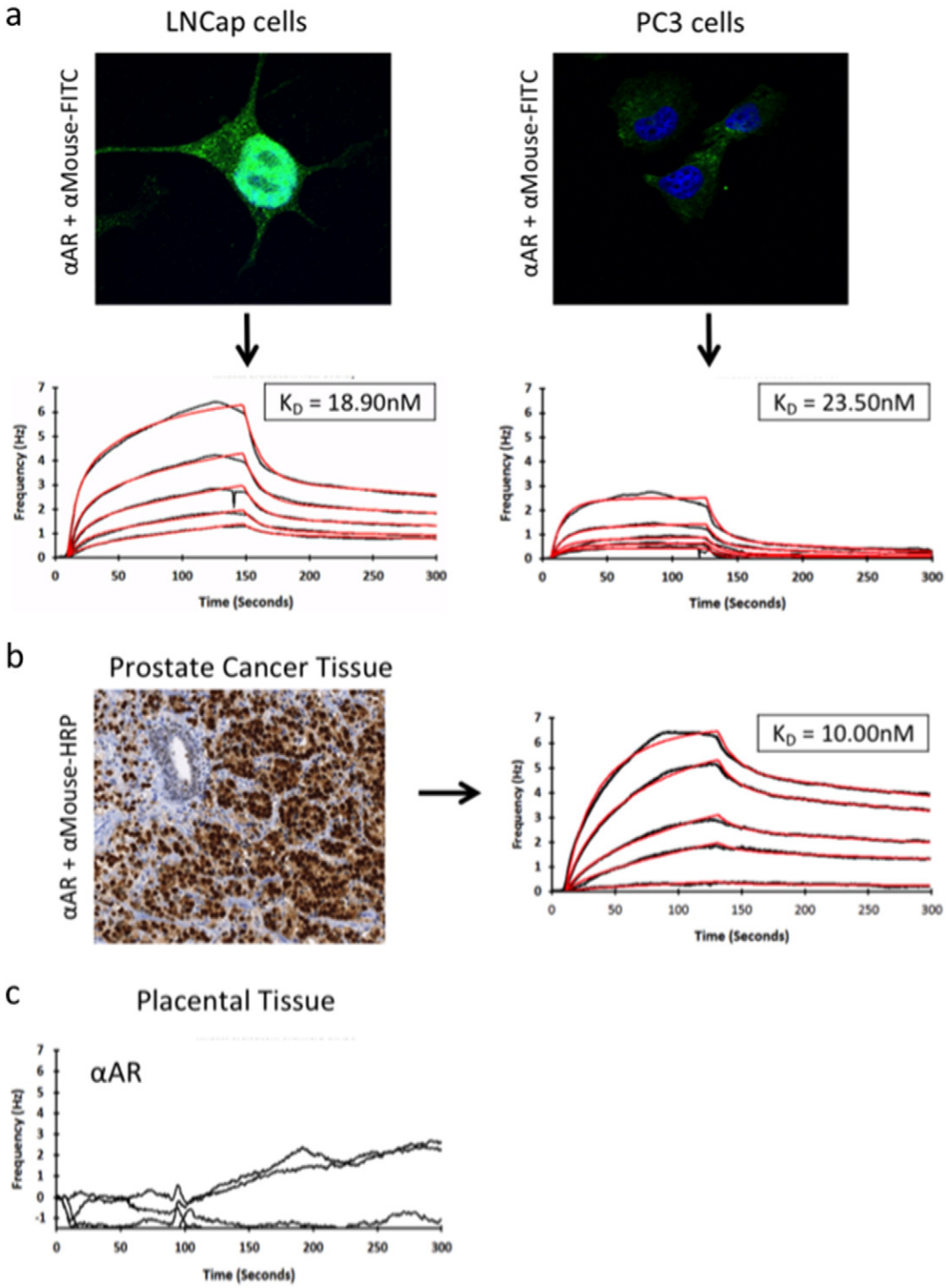

Fig. 4. Investigating the Interaction between clinically relevant monoclonal antibodies and their targets in Cancer Tissue. A) LNCap and PC3 cells were tested for the expression of AR by IF. The cells were fixed to an Attana COP-1 surface. The chips were then subjected to binding analysis with anti-AR (N-20, Santa Cruz) (1:1 dilution 200 nM–3.125 nM) in an Attana Cell 200 instrument. Curve fitting was performed in TraceDrawer. Black curve is original data, red is fitted data. The K_D values are listed. B) A piece of primary prostate cancer tissue was selected for high AR expression in IHC, and a matched piece of tissue was immobilized on a COP-1 surface. Kinetic analysis was performed as in A. C) A piece of primary placental tissue was immobilized on a COP-1 surface and subjected to kinetic analysis as in A. Curve fitting was not possible due to no binding.

that binding of an analyte to a blank chip is not representative of the background seen in binding to a chip coated with cells or tissues. When investigating the interaction between an analyte and a purified receptor in classic SPR, the surface area available for non-specific interactions on the chip can be considered comparable. This is not the case when investigating a chip covered in tissue or cells. Subtracting the signal from the reference chip therefore introduced a negative bias on the 'true' interaction, visualized as a negative spike in the real-time observation of the on-rate (Data not shown). Instead we selected cells and tissues negative for the ligand in question as proper negative controls, and presented them as separate figures to demonstrate the background independently. In this, rVAR2 did not interact with normal tissue (tonsil), confirming our previous observations that rVAR2 staining is placenta and cancer specific [27]. Furthermore, rVAR2 did not interact with the CS negative CHO-A475a cells and binding could be inhibited with soluble CSA, confirming the CS specificity. The analysis

of the AR interaction showed the same correspondence with AR expression in both cell line and tissue setups. It is notable that such analysis was possible using a nuclear target.

Interestingly the data shows that pl-CS is abundantly present in tumour tissue compared to AR. This is evident from the high difference in max binding responses, with the Bmax response for rVAR2 being up to 10 times higher. This difference is not obvious in the IF staining and IHC which with the inherent enzymatic horseradish peroxidase staining is difficult to accurately quantify. The concept of target quantity is interesting for cancer therapy as targeting an abundant target may offer a more efficient *anti*-cancer effect.

We demonstrate that this novel method can be broadly used to determine the relative presence of a cancer specific target as well as the affinity of the targeting reagent for its receptor. Implementation of the method has the potential to inform cancer diagnostics as well as provide an important tool for screening of high affinity targeting reagents in drug development, and aid in patient stratification, companion diagnostics and dosage determination during therapeutic treatment.

Contributions

T.M.C, A.S., M.D., and T.G.T., designed the research; T.M.C, M.A.P., H.Z.O., Y.M., N.S., M.R., and J.L., performed the experiments; L.F., provided useful reagents and helpful discussions; T.M.C., A.S, and M.D. wrote the manuscript.

Conflicts of interest

The authors declare no conflicts of interest.

Acknowledgements

The authors thank the European Research Council (ERC, Grant: MalOnko) and the U.S. Department of Defense (DoD, Grant: W81XWH1310139) for funding the research.

References

[1] B. Becker, M.A. Cooper, A survey of the 2006-2009 quartz crystal microbalance biosensor literature, J. Mol. Recognit. 24 (5) (2011) 754–787.
[2] A. Burgess, S. Vigneron, E. Brioudes, J.C. Labbe, T. Lorca, A. Castro, Loss of human Greatwall results in G2 arrest and multiple mitotic defects due to deregulation of the cyclin B-Cdc2/PP2A balance, Proc. Natl. Acad. Sci. U. S. A. 107 (28) (2010) 12564–12569.
[3] R.D. Cardiff, J.P. Gregg, J.W. Miller, D.E. Axelrod, A.D. Borowsky, Histopathology as a predictive biomarker: strengths and limitations, J. Nutr. 136 (10) (2006) 2673S–2675S.
[4] P. Carter, L. Presta, C.M. Gorman, J.B. Ridgway, D. Henner, W.L. Wong, A.M. Rowland, C. Kotts, M.E. Carver, H.M. Shepard, Humanization of an *anti*-p185HER2 antibody for human cancer therapy, Proc. Natl. Acad. Sci. U. S. A. 89 (10) (1992) 4285–4289.
[5] R. Chu, D. Reczek, W. Brondyk, Capture-stabilize approach for membrane protein SPR assays, Sci. Rep. 4 (2014) 7360.
[6] T.M. Clausen, S. Christoffersen, M. Dahlback, A.E. Langkilde, K.E. Jensen, M. Resende, M.O. Agerbaek, D. Andersen, B. Berisha, S.B. Ditlev, V.V. Pinto, M.A. Nielsen, T.G. Theander, S. Larsen, A. Salanti, Structural and functional insight into how the *Plasmodium falciparum* VAR2CSA protein mediates binding to chondroitin sulfate a in placental malaria, J. Biol. Chem. 287 (28) (2012) 23332–23345.
[7] M. Dahlback, L.M. Jorgensen, M.A. Nielsen, T.M. Clausen, S.B. Ditlev, M. Resende, V.V. Pinto, D.E. Arnot, T.G. Theander, A. Salanti, The chondroitin sulfate A-binding site of the VAR2CSA protein involves multiple N-terminal domains, J. Biol. Chem. 286 (18) (2011) 15908–15917.
[8] L. Elmlund, C. Kack, T. Aastrup, I.A. Nicholls, Study of the interaction of trastuzumab and SKOV3 epithelial cancer cells using a quartz crystal microbalance sensor, Sensors 15 (3) (2015) 5884–5894.
[9] J.D. Esko, T.E. Stewart, W.H. Taylor, Animal cell mutants defective in glycosaminoglycan biosynthesis, Proc. Natl. Acad. Sci. U. S. A. 82 (10) (1985) 3197–3201.
[10] B.M. Fendly, M. Winget, R.M. Hudziak, M.T. Lipari, M.A. Napier, A. Ullrich, Characterization of murine monoclonal antibodies reactive to either the human epidermal growth factor receptor or HER2/neu gene product, Cancer Res. 50 (5) (1990) 1550–1558.
[11] L. Gedda, H. Bjorkelund, L. Lebel, A. Asplund, L. Dubois, K. Wester, N. Penagos, M. Malmqvist, K. Andersson, Evaluation of real-time immunohistochemistry and interaction map as an alternative objective assessment of HER2 expression in human breast cancer tissue, Appl. Immunohistochem. Mol. Morphol. 21 (6) (2013) 497–505.
[12] G.L. Glish, R.W. Vachet, The basics of mass spectrometry in the twenty-first century, Nat. Rev. Drug Discov. 2 (2) (2003) 140–150.
[13] C.A. Heinlein, C. Chang, Androgen receptor in prostate cancer, Endocr. Rev. 25 (2) (2004) 276–308.
[14] C.A. Hudis, Trastuzumab–mechanism of action and use in clinical practice, N. Engl. J. Med. 357 (1) (2007) 39–51.
[15] J.E. Ladbury, Application of isothermal titration calorimetry in the biological sciences: things are heating up! Biotechniques 37 (6) (2004) 885–887.
[16] X. Li, S. Song, Q. Shuai, Y. Pei, T. Aastrup, Y. Pei, Z. Pei, Real-time and label-free analysis of binding thermodynamics of carbohydrate-protein interactions on unfixed cancer cell surfaces using a QCM biosensor, Sci. Rep. 5 (2015) 14066.
[17] G. Lippman, Ann. Chim. Phys. 5 (145) (1881).
[18] S.Y. Madani, A. Tan, M. Dwek, A.M. Seifalian, Functionalization of single-walled carbon nanotubes and their binding to cancer cells, Int. J. Nanomedicine 7 (2012) 905–914.
[19] S.Y. Madani, A. Tan, N. Naderi, A.M. Seifalian, Application of OctaAmmonium-POSS functionalized single walled carbon nanotubes for thermal treatment of cancer, J. Nanosci. Nanotechnol. 12 (12) (2012) 9018–9028.
[20] R.A. McCloy, S. Rogers, C.E. Caldon, T. Lorca, A. Castro, A. Burgess, Partial inhibition of Cdk1 in G 2 phase overrides the SAC and decouples mitotic events, Cell Cycle 13 (9) (2014) 1400–1412.
[21] S. Murthy, M. Wu, V.U. Bai, Z. Hou, M. Menon, E.R. Barrack, S.H. Kim, G.P. Reddy, Role of androgen receptor in progression of LNCaP prostate cancer cells from G1 to S phase, PLoS One 8 (2) (2013) e56692.
[22] Z. Pei, H. Anderson, T. Aastrup, O. Ramstrom, Study of real-time lectin-carbohydrate interactions on the surface of a quartz crystal microbalance, Biosens. Bioelectron. 21 (1) (2005) 60–66.
[23] Z. Pei, J. Saint-Guirons, C. Kack, B. Ingemarsson, T. Aastrup, Real-time analysis of the carbohydrates on cell surfaces using a QCM biosensor: a lectin-based approach, Biosens. Bioelectron. 35 (1) (2012) 200–205.
[24] D. Peiris, A. Markiv, G.P. Curley, M.V. Dwek, A novel approach to determining the affinity of protein-carbohydrate interactions employing adherent cancer cells grown on a biosensor surface, Biosens. Bioelectron. 35 (1) (2012) 160–166.
[25] R.L. Rich, D.G. Myszka, Advances in surface plasmon resonance biosensor analysis, Curr. Opin. Biotechnol. 11 (1) (2000) 54–61.
[26] G.C. Roberts, Applications of NMR in drug discovery, Drug Discov. Today 5 (6) (2000) 230–240.
[27] A. Salanti, T.M. Clausen, M.O. Agerbaek, N. Al Nakouzi, M. Dahlback, H.Z. Oo, S. Lee, T. Gustavsson, J.R. Rich, B.J. Hedberg, Y. Mao, L. Barington, M.A. Pereira, J. LoBello, M. Endo, L. Fazli, J. Soden, C.K. Wang, A.F. Sander, R. Dagil, S. Thrane, P.J. Holst, L. Meng, F. Favero, G.J. Weiss, M.A. Nielsen, J. Freeth, T.O. Nielsen, J. Zaia, N.L. Tran, J. Trent, J.S. Babcook, T.G. Theander, P.H. Sorensen, M. Daugaard, Targeting human cancer by a glycosaminoglycan binding malaria protein, Cancer Cell 28 (4) (2015) 500–514.
[28] A. Salanti, T. Staalsoe, T. Lavstsen, A.T. Jensen, M.P. Sowa, D.E. Arnot, L. Hviid, T.G. Theander, Selective upregulation of a single distinctly structured var gene in chondroitin sulphate A-adhering *Plasmodium falciparum* involved in pregnancy-associated malaria, Mol. Microbiol. 49 (1) (2003) 179–191.
[29] G. Sauerbrey, Verwendung von Schwingquarzen zur Wagung Dunner Schichten und zur Mikrowagung, Z. Phys. 155 (206) (1959).
[30] A.L. Schechter, D.F. Stern, L. Vaidyanathan, S.J. Decker, J.A. Drebin, M.I. Greene, R.A. Weinberg, The neu oncogene: an erb-B-related gene encoding a 185,000-Mr tumour antigen, Nature 312 (5994) (1984) 513–516.
[31] A. Stephenson-Brown, A.L. Acton, J.A. Preece, J.S. Fossey, P.M. Mendes, Selective glycoprotein detection through covalent templating and allosteric click-imprinting, Chem. Sci. 6 (9) (2015) 5114–5119.
[32] S. Tai, Y. Sun, J.M. Squires, H. Zhang, W.K. Oh, C.Z. Liang, J. Huang, PC3 is a cell line characteristic of prostatic small cell carcinoma, Prostate 71 (15) (2011) 1668–1679.
[33] S. Zeng, D. Baillargeat, H.P. Ho, K.T. Yong, Nanomaterials enhanced surface plasmon resonance for biological and chemical sensing applications, Chem. Soc. Rev. 43 (10) (2014) 3426–3452.

Molecular Cancer Research

Oncofetal Chondroitin Sulfate Glycosaminoglycans Are Key Players in Integrin Signaling and Tumor Cell Motility

Thomas Mandel Clausen[1,2,3,4], Marina Ayres Pereira[1], Nader Al Nakouzi[2,3], Htoo Zarni Oo[2,3,5], Mette Ø Agerbæk[1,2,3], Sherry Lee[2], Maj Sofie Ørum-Madsen[1,2], Anders Riis Kristensen[4], Amal El-Naggar[4], Paul M. Grandgenett[6], Jean L. Grem[7], Michael A. Hollingsworth[6], Peter J. Holst[1], Thor Theander[1], Poul H. Sorensen[4], Mads Daugaard[2,3,5], and Ali Salanti[1]

Abstract

Many tumors express proteoglycans modified with oncofetal chondroitin sulfate glycosaminoglycan chains (ofCS), which are normally restricted to the placenta. However, the role of ofCS in cancer is largely unknown. The function of ofCS in cancer was analyzed using the recombinant ofCS-binding VAR2CSA protein (rVAR2) derived from the malaria parasite, *Plasmodium falciparum*. We demonstrate that ofCS plays a key role in tumor cell motility by affecting canonical integrin signaling pathways. Binding of rVAR2 to tumor cells inhibited the interaction of cells with extracellular matrix (ECM) components, which correlated with decreased phosphorylation of Src kinase. Moreover, rVAR2 binding decreased migration, invasion, and anchorage-independent growth of tumor cells *in vitro*. Mass spectrometry of ofCS-modified proteoglycan complexes affinity purified from tumor cell lines on rVAR2 columns revealed an overrepresentation of proteins involved in cell motility and integrin signaling, such as integrin-β1 (ITGB1) and integrin-α4 (ITGA4). Saturating concentrations of rVAR2 inhibited downstream integrin signaling, which was mimicked by knockdown of the core chondroitin sulfate synthesis enzymes β-1,3-glucuronyltransferase 1 (B3GAT1) and chondroitin sulfate *N*-acetylgalactosaminyltransferase 1 (CSGALNACT1). The ofCS modification was highly expressed in both human and murine metastatic lesions *in situ* and preincubation or early intravenous treatment of tumor cells with rVAR2 inhibited seeding and spreading of tumor cells in mice. This was associated with a significant increase in survival of the animals. These data functionally link ofCS modifications with cancer cell motility and further highlights ofCS as a novel therapeutic cancer target.

Implications: The cancer-specific expression of ofCS aids in metastatic phenotypes and is a candidate target for therapy.
Mol Cancer Res; 14(12); 1–12. ©2016 AACR.

Introduction

Glycosaminoglycans are secondary carbohydrate modifications attached to proteoglycans on the cellular plasma membrane or secreted into the extracellular matrix (ECM). During embryogenesis, cell differentiation, and diseases, such as cancer, glycosaminoglycans display radical changes in expression and composition (1–3). Alterations in the glycosaminoglycan component of proteoglycans have been reported in cancer for more than 4 decades (4–7). As part of the cellular glycocalyx, glycosaminoglycans are believed to control the information flow from the ECM to signal transduction pathways stemming from the plasma membrane (8). While the function and mechanistic contribution of glycosaminoglycans in cancer are not fully understood, it is clear that they act as key regulators of the malignant phenotype (9).

Most cancer cells express a distinct chondroitin sulfate glycosaminoglycan epitope that is normally restricted to trophoblastic cells in the placenta (10). These oncofetal chondroitin sulfate (ofCS) chains, previously termed placental-type chondroitin sulfate, are expressed on chondroitin sulfate–modified proteoglycans (CSPG) of tumor and tumor-infiltrated stromal cells across multiple types of malignancies, indicating a possible broad functional importance of ofCS for the disease pathology (10). CSPGs have been associated with proliferation, migration, invasion, angiogenesis, and metastasis (11–15). In these processes, CSPGs act either alone or in concert with membrane components such as integrins, receptor tyrosine kinases (RTK), or metalloproteases to aid cellular attachment, migration, and invasion (16–19). One well-described function of chondroitin sulfate on proteoglycans is to capture growth

[1]Centre for Medical Parasitology at Department of International Health, Immunology and Microbiology, University of Copenhagen, Denmark. [2]Vancouver Prostate Centre, Vancouver, British Columbia, Canada. [3]Department of Urologic Sciences, University of British Columbia, Vancouver, British Columbia, Canada. [4]Department of Molecular Oncology, British Columbia Cancer Research Centre, Vancouver, British Columbia, Canada. [5]Molecular Pathology and Cell Imaging Laboratory, Vancouver Prostate Centre, Vancouver, British Columbia, Canada. [6]Eppley Institute for Research in Cancer and Allied Diseases, University of Nebraska Medical Center, Omaha, Nebraska. [7]Department of Internal Medicine, University of Nebraska Medical Center, Omaha, Nebraska.

Note: Supplementary data for this article are available at Molecular Cancer Research Online (http://mcr.aacrjournals.org/).

Corresponding Authors: Thomas Mandel Clausen, Centre for Medical Parasitology, University of Copenhagen, Bartholinsgade 2, Copenhagen 1356, Denmark. Phone: 454-237-8174; Fax: 454-237-8174; E-mail: tmc@sund.ku.dk; Mads Daugaard, mads.daugaard@ubc.ca; and Ali Salanti, salanti@sund.ku.dk

doi: 10.1158/1541-7786.MCR-16-0103

factors and cytokines and present them to adjacent receptors in the membrane. As such, chondroitin sulfate can act as a scaffold or reservoir for sustained proliferative and oncogenic signaling (20–24). Glycosaminoglycans are made up of repeated disaccharide units making up long, linear polymers. Chondroitin sulfate consists of alternating glucuronic acid (GlcA) and *N*-acetyl-D-galactosamine (GalNac) residues (24). While the base structure is simple, heterogeneity is achieved through secondary modification of the chondroitin sulfate carbohydrate backbone, such as alternate sulfation of hydroxyl groups (25). Erythrocytes infected with malaria parasites expressing the VAR2CSA protein adhere to chondroitin sulfate only in the placenta, despite the fact that chondroitin sulfate is present in most organs of the human host (24, 26–28). This suggests that chondroitin sulfate in the placenta is distinct from chondroitin sulfate present in other organs. The interaction between malarial VAR2CSA and the placenta is the key molecular event underlying placental malaria (26, 28).

The ofCS motif on cancer and placental cells can be detected using a 72-kDa recombinant fragment of the *Plasmodium falciparum* VAR2CSA protein (rVAR2; refs/ 10, 29). VAR2CSA is a large complex multidomain protein (28). The 72-kDa functional chondroitin sulfate–binding domain ID1–ID2a has an unprecedented high specificity and affinity for 4-*O*-sulfated chondroitin sulfate (C4S; refs. 29, 30).

Using rVAR2 as an ofCS-binding reagent, we have investigated the role of ofCS in human cancer. We report that ofCS is required for cellular attachment, migration, and invasion of tumor cells *in vitro* and *in vivo*. Furthermore, we identify a number of proteins that are modified or associated with ofCS in human tumor cells including components of the integrin complexes. Our study confirms a pivotal role for ofCS in integrin-mediated signaling and supports current efforts using rVAR2 as a broad therapeutic targeting reagent against ofCS in cancer.

Materials and Methods

Reagents and cell culture

Recombinant proteins were expressed in SHuffle T7 Express Competent *Escherichia coli* (NEB) and purified using HisTrap columns from GE Healthcare followed by size exclusion chromatography, as previously described (10). Purified monomeric proteins were validated by SDS-PAGE. Purified chondroitin sulfate A (CSA) was obtained from Sigma. Anti-V5-FITC antibodies were obtained from Invitrogen. Most cell lines were obtained from ATCC and grown in their suggested growth media with 1× penicillin and streptomycin cocktail. The Myla2059 Lymphoma cell lines were donated by Niels Ødum at the University of Copenhagen (Copenhagen, Denmark). Mice for animal studies were acquired from Taconic Biosciences.

ECM-binding assay

Cells were grown in 10-cm dishes to about 70% confluency. The cells were then serum-starved in the presence of 450 nmol/L rVAR2, rDBL4 (a non–ofCS-binding domain of the VAR2CSA protein) or PBS for 18 to 24 hours. The cells were collected using Cellstripper, counted, and adjusted to 0.2×10^6 cell/mL in serum-free media containing inhibitor as above. One hundred microliters was added to wells in a 96-well plate coated with fibronectin (10 μg/mL, Sigma), collagen-I (23 μg/mL, Sigma), collagen IV (23 μg/mL, Sigma), or uncoated plastic. Plastic blocked with BSA was included as a negative control. All samples were run in triplicates. Following a 25-minute incubation, the adherent cells were stained with methylene blue in methanol for 10 minutes. The plates were washed in water and dried. The color was dissolved in 0.2 mol/L sodium citrate in 50% ethanol and absorbance was read at 650 nm.

Scratch assay

Cells were seeded into 6-well plates and allowed to grow to confluency. The cells were then washed in PBS and serum-starved for 24 hours in the presence of 450 nmol/L rVAR2, rDBL4, or PBS. CSA (400 μg/mL; Sigma) was used to outcompete rVAR2 effect. A scratch was made in the cell monolayer with a 20-μL pipette tip. The cells were washed in PBS and serum-free media containing the inhibitors was added. Pictures were taken at 0, 19, 30, and 46 hours at 2 fixed points per sample.

For the siRNA experiments, MG63 cells were transfected with siRNAs (Qiagen; 50 nmol/L final) against CSGALNACT1, using RNAiMAX (Invitrogen). Scratch was made 48 hours after transfection.

Boyden chamber invasion and migration assays

The cells were grown to 70% confluency. They were then serum-starved in the presence of 450 nmol/L rVAR2 or rDBL4 for 24 hours. The cells were dislodged with Cellstripper and counted 3 times. Then, 100,000 cells were added to each insert of a Boyden chamber plate (Chemi-Con). Separate kits were used for migration and invasion. Invasion kit included membranes coated in basement membrane extract. Media with or without chemoattractant were added to the lower well. Plates were then incubated for 18 to 36 hours at 37°C. The number of migrating cells was determined by a fluorescent probe and compared to a standard curve.

Identification of ofCS-conjugated CSPGs

Column-based pull down. Membrane proteins were extracted with EBC lysis buffer (150 mmol/L NaCl, 50 mmol/L Tris-HCl, 2.5 mmol/L MgCl2, 1 mmol/L EDTA, 1% CHAPS, and a protease inhibitor cocktail; Roche). The lysate was loaded onto a Hitrap NHS HP column (GE) containing immobilized rVAR2 or rContrl (rDBL4) control protein. The column was washed in lysis buffer as well as lysis buffer containing 250 mmol/L NaCl. Bound protein was eluded with 0.5 mol/L NaCl in lysis buffer and Upconcentrated on a Vivaspin Column (MWCO; 10,000 kDa). Protein samples, dissolved in SDS loading buffer, and a high-molecular-weight marker (LC5699, Life Technologies) were loaded onto a NuPAGE Tris-acetate gel (Life Technologies). Proteins were subsequently transferred to a nitrocellulose membrane overnight at 4°C at 75 mA. The membranes were stained with anti-CSPG4 antibody (LHM2, Abcam) or antibodies against the α4-, α5-, or β1-integrin subunits. The staining was developed in ECL and scanned.

Bead-based pull down. Membrane proteins were extracted in EBC lysis buffer (150 mmol/L NaCl, 50 mmol/L Tris-HCl, 2.5 mmol/L MgCl2, 1 mmol/L EDTA, 1% CHAPS, and a protease inhibitor cocktail; Roche). Biotinylated rVAR2 protein was added to the lysate and the mix was incubated overnight at 4°C. The rVAR2 and bound protein were pulled down on streptavidin dynabeads (Invitrogen).

Proteomics. The pulled-down material was dissolved in nonreducing LDS loading buffer (Invitrogen), reduced in 1 mmol/L dithiothreitol (DTT), and alkylated with 5.5 mmol/L iodoacetamide. The samples were then run 1 cm into Bis–Tris gels and stained with Coomasie Blue. The protein was cut out, washed, and in-gel digested with trypsin. The resulting peptides were captured and washed using C18 resin. The peptides were sequenced using a Fusion Orbitrap Mass Spectrometer. Sample analysis and hit verification were performed using the MaxQuant software. All samples were verified against control samples being either a control protein coupled columns or empty beads. For the Ingenuity Pathways Analysis (IPA), proteins that were found to be significantly different between rVAR2 and rControl were analyzed using the IPA software (Quiagen) against their involvement in cellular function and disease.

Proximity ligation analysis

The proximity ligation analysis (PLA) experiment was done according to the manufacturer's guidelines (Sigma). In short, adherent cells were fixed in 4% paraformaldehyde. The cells were blocked in 1% BSA and 5% FBS in PBS. The cells were then stained with primary antibodies together with rVAR2 or rDBL4 overnight in these concentrations: rVAR2 (50 nmol/L), anti-integrin-α4 (MAB16983; 1:100), anti-integrin-α5 (H-104, sc-10729; 1:50), anti-NG2 (LHM 2, ab20156; 1:400), anti-panCD44 (2C5, BBA10; 1:400) anti-integrin-β1 (EP1041Y, ab52971; 1:200), and anti-integrin-β1 antibody (4B7R, sc-9970; 1:50). Cells were washed in Wash Buffer A (DUO82047) between incubations. An anti-V5 (mouse or rabbit) antibody was used for rVAR2 detection. The cells were then stained with Duolink In Situ PLA Probe Anti-Mouse MINUS (DUO92004) and Duolink In Situ PLA Probe Anti-Rabbit PLUS (DUO92002) diluted in Antibody Diluent (DUO82008). The cells were then treated with the ligation solution, followed by incubation with the amplification solution. Both reagents were provided with the kit Duolink In Situ Detection Reagents Orange (DUO92007). The cells were washed with Wash Buffer B (DUO82048). Slides were mounted using Duolink In Situ Mounting Medium with DAPI (DUO82040). Results were analyzed under a Nikon C1 confocal microscope with a 60× oil objective. A total of 75 to 100 cells were imaged per sample. The images were analyzed using the BlobFinder software (version 3.2.).

Flow cytometry–binding analysis

Cells were grown to 70% to 80% confluency and harvested using Cellstripper. Cells (200,000) were added to each well in a 96-well plate. All incubations were in PBS containing 2% FBS. Cells were incubated with protein (400 nmol/L–25 nmol/L) for 30 minutes at 4°C. Cells were washed 2 times and incubated with secondary antibody (anti-V5-FITC) for 30 minutes at 4°C, washed 2 times, and analyzed in a FACSCalibur (BD Biosciences) for FL-1 signal intensity. Results were analyzed using the FlowJo software.

Signaling stimulation assays

Cells were seeded into 6-well plates and allowed to adhere overnight. The cells were washed in PBS and serum-starved in the presence of 450 nmol/L rVAR2 or rDBL4 control for 18 to 24 hours. The cells were stimulated with 1% to 3% FBS, 5 μg/mL fibronectin (Sigma), or 10 to 80 μg/mL fibronectin CS1 peptide (GeneArt) for the given timepoints. The cells were put on ice, washed 3 times in PBS, and lysed in EBC lysis buffer, containing 0.5% NP40 and phosphatase and protease inhibitor cocktails (Roche). The samples were balanced on protein concentrations (Bradford assay). The samples were run in Western blotting and probed for the indicated phosphoproteins. For total protein determination, the membranes were stripped and reprobed with antibodies for the indicated proteins.

For the siRNA experiments, cells were transfected with siRNAs (Qiagen; 10 nmol/L final) against B3GAT1 and CSGALNACT1, using RNAiMAX (Invitrogen) and analyzed for rVAR2 binding by flow cytometry and for mRNA expression by RT-PCR, following 72-hour exposure. The evaluation of intracellular signaling in these cells was performed as described above.

The adhesion signaling experiments were performed as follows. The cells were grown to 70% confluency in 10-cm dishes. They were serum-starved 18 to 24 hours prior to the assay in the presence of 450 nmol/L rVAR2 or rDBL4. The cells were dislodged in Cellstripper, counted, and seeded into the wells of a 6-well plate for 120 minutes. Cell lysates were collected and analyzed as described above.

Antibodies used were: α-phospho-Erk1/2 (thr202/tyr204; Cell Signaling, 9101), α-Erk 1/2 (Cell Signaling, 9102), α-Src (Cell Signaling, 2108), α-phospho-Src (Tyr416; Cell Signaling, 2101), α-Akt (Cell Signaling, 9272), α-phospho-Akt (Thr308; Cell Signaling, 2965), α-FAK (Cell signaling, 3285), α-phospho-P130Cas (Tyr410; Cell Signaling, 4011), and α-p130Cas (Santa Cruz, sc-20029).

Tissue samples and immunohistochemistry

A tissue microarray (TMA) containing 38 patients with primary human pancreatic cancer and corresponding metastatic tissues, as well as control normal pancreas, was obtained from the UNMC Rapid Autopsy Pancreas (RAP) program and stained using the Ventana Discovery platform. Sectioned, paraffin-embedded TMA was stained with 500 picomolar V5–tagged recombinant VAR2CSA (rVAR2) without antigen retrieval followed by 1:700 monoclonal anti-V5 step and an anti-mouse-HRP detection step. Mounted and stained TMA was subsequently scored for membranous staining intensity on a 0–3 scale. Score 2 reflects a staining intensity equal to that of placenta (included as a positive control in each staining run). Expression is considered "low" when ofCS expression is present only in cellular or stromal compartment with intensity score 1 and considered "high" when ofCS expression is present either in cellular or stromal compartment or both with intensity score 2 or 3.

Immunocytochemistry

We obtained formalin-fixed, paraffin-embedded (FFPE) slides of metastatic lesions in murine allografts, created by injecting C57BL/6 mice with 4T1 mammary tumor cells in the left cardiac ventricle, in the animal model (published in ref. 10). The slides were deparaffinized and stained with rVAR2-Alexa488. The staining of ofCS was visualized using confocal microscopy.

Animal studies

The methodologies described were reviewed and approved by the Institutional Animal Care Committee (IACC) at the University of British Columbia (Vancouver, BC, Canada) and the animal experiments inspectorate at the University of Copenhagen before conducting the study. During the study, the care, housing, and use of animals were performed in accordance with the Canadian Council on Animal Care Guidelines and the Danish animal experiments inspectorate guidelines.

For the Lewis lung carcinoma seeding model, 5- to 6-week-old C57black/6 female mice were maintained under isoflurane anesthesia and 5×10^5 Lewis luciferase cells suspended in 100 μL of 100 nmol/L of rVAR2 or saline solution were injected into the left ventricle under ultrasound guidance using a 30-gauge needle. The location of the tip of the needle in the left ventricle was confirmed by pulsatile blood flow in the hub of the needle. Animals were monitored until 7 weeks after injection using IVIS imaging system. Metastasis sites were collected at day of sacrifice and fixed in formalin for pathology studies. Mice were sacrificed when they reached the predefined humane end point.

For the B16 melanoma model, 5×10^5 B16-F10GP cells in 100 μL PBS were injected into the right flank of C57BL/6 mice. The animals were randomized into 2 groups of 10 mice. One group was treated by intravenous injection of 100 μg rVAR2 at days 0, 6, and 9. The control group was treated with equal volume PBS. Tumor size was monitored by manual measurements using a caliper-measuring tool, taking measurements at the 2 longest perpendicular axes in the x/y plane of each tumor. Tumor volume was calculated according to the standard formula: volume $= xy^2 \times 0.5236$ (31).

Statistical methods

Correlations between clinicopathologic parameters and ofCS expression were analyzed by the Fisher exact test. $P < 0.05$ was considered statistically significant. Statistical analyses were performed with GraphPad Prism (version 6, GraphPad Software, Inc.). Survival of mice was analyzed by Kaplan–Meier survival plot. Statistical significance was determined with Prism GraphPad version 6.0 using the log-rank (Mantel–Cox) test (χ^2: 3.84; $P < 0.05$).

Results

rVAR2 blocks cellular adhesion to ECM components

We have shown that placental and tumor cells share the expression of a placental-type chondroitin sulfate now designated ofCS (10). The expression of this modification in human cancers suggests a pivotal role for ofCS in malignant disease. On the basis of the preliminary observation that cellular attachment of tumor cells to normal culture flask plastic surfaces was impaired after rVAR2 incubation, we hypothesized that ofCS may play a role in cell motility. To test our hypothesis, we investigated whether rVAR2 targeting of ofCS on U2OS and MG63 osteosarcoma cells would block cellular adhesion to plastic (PL), fibronectin (FN), and collagens I (CI) and IV (CIV). While different binding preferences for individual ECM components could be observed, both cell lines displayed a significant reduction in adhesion to fibronectin, collagen I, and collagen IV (Fig. 1A and B). The same was true for cell lines representing other cancers, such as RH30 rhabdomyosarcoma cells (Fig. 1C) and MDA-MB-231 breast

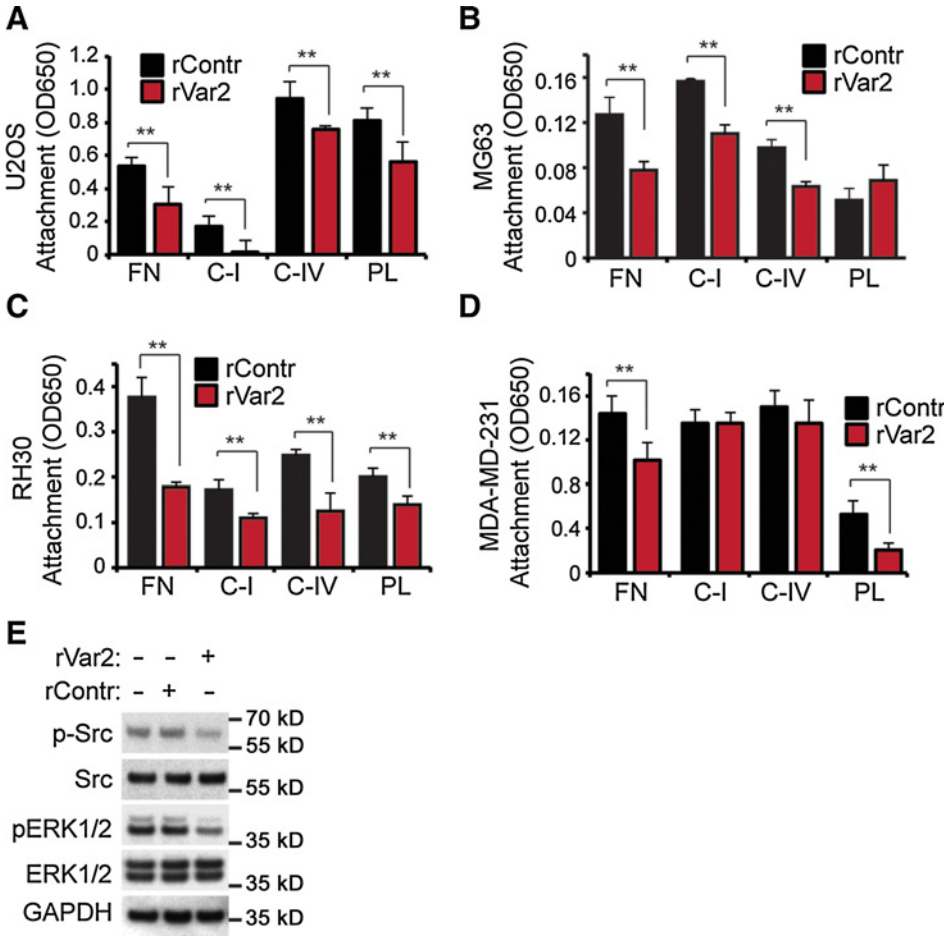

Figure 1.
rVAR2 impedes attachment and detachment mechanics in tumor cells. **A,** U2OS cells were preincubated with rVAR2 and tested for their capacity to adhere to fibronectin (FN), collagen I (C-I), collagen IV (C-IV), and plastic (PL). Adherent cells were stained with methylene blue and quantified by reading absorbance at 650 nm. **B,** MG63 cells were preincubated with rVAR2 and tested for their capacity to adhere to fibronectin (FN), collagen I (C-I), collagen IV (C-IV), and plastic (PL). Adherent cells were stained with methylene blue and quantified by reading absorbance at 650 nm. **C,** RH30 cells were preincubated with rVAR2 and tested for their capacity to adhere to fibronectin (FN), collagen I (C-I), collagen IV (C-IV), and plastic (PL). Adherent cells were stained with methylene blue and quantified by reading absorbance at 650 nm. **D,** MDA-MB-231 cells were preincubated with rVAR2 and tested for their capacity to adhere to fibronectin (FN), collagen I (C-I), collagen IV (C-IV), and plastic (PL). Adherent cells were stained with methylene blue and quantified by reading absorbance at 650 nm. **E,** U2OS cells were preincubated with rVAR2 or rContrl and allowed to adhere to plastic. The phosphorylation of Src and Erk1/2 kinases in response to the adhesion event was monitored by Western blotting.

cancer cells (Fig. 1D). MDA-MB-231 was not inhibited in binding to collagen, suggesting another mode of binding in this cell type (Fig. 1D).

The Src and Erk kinases are activated by cellular adhesion (32, 33). Given the effects of rVAR2 incubation on functional cell adhesion, we tested whether these pathways were affected in rVAR2-treated U2OS cells. Indeed, we observed a clear inhibition of the phosphorylation of Src and Erk (Fig. 1E), in line with the shown effect on cellular adhesion (Fig. 1A–C).

rVAR2 inhibits cellular migration, invasion, and anchorage-independent growth in cancer

We next wanted to test whether blocking ofCS function impacts cellular migration. We therefore performed scratch assays using the invasive MG63 osteosarcoma cell line. Confluent monolayers of MG63 cells were scratched and incubated with rVAR2 for 24 hours under serum starvation. We then observed and documented wound closure over time. The cells incubated with rVAR2 failed to close the wound, whereas the control cells effectively filled in the scratch (Fig. 2A and B). MG63 cells treated with siRNAs against CSGALNACT1, which is involved key enzyme involved in chondroitin sulfate synthesis, showed similar effects (Supplementary Fig. S1). The antimigratory effect of rVAR2 on the cells could be inhibited by the addition of soluble CSA to outcompete rVAR2 cell binding (Fig. 2C). Furthermore, rVAR2 significantly inhibited the migration of MG63 cells across a membrane in a Boyden chamber assay (Fig. 2D). Next, we tested the ability of rVAR2 to block cancer cell invasion across an ECM-modified membrane in the same Boyden chamber assay. This showed that rVAR2 potently inhibited the invasive capacity of cancer cells (Fig. 2E). Finally, we tested the ability of rVAR2 to inhibit anchorage-independent growth of MG63 cells in soft agar colony growth assays (Fig. 2F). rVAR2 efficiently reduced the number of colonies formed compared with the control. The effect was shown to be ofCS specific, as addition of soluble CSA to outcompete rVAR2 cell binding efficiently rescued the colony formation. Collectively, this shows that blocking the function of ofCS with rVAR2 inhibits the metastatic potential of cancer cells.

rVAR2 interacts with ofCS-modified proteoglycans

Chondroitin sulfate is a posttranslational modification to many CSPGs within the cell membrane. Although these CSPGs differ greatly in their protein cores, they have many overlapping functions in cancer development (11–19). We previously showed that rVAR2, through ofCS chains, interacts with numerous cancer-associated proteoglycans including CSPG4 and CD44, based on overexpression of membrane receptors in HEK cells (10). In continuation of this work, we wanted to explore the significance of ofCS targeting in terms of the number and diversity of CSPG targets in different cancers. To do this, we selected 5 cell lines derived from different cancer types: melanoma (C32), T-cell lymphoma (Myla2059), prostate cancer (PC3), osteosarcoma (U2OS),

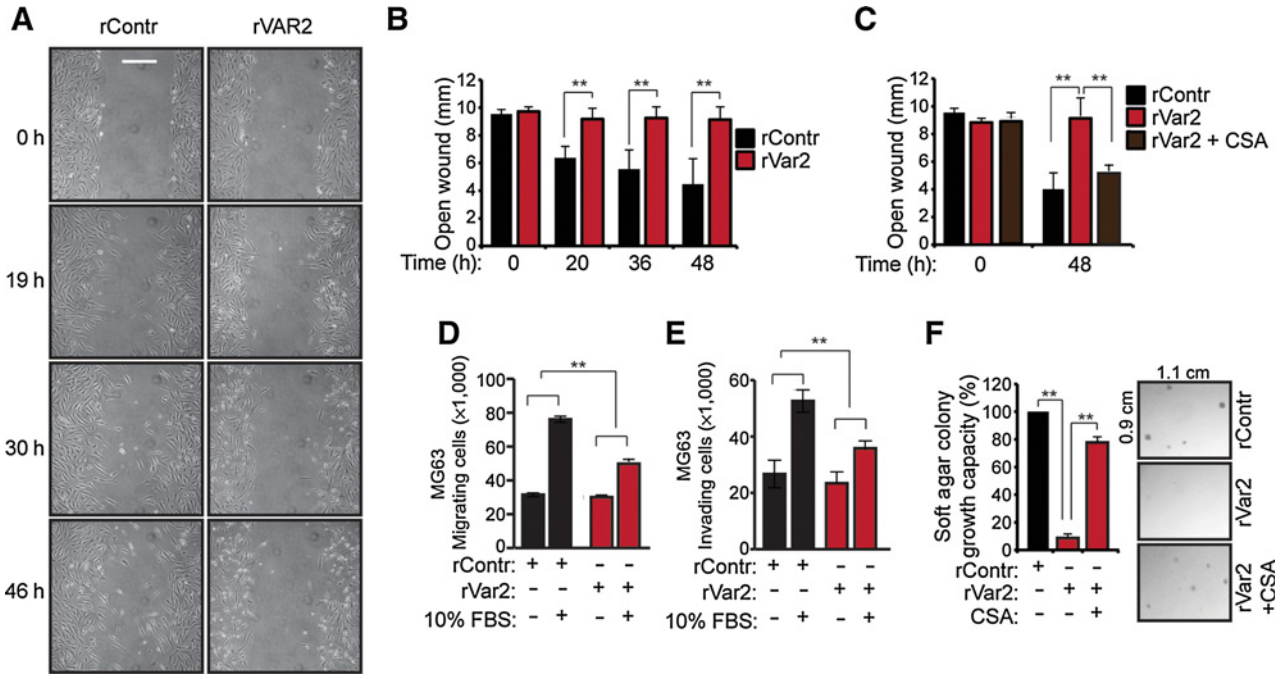

Figure 2.

Chondroitin sulfate–dependent motility and anchorage-independent growth in tumor cells. **A,** MG63 cells were tested for their ability to migrate in the presence of rVAR2 or saline in a scratch wound heal assay. The figure shows representative pictures of the analysis taken at time 0, 19, 30, and 46 hours. **B,** Column graph showing the statistical analysis of the MG63 scratch wound heal assay. **C,** Scratch wound heal assay was repeated with rVAR2 treatment in the presence of CSA to illustrate ofCS specificity. **D,** MG63 cells were tested for their ability to migrate across a membrane in a Boyden chamber assay in the presence of rVAR2 or rContr. **E,** MG63 cells were tested for their ability to invade across an ECM-modified membrane in a Boyden chamber assay in the presence of rVAR2 or rContr. **F,** MG63 cells were tested for their ability to elicit anchorage-independent growth in the presence of rVAR2, rContr, or rVAR2 + CSA in a soft agar colony formation assay.

Table 1. List of known CSPGs identified in the rVAR2 pull-down screen

Protein name	Gene	Source
Cell surface CSPGs		
Chondroitin sulfate proteoglycan 4	*CSPG4*	U2OS, C32, RH30
Amyloid-like protein 2	*APLP2*	U2OS, PC3, Myla2059, C32
Syndecan-1	*SDC1*	U2OS, PC3, C32, RH30
CD44	*CD44*	U2OS, C32, Myla2059, RH30
Integrin-β1	*ITGB1*	U2OS, C32
Syndecan-4	*SDC4*	U2OS, C32, Myla2059
Glypican-1	*GPC1*	U2OS
Sushi repeat–containing protein	*SRPX*	U2OS, C32
Neuropilin-1	*NRP1*	U2OS, PC3
Sushi repeat–containing protein 2	*SRPX2*	U2OS
Syndecan 2	*SDC2*	C32
Neuropilin-2	*NRP2*	C32
Glypican-2	*GPC2*	C32
Glypican-6	*GPC6*	C32
Glypican-4	*GPC4*	C32
Endorepellin	*HSPG2*	C32
Delta-sarcoglycan	*SGCD*	C32
Agrin	*AGRN*	C32, Myla2059
Syndecan-3	*SDC3*	C32
HLA class II histocompatibility antigen gamma chain	*CD74*	C32, Myla2059
Laminin subunit alpha-4	*LAMA4*	C32
Leukocyte surface antigen CD47	*CD47*	Myla2059
Testican-1	*SPOCK1*	Myla2059
Secreted CSPGs		
Serglycin	*SRGN*	PC3, Myla2059

NOTE: Each CSPG hit is listed at either cell surface or secreted. The hits are given by name and gene. The source of these hits is given in the right column.

and rhabdomyosarcoma (RH30). We then performed pull-downs from cell extracts using rVAR2 coupled columns or biotinylated rVAR2 captured on streptavidin-coated beads. The elution extracts were then analyzed by mass spectrometry. Using this method, we identified 24 proteins previously reported to carry chondroitin sulfate (Table 1). Interestingly, all cell lines tested co-expressed different CSPGs, and several CSPGs were shared between tumor cell lines of different origin.

Cancer-associated CSPG complexes are involved in cell motility

The combined pull down and mass spectrometric analysis identified many ofCS CSPGs across diverse tumor types. Furthermore, we noted that several known CSPG-associated partners were among the identified proteins. To gain insights into the CSPG-related proteome and its impact on cellular function, we subjected the full list of pulldown hits to IPA. This revealed an involvement of CSPG complexes in cellular motility and metastasis (Fig. 3A and B).

Several integrin subunits were consistently among the most significant hits in the pulldown analysis (Fig. 3C). To verify this, we investigated the interaction between rVAR2 staining and integrin-β1, integrin-α4, and the heterodimeric integrin-α5β1 complex by colocalization in immunofluorescence (Fig. 3D), coprecipitation using an rVAR2-coupled column (Fig. 3E; Supplementary Fig. S2A), and PLA (refs. 34, 35; Fig. 3F and G; Supplementary Fig. S2B and S2C). This suggested a strong interaction between rVAR2-targeted ofCS and integrin-β1, integrin-α4, and integrin-α5β1.

ofCS is involved in integrin-related intracellular signaling

Several studies have shown that targeting the CSPG4 core protein on diverse cancer cell types has a direct effect on integrin-related intracellular signaling through effectors such as FAK, Src, and Erk1/2 (15, 36, 37). To test whether targeting of the ofCS part of these CSPG/integrin complexes had a similar effect, we incubated the osteosarcoma cell line, U2OS, with rVAR2 and analyzed the intracellular response to FBS stimulation. We used 450 nmol/L rVAR2 as this concentration effectively saturated the rVAR2-binding sites on the cells, shown by FACS-binding analysis (Fig. 4A). A non–chondroitin sulfate–binding part of VAR2CSA, rDBL4, was used as a recombinant protein negative control (rContr). This showed that phosphorylation of Src and P130Cas was indeed inhibited in response to FBS stimulation (Fig. 4B). There was an effect of rVAR2 on the signaling prior to FBS stimulation as well.

To test whether these effects were isolated to U2OS cells, we performed the same analysis on MG63 osteosarcoma (Fig. 4C) and MDA-MB-231 breast cancer cells (Fig. 4D). The latter has previously been tested in an anti-CSPG4 targeting strategy (15). Again, we saw that phosphorylation of Src was inhibited (Fig. 4C and D).

We have previously shown that siRNA-mediated knockdown of the enzymes B3GAT1 and CSGALNACT1, which are involved in chondroitin sulfate biosynthesis, reduces binding of rVAR2 to the cell surface (10). To test whether the effects seen on intracellular signaling were due to inhibition of the ofCS-binding epitope, we tested the effects of B3GAT1 and CSGalNAcT1 knockdown in our FBS stimulation assay (Fig. 4E and F). This showed inhibition of phosphorylation of Src and P130Cas with knockdown of both B3GAT1 and CSGALNACT1. This supports our hypothesis that the rVAR2 ofCS-binding epitope is involved in integrin-mediated signaling in cancer.

While stimulation with FBS revealed inhibition of several integrin related effector proteins, such broad stimulation may show effects through other signaling pathways converging on the same effectors. To narrow down the source of stimulation, we wanted to investigate the specific cellular activation of integrin complexes, with a ligand such as fibronectin. Fibronectin is a large complex molecule containing binding sites for numerous cell surface receptors and ECM components. The integrin subunits of various types can interact with several of these sites both with and without CSPGs (38–42). However, one region of fibronectin, called the CS1 region, has been shown to support integrin-α4β1 binding only when it is in complex with a CSPG (43). We therefore tested whether rVAR2 would inhibit cellular activation in response to stimulation with recombinant CS1 peptide, which has been shown to stimulate the phosphorylation of FAK (44). Accordingly, rVAR2 blocked phosphorylation of FAK (Y397) in response to stimulation with the CS1 peptide on U2OS cells (Fig. 4G). This work shows the importance of ofCS in integrin-mediated signaling.

ofCS is expressed in metastasis

We have shown the implication of ofCS in integrin-mediated cellular function and in cellular adhesion, migration, and invasion, pointing to a potential role for ofCS in metastasis. To investigate the presence of ofCS at metastatic sites, we stained metastatic lesions in murine allografts from C57BL/6 mice injected with 4T1 mammary tumor cells in the left cardiac ventricle (10), using rVAR2-Alexa488. The analysis showed that ofCS was highly and specifically expressed in liver and bone metastasis

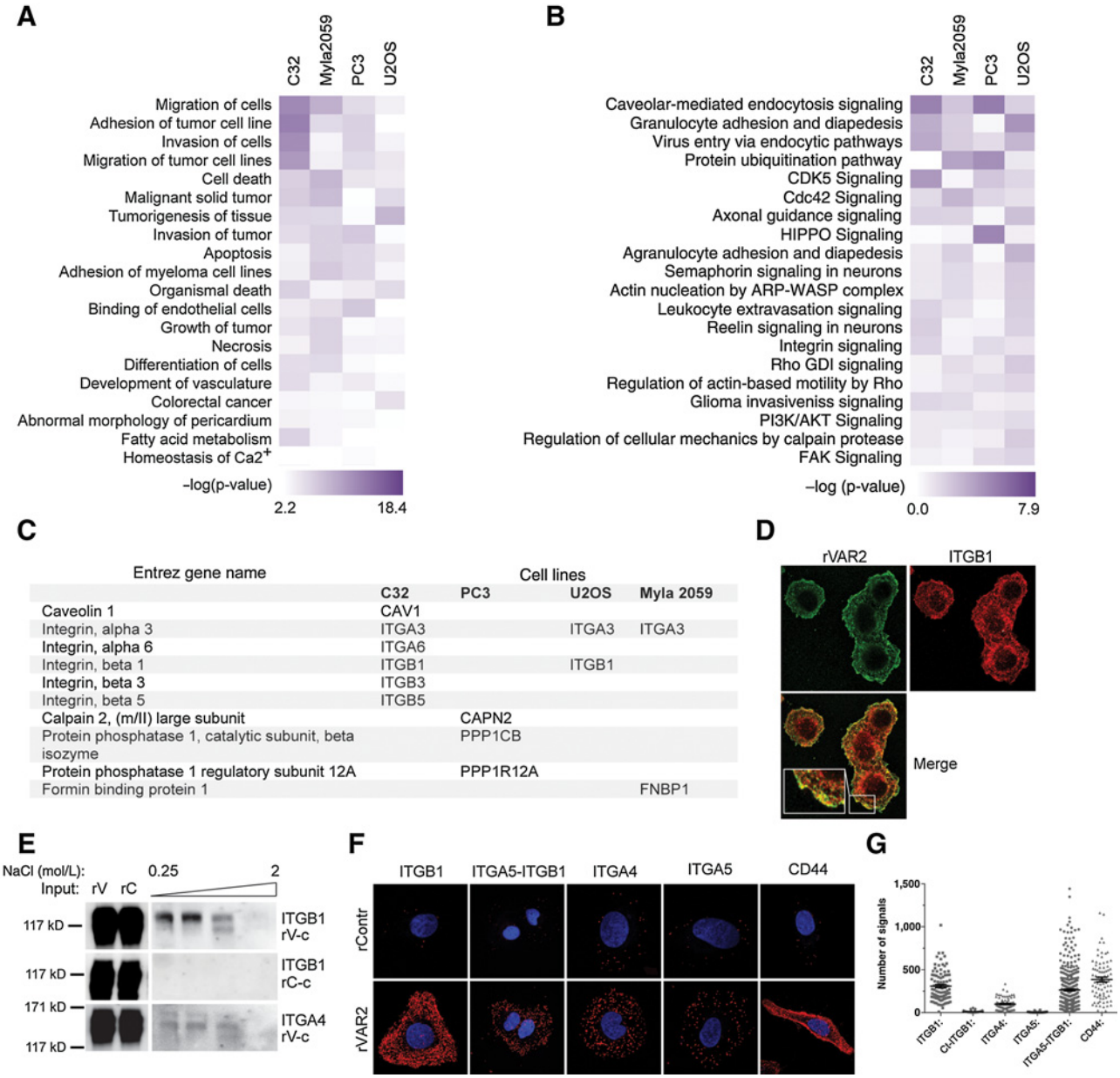

Entrez gene name	Cell lines			
	C32	PC3	U2OS	Myla 2059
Caveolin 1	CAV1			
Integrin, alpha 3	ITGA3		ITGA3	ITGA3
Integrin, alpha 6	ITGA6			
Integrin, beta 1	ITGB1		ITGB1	
Integrin, beta 3	ITGB3			
Integrin, beta 5	ITGB5			
Calpain 2, (m/II) large subunit		CAPN2		
Protein phosphatase 1, catalytic subunit, beta isozyme		PPP1CB		
Protein phosphatase 1 regulatory subunit 12A		PPP1R12A		
Formin binding protein 1				FNBP1

Figure 3.

The chondroitin sulfate–modified tumor cells proteome in enriched for proteins involved in motility. **A,** Network analysis of pulled down proteins using the IPA software. Proteins that were found to be significantly different between rVAR2 and rControl in the pulldown analysis were analyzed. The top 20 diseases and biofunctions involved are shown in a heatmap. We generated the heatmap by comparing independent analyses of rVAR2 pull downs in different cell lines. **B,** IPA heatmap analysis of canonical pathways most significantly enriched in proteins pulled-down with rVAR2. **C,** List of the significant rVAR2 pulled-down proteins involved in the integrin signaling. **D,** Colocalization analysis between ofCS [rVAR2 stain (green)] and ITGB1 antibody stain (red). **E,** Column-based pull down of integrin subunits using rVAR2 (rV-c) from U2OS cells. Figure shows Western blot analysis of eluates in increasing NaCl concentration. An rContr coupled column is used as negative control (rC-c). **F,** PLA analysis of colocalization between ofCS (rVAR2 stain) and integrin subunits. CD44 is used as the positive control. **G,** Quantification of the PLA analysis.

(Fig. 5A). A stain for the Ki-67 proliferation marker showed that the rVAR2-staining metastatic cancer cells were rapidly proliferating (Fig. 5A).

To investigate the presence of ofCS in metastatic sites in human tumors, we stained pancreatic cancer specimens collected in the UNMC RAP program from primary tumor tissue as well as tissue from metastatic sites in different organs. As in the murine model, rVAR2 showed strong staining of the primary tumor as well as all metastatic sites, with little staining of normal pancreatic tissue (Fig. 5B and C). Notably, high ofCS expression was unrelated to all annotated clinical parameters (Supplementary Table S1). These data

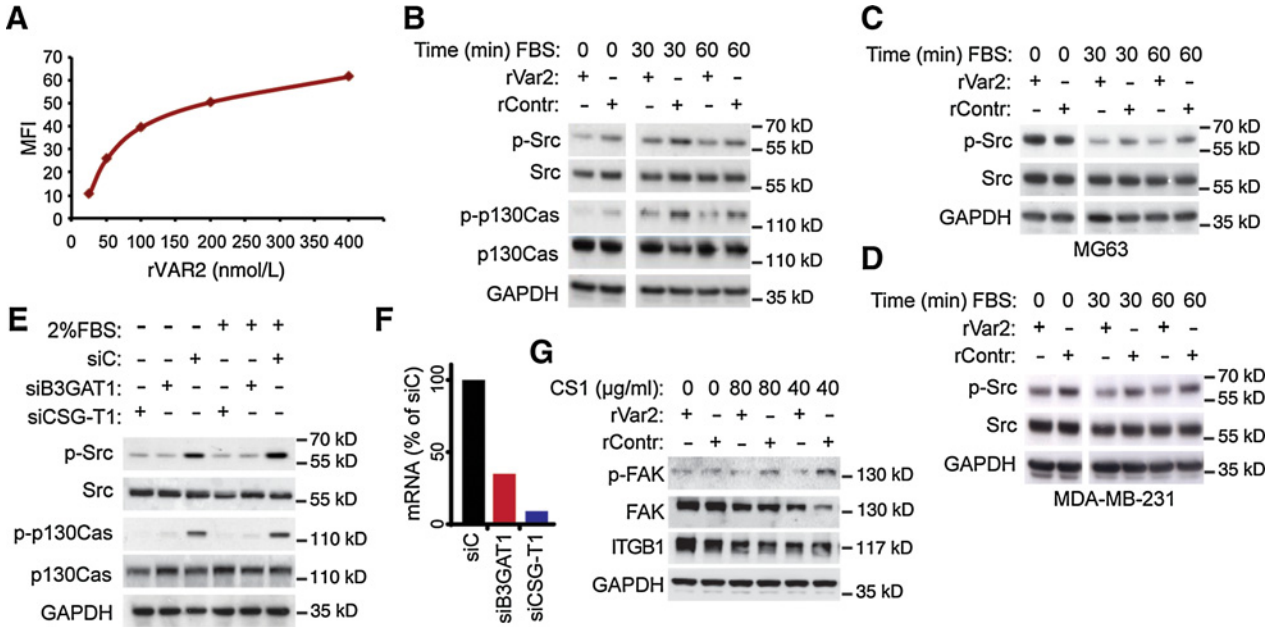

Figure 4.

A role for ofCS in signaling downstream integrin-β1. **A,** Titration of rVAR2 staining of U2OS cells in flow cytometric analysis. **B,** Analysis of downstream integrin signaling in rVAR2- or rContr-treated U2OS cells in response to FBS stimulation. Figure shows effect on Src and p130Cas phosphorylation. **C,** Analysis of downstream integrin signaling in rVAR2- or rContr-treated MG63 cells in response to FBS stimulation. Figure shows effect on Src. **D,** Analysis of downstream integrin signaling in rVAR2- or rContr-treated MDA-MB-231 cells in response to FBS stimulation. Figure shows effect on Src. **E,** Analysis of downstream integrin signaling in U2OS cells treated with siRNA (72 hours) against B3GAT1 and CSGALNACT1 (CSGT-1). A scrambled siRNA is used as control. Figure shows effect on Src and p130Cas phosphorylation. **F,** RT-PCR analysis of cells treated with siRNA against B3GAT1 and CSGALNACT1 for the analysis shown in **E**. **G,** Analysis of FAK phosphorylation in rVAR2- or rContr-treated U2OS cells in response to stimulation with the CS1 fibronectin peptide.

support a role for ofCS in both primary and metastatic tumor compartments.

rVAR2 adhesion to ofCS inhibits metastasis

Having shown that ofCS is present in metastatic tumors, we wanted to investigate the effect of rVAR2 treatment on metastasis formation *in vivo*. First, we tested the effect of intravenous administration of rVAR2 on the implementation of B16 melanoma tumors in subcutaneous allotransplanted mice. After B16 cell inoculation, the mice were randomized into 2 groups ($n = 10$ each) and treated with rVAR2 at days 0, 6, and 9. The control group was treated with saline. The results showed that 100% of mice in the saline group developed tumors within 12 days whereas tumor growth in the mice treated with rVAR2 at days 0, 6, and 9 was significantly delayed (Fig. 6A; Supplementary Fig. S3, $P = 0.008178$). These data show that rVAR2 binding to ofCSA on the cell surface of B16 melanoma cells inhibits tumor implantation.

To analyze the impact of rVAR2–ofCS binding on metastatic spread, luciferase-positive Lewis lung carcinoma cells were preincubated with 100 nmol/L of rVAR2 or saline and injected into the left cardiac ventricle of mice ($n = 7$ each). In the control arm, 42% ($n = 3$) of the mice formed metastases as visualized by bioluminescence imaging, whereas no metastases were found in any of the rVAR2-treated mice ($P < 0.05$; Fig. 6B and C). Of the mice in the rVAR2 arm, 100% were alive after 45 days. One mouse in the saline group died unexplainably without signs of metastasis and is therefore excluded from the survival graph. With this in mind, 50% of the saline control group were dead by day 45 days ($n = 3$; $P < 0.05$; Fig. 6D). At the experimental endpoint, autopsy and immunohistochemical (IHC) analysis were performed. The control mice treated with PBS had visible metastases in different organs, including kidney and ovary, which stained strongly for ofCS using rVAR2-alexa 488 (Fig. 6E). No metastases were found in the lung, liver, and kidney of the rVAR2-treated mice (Fig. 6F). This shows that interfering with ofCS on cancer cells significantly ($P < 0.05$) inhibits the seeding of cancer cells *in vivo*.

Discussion

We have recently shown that tumor and placental cells carry a common ofCS secondary modification that can be targeted by the malarial VAR2CSA protein (10). The binding of rVAR2 to cancer is nearly universal and highly specific with minimal to absent binding in normal tissue compartments, except for placenta. As such, rVAR2 can potentially be utilized in various diagnostic and therapeutic settings (10).

Chondroitin sulfate in cancer is well described (14, 15, 45–51). The roles of chondroitin sulfate and CSPGs have been described in many cellular functions including proliferation, migration, invasion, metastasis, angiogenesis, and capture of growth factors, cytokines, and chemokines (11–15, 20–24). A well-described function of chondroitin sulfate, and of many of the distinct CSPGs, is their interaction with, and potentiation of integrin function (18, 39, 40, 43, 52). In this article, we investigated the link between ofCS modification and cellular function in cancer.

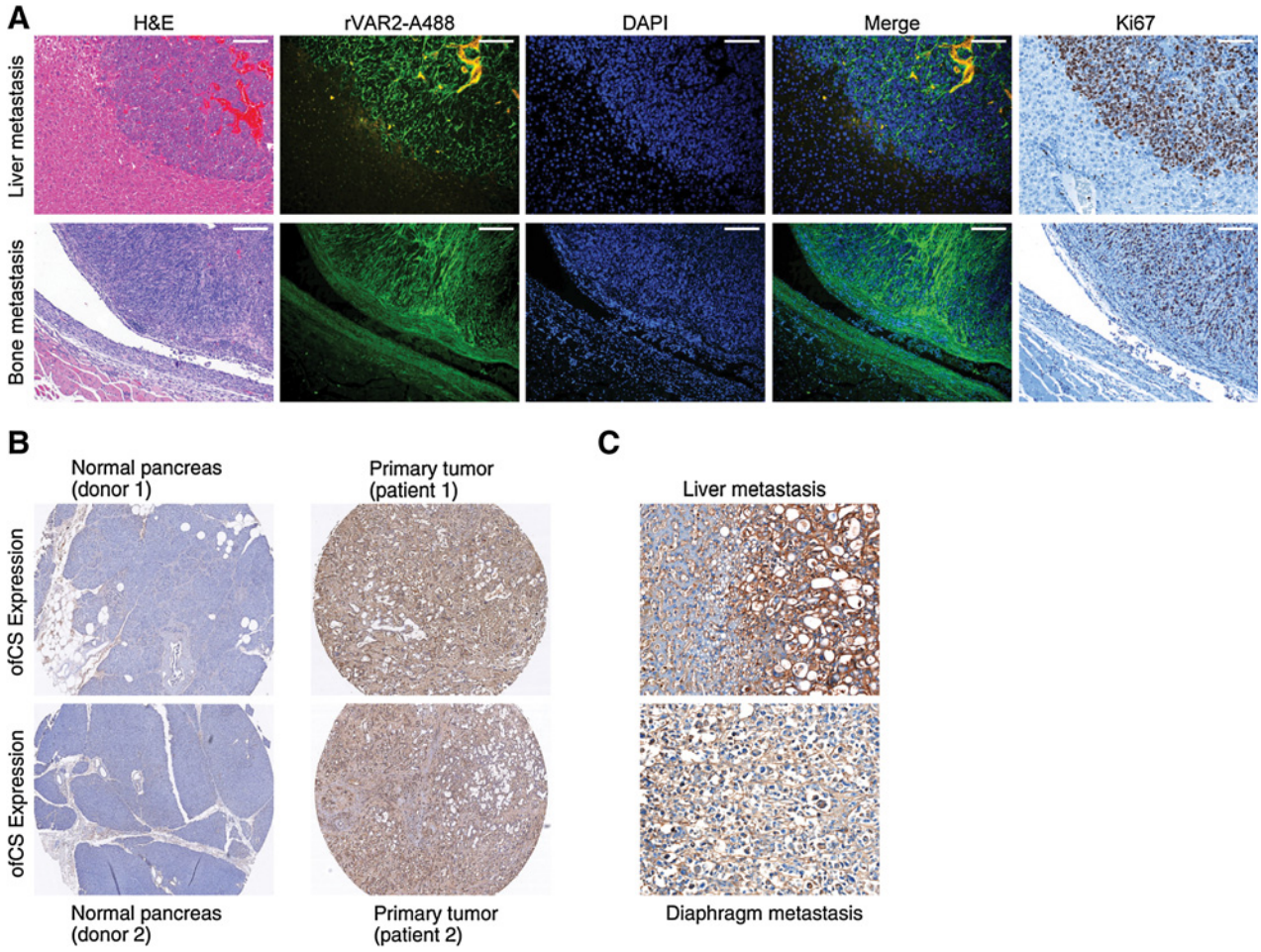

Figure 5.

Expression of oncofetal CS in metastatic lesions. **A,** Hematoxylin and eosin (H&E) images (left), immunofluorescent (rVAR2-Alexa 488, DAPI and merged; middle), and Ki-67 cell proliferative marker staining (right) images of murine liver and bone metastases derived from Balb/C mice inoculated with 4T1 murine mammary cancer cells by intracardiac injection. The scale bars represent 100 μm. **B,** IHC analysis of ofCS, stained with rVAR2-V5 using anti-V5-HRP antibody, in human normal pancreas (left), pancreatic cancer tissues (right). **C,** Liver and diaphragm metastases.

There are more than 50 known proteoglycans in human tissues. They are found in the cell membranes, in the ECM, excreted into the body fluids, or kept in intracellular granules (24, 53). We recently tested rVAR2 binding in a functional screen where 3,500 cell surface receptors were overexpressed in HEK cells. We identified 17 positive binding partners of which some were known proteoglycans (10). Overexpression of receptors in a non-cancer cell line is unlikely to be fully representative of how the receptors are modified during expression in cancer cells. To more directly analyze proteins associated with ofCS, we performed co-precipitation from tumor cell extracts using rVAR2. Here, we identified 24 known CSPGs as well as known CSPG-associated proteins, including integrin subunits (Table 1). Furthermore, the analysis identified several proteins not previously described in relation to CSPGs (data not shown). The co-precipitated proteins included both cell membrane CSPGs and secreted serglycin. Several CSPGs were coprecipitated from each cell type and some were common among tumor cell lines of diverse origin. The broad presence of ofCS on so many CSPGs emphasizes the significance of ofCS substitution in cancer rather than the expression of a specific CSPG. This promotes ofCS-modified CSPG as potential candidate targets in anticancer therapy. Our results are refined by the current knowledge of chondroitin sulfate–carrying proteoglycans. The part-time glycosylation status of many proteoglycans, meaning that they are not always glycosaminoglycan-modified, does however make CSPGs difficult to identify. It is therefore possible that proteoglycans not previously associated with a chondroitin sulfate chain are modified with ofCS during transformation to fuel proliferation and tumor cell motility. A thorough and detailed analysis into glycosaminoglycan displacement at the proteome level is needed.

The interaction of CSPGs, including CSPG4, CD44, and the syndecans, with integrin subunits are well described (38–40, 52, 54). Furthermore, it has been shown that the α5β1 complex can be modified with a chondroitin sulfate chain itself (55, 56). In line with this, α4- and β1-integrins were co-precipitated with rVAR2. The association of ofCS with the integrin complexes was further verified using PLA that allows for colocalization analysis at the resolution of a single molecule (35). This

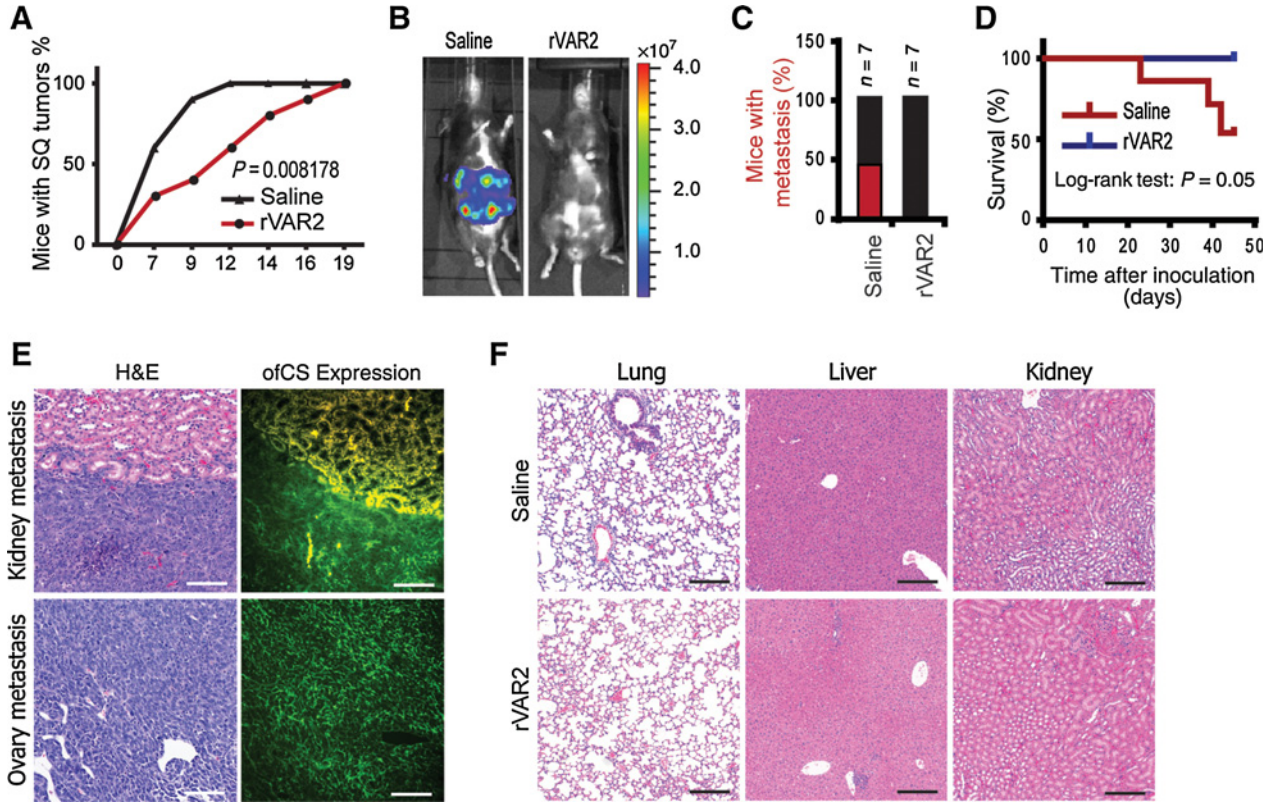

Figure 6.

Inhibition of tumor initiation and metastatic spread by rVAR2. **A,** Mice were inoculated with subcutaneous B16 tumors and randomized into 2 groups ($n = 10$) and treated with rVAR2 at days (0, 6, 9). The control group was treated with saline. Figure shows tumor size progression over time (days). **B,** Two groups of C57black/6 mice were inoculated with murine Lewis lung cancer cells preincubated with control (saline) or rVAR2. Representative luciferase images 39 days after inoculation. **C,** Percentage of C57black/6 mice carrying Lewis cell metastasis (luciferase-positive) in saline and rVAR2 group; $n = 7$. **D,** Kaplan–Meier plot of disease-free survival ($P = 0.05$). **E,** Metastatic kidney and ovary from control group stained with hematoxylin and eosin (H&E) and immunofluorescence using rVAR2-Alexa488 (right). **F,** Lung, liver, and kidney tissue from control group (top) and the rVAR2 group (bottom) were stained with H&E. The white scale bars represent 100 μm; the black scale bars represent 200 μm.

method confirmed a strong correlation between integrin-α4, -β1, and -α5β1 and rVAR2 cell binding. These data confirm the findings of others (18, 39, 40, 43) and emphasize the involvement of CSPGs in tumor-associated integrin signaling.

Several articles have shown that targeting the CSPG4 protein core with monoclonal antibodies has an effect on integrin-related cellular function (15, 36, 37, 57). Here, we show that targeting the ofCS modification present on the proteoglycan component of the integrin complexes has similar effects. These effects include inhibition of intracellular signaling through Src, FAK, P130Cas, and Erk in stimulation and adhesion experiments. The mode of action could be 2-fold. On one hand, a bulky protein bound to ofCS chains could prevent formation of the CSPG-integrin complexes at the cell surface, whereas on the other hand, shielding of the ofCS epitope could abrogate its cancer-promoting effects. We have previously shown that knockdown of key enzymes in the chondroitin sulfate biosynthesis pathway reduces rVAR2 binding, suggesting that these enzymes are involved in producing the distinct ofCS epitope (10). In the present study, we show that targeting the same enzymes has a similar effect on integrin-related signaling, which suggests that the ofCS epitope is indeed crucial for these events to take place. It is likely that targeting the ofCS modification rather than the protein component of proteoglycans such as CSPG4 will present a more universal and efficacious treatment strategy.

We have presented evidence for a function of ofCS in cellular adhesion, migration, and invasion. These are all driver functions of metastatic disease. Indeed we found that ofCS was present in both the primary and the metastatic lesions of human pancreatic cancer.

Finally, we wanted to see whether targeting ofCS with rVAR2 would interfere with tumor settlement *in vivo*. For this purpose, we established 2 animal models exploring 2 essential events of metastatic spread; cell settlement and tumor implementation. Preincubating Lewis lung carcinoma cells with rVAR2 strongly inhibited settlement in distant organs and significantly prolonged lifespan of the treated mice. The same was evident for treatment of subcutaneous B16 melanoma tumors at time of implementation. This aligns with our data showing that rVAR2 inhibits cellular attachment, migration, invasion, and integrin function. It also confirms what others have shown in targeting specific CSPG components of cancer cells using monoclonal antibodies (15).

Taken together, these data demonstrate the involvement of ofCS chains in cancer cell growth and motility, promoting ofCS as a candidate target for therapy.

Disclosure of Potential Conflicts of Interest

S. Lee is the Research Assistant at Vancouver Prostate Centre. A. Salanti is the CEO of and has Ownership Interest (including patents) in VAR2Pharmaceuticals. No potential conflicts of interest were disclosed by the other authors.

Authors' Contributions

Conception and design: T.M. Clausen, H.Z. Oo, M. Daugaard, A. Salanti
Development of methodology: T.M. Clausen, N.A. Nakouzi, H.Z. Oo, M. Daugaard
Acquisition of data (provided animals, acquired and managed patients, provided facilities, etc.): T.M. Clausen, M.A. Pereira, N.A. Nakouzi, H.Z. Oo, M.Ø. Agerbæk, S. Lee, M.S. Ørum-Madsen, A.R. Kristensen, P.M. Grandgenett, J. L. Grem, M.A. Hollingsworth, P.J. Holst
Analysis and interpretation of data (e.g., statistical analysis, biostatistics, computational analysis): T.M. Clausen, M.A. Pereira, N.A. Nakouzi, H.Z. Oo, A. El-Naggar, P.M. Grandgenett, T. Theander
Writing, review, and/or revision of the manuscript: T.M. Clausen, M.A. Pereira, H.Z. Oo, A. El-Naggar, P.M. Grandgenett, P.J. Holst, T. Theander, P.H.B. Sorensen, M. Daugaard, A. Salanti
Administrative, technical, or material support (i.e., reporting or organizing data, constructing databases): H.Z. Oo, M.A. Hollingsworth, A. Salanti
Study supervision: T.M. Clausen, M. Daugaard, A. Salanti
Other (*conducted motility studies, analyzed and interpreted the data, and providedfigures*): A. El-Naggar

Acknowledgments

The authors would like to thank Birita Kjærbæk and Elham Alijazaeri for their technical assistance in the above-mentioned experiments.

Grant Support

T.M. Clausen, M.A. Pereira, M.Ø. Agerbæk, P.J. Holst, T. Theander, M. Daugaard, and A. Salanti were funded by the European Research Council (ERC) and the US Department of Defense (DoD). T.M. Clausen, N.A. Nakouzi, H.Z. Oo, S. Lee, and M. Daugaard were funded by Prostate Cancer Canada funded by Canada Safeway (Grant # RS2014-02). P.M. Grandgenett, J.L. Grem, and M.A. Hollingsworth were funded by SPORE in Pancreatic Cancer (Rapid Autopsy Pancreas program), CA127297, TMEN Tumor Microenvironment Network, U54 CA163120, and NCI Cancer Center Support GrantP30 CA36727.

The costs of publication of this article were defrayed in part by the payment of page charges. This article must therefore be hereby marked *advertisement* in accordance with 18 U.S.C. Section 1734 solely to indicate this fact.

Received April 6, 2016; revised August 8, 2016; accepted September 2, 2016; published OnlineFirst September 21, 2016.

References

1. Esko JD, Kimata K, Lindahl U. Proteoglycans and sulfated glycosaminoglycans. In:Varki A, Cummings RD, Esko JD, Freeze HH, Stanley P, Bertozzi CR, et al. , editors. Essentials of glycobiology. 2nd ed. Cold Spring Harbor, NY: Cold Spring Harbor Laboratory Press;2009. Chapter 16. Available from: https://www.ncbi.nlm.nih.gov/books/NBK1900/.
2. Lanctot PM, Gage FH, Varki AP. The glycans of stem cells. Curr Opin Chem Biol 2007;11:373–80.
3. Kalathas D, Theocharis DA, Bounias D, Kyriakopoulou D, Papageorgakopoulou N, Stavropoulos MS, et al. Alterations of glycosaminoglycan disaccharide content and composition in colorectal cancer: structural and expressional studies. Oncol Rep 2009;22:369–75.
4. Chandrasekaran EV, Davidson EA. Glycosaminoglycans of normal and malignant cultured human mammary cells. Cancer Res 1979; 39:870–80.
5. De Klerk DP. The glycosaminoglycans of human bladder cancers of varying grade and stage. J Urol 1985;134:978–81.
6. De Klerk DP, Lee DV, Human HJ. Glycosaminoglycans of human prostatic cancer. J Urol 1984;131:1008–12.
7. Sweet MB, Thonar EM, Immelman AR. Glycosaminoglycans and proteoglycans of human chondrosarcoma. Biochim Biophys Acta 1976; 437:71–86.
8. Paszek MJ, DuFort CC, Rossier O, Bainer R, Mouw JK, Godula K, et al. The cancer glycocalyx mechanically primes integrin-mediated growth and survival. Nature 2014;511:319–25.
9. Pinho SS, Reis CA. Glycosylation in cancer: mechanisms and clinical implications. Nat Rev Cancer 2015;15:540–55.
10. Salanti A, Clausen TM, Agerbaek MO, Al Nakouzi N, Dahlback M, Oo HZ, et al. Targeting human cancer by a glycosaminoglycan binding malaria protein. Cancer Cell 2015;28:500–14.
11. Cooney CA, Jousheghany F, Yao-Borengasser A, Phanavanh B, Gomes T, Kieber-Emmons AM, et al. Chondroitin sulfates play a major role in breast cancer metastasis: a role for CSPG4 and CHST11 gene expression in forming surface P-selectin ligands in aggressive breast cancer cells. Breast Cancer Res 2011;13:R58.
12. Denholm EM, Lin YQ, Silver PJ. Anti-tumor activities of chondroitinase AC and chondroitinase B: inhibition of angiogenesis, proliferation and invasion. Eur J Pharmacol 2001;416:213–21.
13. Fthenou E, Zong F, Zafiropoulos A, Dobra K, Hjerpe A, Tzanakakis GN. Chondroitin sulfate A regulates fibrosarcoma cell adhesion, motility and migration through JNK and tyrosine kinase signaling pathways. In Vivo 2009;23:69–76.
14. Garusi E, Rossi S, Perris R. Antithetic roles of proteoglycans in cancer. Cell Mol Life Sci 2012;69:553–79.
15. Wang X, Osada T, Wang Y, Yu L, Sakakura K, Katayama A, et al. CSPG4 protein as a new target for the antibody-based immunotherapy of triple-negative breast cancer. J Natl Cancer Inst 2010;102:1496–512.
16. Yang J, Price MA, Li GY, Bar-Eli M, Salgia R, Jagedeeswaran R, et al. Melanoma proteoglycan modifies gene expression to stimulate tumor cell motility, growth, and epithelial-to-mesenchymal transition. Cancer Res 2009;69:7538–47.
17. Iida J, Wilhelmson KL, Ng J, Lee P, Morrison C, Tam E, et al. Cell surface chondroitin sulfate glycosaminoglycan in melanoma: role in the activation of pro-MMP-2 (pro-gelatinase A). Biochem J 2007;403:553–63.
18. Iida J, Skubitz AP, Furcht LT, Wayner EA, McCarthy JB. Coordinate role for cell surface chondroitin sulfate proteoglycan and alpha 4 beta 1 integrin in mediating melanoma cell adhesion to fibronectin. J Cell Biol 1992; 118:431–44.
19. Price MA, Colvin Wanshura LE, Yang J, Carlson J, Xiang B, Li G, et al. CSPG4, a potential therapeutic target, facilitates malignant progression of melanoma. Pigment Cell Melanoma Res 2011;24:1148–57.
20. Sugiura N, Shioiri T, Chiba M, Sato T, Narimatsu H, Kimata K, et al. Construction of a chondroitin sulfate library with defined structures and analysis of molecular interactions. J Biol Chem 2012;287: 43390–400.
21. ten Dam GB, van de Westerlo EM, Purushothaman A, Stan RV, Bulten J, Sweep FC, et al. Antibody GD3G7 selected against embryonic glycosaminoglycans defines chondroitin sulfate-E domains highly up-regulated in ovarian cancer and involved in vascular endothelial growth factor binding. Am J Pathol 2007;171:1324–33.
22. Deepa SS, Umehara Y, Higashiyama S, Itoh N, Sugahara K. Specific molecular interactions of oversulfated chondroitin sulfate E with various heparin-binding growth factors. Implications as a physiological binding partner in the brain and other tissues. J Biol Chem 2002;277:43707–16.
23. Nikitovic D, Assouti M, Sifaki M, Katonis P, Krasagakis K, Karamanos NK, et al. Chondroitin sulfate and heparan sulfate-containing proteoglycans are both partners and targets of basic fibroblast growth factor-mediated proliferation in human metastatic melanoma cell lines. Int J Biochem Cell Biol 2008;40:72–83.
24. Afratis N, Gialeli C, Nikitovic D, Tsegenidis T, Karousou E, Theocharis AD, et al. Glycosaminoglycans: key players in cancer cell biology and treatment. FEBS J 2012;279:1177–97.
25. Gama CI, Tully SE, Sotogaku N, Clark PM, Rawat M, Vaidehi N, et al. Sulfation patterns of glycosaminoglycans encode molecular recognition and activity. Nat Chem Biol 2006;2:467–73.
26. Fried M, Duffy PE. Adherence of Plasmodium falciparum to chondroitin sulfate A in the human placenta. Science 1996;272:1502–4.

27. Salanti A, Dahlback M, Turner L, Nielsen MA, Barfod L, Magistrado P, et al. Evidence for the involvement of VAR2CSA in pregnancy-associated malaria. J Exp Med 2004;200:1197–203.
28. Salanti A, Staalsoe T, Lavstsen T, Jensen AT, Sowa MP, Arnot DE, et al. Selective upregulation of a single distinctly structured var gene in chondroitin sulphate A-adhering Plasmodium falciparum involved in pregnancy-associated malaria. Mol Microbiol 2003;49:179–91.
29. Clausen TM, Christoffersen S, Dahlback M, Langkilde AE, Jensen KE, Resende M, et al. Structural and functional insight into how the Plasmodium falciparum VAR2CSA protein mediates binding to chondroitin sulfate A in placental malaria. J Biol Chem 2012;287:23332–45.
30. Dahlback M, Jorgensen LM, Nielsen MA, Clausen TM, Ditlev SB, Resende M, et al. The chondroitin sulfate A-binding site of the VAR2CSA protein involves multiple N-terminal domains. J Biol Chem 2011;286: 15908–17.
31. Janik P, Briand P, Hartmann NR. The effect of estrone-progesterone treatment on cell proliferation kinetics of hormone-dependent GR mouse mammary tumors. Cancer Res 1975;35:3698–704.
32. Kim LC, Song L, Haura EB. Src kinases as therapeutic targets for cancer. Nat Rev Clin Oncol 2009;6:587–95.
33. Webb DJ, Donais K, Whitmore LA, Thomas SM, Turner CE, Parsons JT, et al. FAK-Src signalling through paxillin, ERK and MLCK regulates adhesion disassembly. Nat Cell Biol 2004;6:154–61.
34. Fredriksson S, Gullberg M, Jarvius J, Olsson C, Pietras K, Gustafsdottir SM, et al. Protein detection using proximity-dependent DNA ligation assays. Nat Biotechnol 2002;20:473–7.
35. Soderberg O, Gullberg M, Jarvius M, Ridderstrale K, Leuchowius KJ, Jarvius J, et al. Direct observation of individual endogenous protein complexes in situ by proximity ligation. Nat Methods 2006;3:995–1000.
36. Rivera Z, Ferrone S, Wang X, Jube S, Yang H, Pass HI, et al. CSPG4 as a target of antibody-based immunotherapy for malignant mesothelioma. Clin Cancer Res 2012;18:5352–63.
37. Wang J, Svendsen A, Kmiecik J, Immervoll H, Skaftnesmo KO, Planaguma J, et al. Targeting the NG2/CSPG4 proteoglycan retards tumour growth and angiogenesis in preclinical models of GBM and melanoma. PLoS One 2011;6:e23062.
38. Moyano JV, Carnemolla B, Albar JP, Leprini A, Gaggero B, Zardi L, et al. Cooperative role for activated alpha4 beta1 integrin and chondroitin sulfate proteoglycans in cell adhesion to the heparin III domain of fibronectin. Identification of a novel heparin and cell binding sequence in repeat III5. J Biol Chem 1999;274:135–42.
39. Verfaillie CM, Benis A, Iida J, McGlave PB, McCarthy JB. Adhesion of committed human hematopoietic progenitors to synthetic peptides from the C-terminal heparin-binding domain of fibronectin: cooperation between the integrin alpha 4 beta 1 and the CD44 adhesion receptor. Blood 1994;84:1802–11.
40. Iida J, Meijne AM, Spiro RC, Roos E, Furcht LT, McCarthy JB. Spreading and focal contact formation of human melanoma cells in response to the stimulation of both melanoma-associated proteoglycan (NG2) and alpha 4 beta 1 integrin. Cancer Res 1995;55:2177–85.
41. Pierschbacher MD, Ruoslahti E. Variants of the cell recognition site of fibronectin that retain attachment-promoting activity. Proc Natl Acad Sci U S A 1984;81:5985–8.
42. Hynes RO. Integrins: a family of cell surface receptors. Cell 1987;48: 549–54.
43. Iida J, Meijne AM, Oegema TRJr, Yednock TA, Kovach NL, Furcht LT, et al. A role of chondroitin sulfate glycosaminoglycan binding site in alpha4beta1 integrin-mediated melanoma cell adhesion. J Biol Chem 1998;273:5955–62.
44. Kamarajan P, Garcia-Pardo A, D'Silva NJ, Kapila YL. The CS1 segment of fibronectin is involved in human OSCC pathogenesis by mediating OSCC cell spreading, migration, and invasion. BMC Cancer 2010;10:330.
45. Wang X, Wang Y, Yu L, Sakakura K, Visus C, Schwab JH, et al. CSPG4 in cancer: multiple roles. Curr Mol Med 2010;10:419–29.
46. Korpetinou A, Skandalis SS, Moustakas A, Happonen KE, Tveit H, Prydz K, et al. Serglycin is implicated in the promotion of aggressive phenotype of breast cancer cells. PLoS One 2013;8:e78157.
47. Labropoulou VT, Theocharis AD, Ravazoula P, Perimenis P, Hjerpe A, Karamanos NK, et al. Versican but not decorin accumulation is related to metastatic potential and neovascularization in testicular germ cell tumours. Histopathology 2006;49:582–93.
48. Stallcup WB, Huang FJ. A role for the NG2 proteoglycan in glioma progression. Cell Adh Migr 2008;2:192–201.
49. Wegrowski Y, Maquart FX. Chondroitin sulfate proteoglycans in tumor progression. Adv Pharmacol 2006;53:297–321.
50. Theocharis AD, Tsolakis I, Tzanakakis GN, Karamanos NK. Chondroitin sulfate as a key molecule in the development of atherosclerosis and cancer progression. Adv Pharmacol 2006;53:281–95.
51. Ricciardelli C, Sakko AJ, Ween MP, Russell DL, Horsfall DJ. The biological role and regulation of versican levels in cancer. Cancer Metastasis Rev 2009;28:233–45.
52. Woods A, Couchman JR. Syndecan 4 heparan sulfate proteoglycan is a selectively enriched and widespread focal adhesion component. Mol Biol Cell 1994;5:183–92.
53. Theocharis AD, Seidel C, Borset M, Dobra K, Baykov V, Labropoulou V, et al. Serglycin constitutively secreted by myeloma plasma cells is a potent inhibitor of bone mineralization*in vitro*. J Biol Chem 2006;281:35116–28.
54. Woods A, McCarthy JB, Furcht LT, Couchman JR. A synthetic peptide from the COOH-terminal heparin-binding domain of fibronectin promotes focal adhesion formation. Mol Biol Cell 1993;4:605–13.
55. Veiga SS, Elias M, Gremski W, Porcionatto MA, da Silva R, Nader HB, et al. Post-translational modifications of alpha5beta1 integrin by glycosaminoglycan chains. The alpha5beta1 integrin is a facultative proteoglycan. J Biol Chem 1997;272:12529–35.
56. Franco CR, Trindade ES, Rocha HA, da Silveira RB, Paludo KS, Chammas R, et al. Glycosaminoglycan chains from alpha5beta1 integrin are involved in fibronectin-dependent cell migration. Biochem Cell Biol 2009;87:677–86.
57. Yu L, Favoino E, Wang Y, Ma Y, Deng X, Wang X. The CSPG4-specific monoclonal antibody enhances and prolongs the effects of the BRAF inhibitor in melanoma cells. Immunol Res 2011;50:294–302.